Harnessing Exosomes from Human Dermal Fibroblasts and Pirfenidone-exosomes as Innovative Strategies for Scarless Tissue Repair in Wound Healing

by

Jin Wang

A thesis

presented to the University of Waterloo

in fulfilment of the

thesis requirement for the degree of

Doctor of Philosophy

in

Pharmacy

Waterloo, Ontario, Canada, 2025

© Jin Wang 2025

Examining Committee Membership

The following served on the Examining Committee for this thesis. The decision of the Examining Committee is by majority vote.

Supervisor	Dr. Emmanuel A. Ho Professor, School of Pharmacy, Faculty of Science University of Waterloo
Internal examiner	Dr. Michael Beazely Associate Professor, School of Pharmacy, Faculty of Science University of Waterloo
Internal-External examiner	Dr. Shirley Tang Professor, Department of Chemistry, Faculty of Science University of Waterloo
Internal-External examiner	Dr. Juewen Liu Professor, Department of Chemistry, Faculty of Science University of Waterloo
External examiner	Dr. Ildiko Badea Professor University of Saskatchewan

Author's Declaration

I hereby declare that I am the sole author of this thesis. This is a true copy of the thesis, including any required final revisions, as accepted by my examiners. I understand that my thesis may be made electronically available to the public.

Abstract

The wound healing process often leads to scar formation that can negatively affect patients both physically and psychologically. The management and treatment of scars also place a considerable financial burden on healthcare systems. Significant efforts are being made to improve wound healing outcomes by accelerating closure while simultaneously minimizing scar formation. To facilitate scarless wound healing, developing an anti-scarring treatment that modulates dermal fibroblast activity is a promising strategy, with pirfenidone (PFD) showing potential due to its anti-fibrotic properties by targeting intracellular pathways that regulate collagen disposition. PFD, particularly when delivered via dermal fibroblast-derived exosomes, may further enhance therapeutic effectiveness and promote scarless healing.

To achieve this goal, we began by isolating high-purity exosomes from *in vitro* cultured human dermal fibroblasts. Two common isolation methods—PEG precipitation and affinity-based techniques—were compared to identify the most efficient approach for obtaining high-purity and relatively homogenous exosomes. A range of characterization techniques, including transmission electron microscopy (TEM), atomic force microscopy (AFM), antibody arrays, and enzyme-linked immunosorbent assays (ELISA), confirmed the successful isolation of high-purity exosomes. The affinity-based method demonstrated superior performance, yielding well-dispersed and highly pure exosomes. Due to the difficulties in achieving efficient drug encapsulation in exosomes, the following chapter specifically focused on the encapsulation and formulation optimization of the antifibrotic compound PFD and explored the use of exosomes as a drug delivery platform. We optimized an active drug loading method using sonication to enhance encapsulation efficiency (EE%) and loading efficiency (LE%), ensuring that careful control of the sonication process maintained exosome integrity. The optimal formulation of PFD-exosomes achieved an EE% of

11.14% ± 1.27% and an LE of 10.01% ± 1.03%, with a particle recovery rate of exosomes at 64.21% ± 8.49%. Then, we investigated how to harness exosomes from dermal fibroblasts and PFD-exosomes as innovative strategies for achieving scarless tissue repair in wound healing. Our findings showed that exosomes enhanced fibroblast migration and proliferation through an autocrine mechanism, highlighting their potential as a stand-alone cell-free therapy for wound healing. Additionally, this study was ground-breaking in demonstrating that exosomes can improve the efficacy of PFD as a drug carrier, amplifying its anti-fibrotic effects in both *in vitro* and *in vivo* models. The *in vivo* results indicated that PFD-exosomes accelerated wound healing while organizing the extracellular matrix (ECM) by reducing excessive collagen deposition. Overall, PFD-exosomes present an innovative strategy for pre-scarring interventions, offering benefits of enhanced wound healing outcomes while minimizing scarring.

Acknowledgment

I would like to express my heartfelt gratitude to my supervisor, Dr. Emmanuel A. Ho, for his unwavering support and guidance. His mentorship has been instrumental in helping me reach this stage in my career. I am deeply appreciative of his belief in me and the inspiration he has provided, which has motivated me to pursue my goal of becoming a scientist. It is a true honor to be mentored by someone whose passion for research has profoundly shaped my journey. Dr. Ho's impact on my research has been immense, and I aspire to embody the leadership qualities he has instilled in me. I will always be thankful for his support and mentorship.

My gratitude extends to Dr. Michael Beazely and Dr. Shirley Tang for their insightful feedback and constructive criticism throughout the years. I appreciate the contributions of my thesis examiners, Dr. Juewen Liu and Dr. Ildiko Badea, for their role in my thesis examination committee. I would also like to thank the former members of my committee, Dr. Jonathan Blay and Dr. Mungo Marsden, for their invaluable guidance.

I am sincerely grateful to all my colleagues at the Laboratory for Drug Delivery and Biomaterials for their support over the years. A special thanks goes to Dr. Yannick Leandre Traore for his valuable knowledge, training, and friendship. I appreciate Dr. Chen Sun for his ongoing support and guidance throughout my Ph.D. studies. I would like to acknowledge my colleagues, including Derek Chen, Chuying Feng, Sihan Dong, Alistair Chan, Calvin Wong, Ethan Watt, Ryan Nodder, Kaidy Orellana, and Qi Sun, for their encouragement and help. I also want to recognize the contributions of every co-op student.

Additionally, I would like to thank our research technician in School of Pharmacy, Dr. Monica Tudorancea, along with Antoine Hakim and Dr. Ahmed Abdallah, for their prompt

assistance with technical issues. I would like to express my gratitude to Jeanie Flanagan for training me on all animal procedures at the Animal Research and Teaching Facilities. I am also grateful to my former colleagues, Dr. Jiahao Huang and Dr. Yusheng Zhao from the School of Pharmacy, as well as Dr. Pei Zhao and Dr. Weijia Cui from the Department of Mechanical and Mechatronics Engineering, for their valuable guidance and support in my research.

Dedication

To my beloved parents, Jingru Dong and Quanxin Wang. Your unwavering belief in me and your unconditional love and support have been my guiding light. This thesis is a testament to your love and encouragement, for which I am eternally grateful. Thank you for inspiring me to reach for my dreams.

Table of contents

Examining Committee Membership ii
Author's Declaration iii
Abstract iv
Acknowledgment vi
Dedication viii
Abbreviations and Terms xi
List of Tables xvi
List of Figures xvii
Chapter 1 Introduction 1
1.1 Physiology of wound healing 2
1.2 Strategies for mitigating scar formation 8
1.3 Exosomes 10
Chapter 2 High-Purity Exosome Isolation from *In Vitro* Cultured Human Dermal Fibroblasts and Characterization Techniques 20
2.1 Overview 21
2.2 Introduction 22
2.3 Material and methods 28
2.4 Results 36
2.5 Discussion 50
2.6 Conclusion 54
Chapter 3 Active Drug Encapsulation and Formulation Optimization for Utilizing Exosomes as Drug Carriers 55
3.1 Overview 56
3.2 Introduction 57
3.3 Material and methods 65
3.4 Results 69
3.5 Discussion 83
3.6 Conclusion 87
Chapter 4 *In Vitro* and *In Vivo* Assessment of Human Dermal Fibroblast-Derived Exosomes and Pirfenidone- exosomes for Scarless Tissue Repair in Wound Healing 88
4.1 Overview 89
4.2 Introduction 91
4.3 Materials and methods 94

4.4 Results 104
4.5 Discussion 129
4.6 Conclusion 135
Chapter 5 Conclusion and Future Direction 136
5.1 Result conclusion and significance of study 137
5.2 Limitations and future directions 139
References 143

Abbreviations and Terms

AFM	Atomic Force Microscopy
ADSCs	Human Adipose-Derived Stem Cells
ALIX	Programmed Cell Death 6-Interacting Protein
ANXA5	Annexin A5
ASA	Aspirin
ASMA	Alpha-Smooth Muscle Actin
BCA	Bicinchoninic Acid
Ber	Berberine
bFGF	Basic Fibroblast Growth Factor
BSA	Bovine Serum Albumin
Ca^{2+}	Calcium Ion
CD37	Leukocyte Antigen CD37
CD53	Tetraspanin CD53
CD63	Tetraspanin CD63
CD81	Tetraspanin CD81
CD82	Tetraspanin CD82
CD9	Tetraspanin CD9
COL1A1	Collagen Type I Alpha 1
CRY2	Cryptochrome 2
Cur	Curcumin
D90	Diameter of 90% of Particles Below This Value
DAPI	4',6-Diamidino-2-Phenylindole
DG-UC	Density Gradient Ultracentrifugation
DiI	1,1'-Dioctadecyl-3,3,3',3'-Tetramethylindocarbocyanine Perchlorate
DLS	Dynamic Light Scattering
DMSO	Dimethyl Sulfoxide
DNA	Deoxyribonucleic Acid
DOX	Doxorubicin
ECM	Extracellular Matrix

EDTA	Ethylenediaminetetraacetic Acid
EE	Encapsulation Efficiency
EGF	Epidermal Growth Factor
EGFR	Epidermal Growth Factor Receptor
ELISA	Enzyme-Linked Immunosorbent Assay
EMEM	Eagle's Minimum Essential Medium
EpCAM	Epithelial Cell Adhesion Molecule
ER	Endoplasmic Reticulum
Er	Erastin
ESCRT	Endosomal Sorting Complexes Required for Transport
EVs	Extracellular Vesicles
FBS	Fetal Bovine Serum
FGF	Fibroblast Growth Factor
FLOT1	Flotillin-1
GEM	Gemcitabine
GM130	Cis-Golgi Matrix Protein
GMP	Good Manufacturing Practices
GRO-α	Growth-Regulated Protein Alpha
HA-PEG	Hyaluronic Acid-Polyethylene Glycol
HA-PEI	Hyaluronic Acid-Polyethyleneimine
hCG	Human Chorionic Gonadotropin
HDL	High-Density Lipoprotein
HE	Hematoxylin and Eosin
HRP	Horseradish Peroxidase
HSP	Heat Shock Protein
hUCMSCs	Human Umbilical Cord Mesenchymal Stem Cells
hUVECs	Human Umbilical Vein Endothelial Cells
ICAM	Intercellular Adhesion Molecule 1
IgG	Immunoglobulin G
IL-6	Interleukin 6
ILVs	Intraluminal Vesicles

LDL	Low-Density Lipoprotein
LE	Loading Efficiency
LOD	Limit of Detection
LOQ	Limit of Quantification
MCP-1	Monocyte Chemoattractant Protein-1
MHC	Major Histocompatibility Complex
miRNA	MicroRNA
MMP-1	Matrix Metalloproteinase 1
MMPs	Matrix Metalloproteinases
mRNA	Messenger RNA
MSC	Mesenchymal Stem Cell
MTS	3-(4,5-Dimethylthiazol-2-Yl)-5-(3-Carboxymethoxyphenyl)-2-(4-Sulfophenyl)-2H-Tetrazolium
MTX	Methotrexate
MVBs	Multivesicular Bodies
MVs	Microvesicles
MW	Molecular Weight
NTA	Nanoparticle Tracking Analysis
PBS	Phosphate-Buffered Saline
PC	Phosphatidylcholine
PDA	Photo Diode Array (Detector Type)
PDGF	Platelet-Derived Growth Factor
PE	Phosphatidylethanolamine
PEG	Polyethylene Glycol
PEI	Polyethylenimine
PFD	Pirfenidone
PFD-Exosomes	Pirfenidone-Loaded Exosomes
PDI	Polydispersity Index
PI	Phosphatidylinositol
piRNAs	Piwi-Interacting RNAs
Pro-Collagen I Alpha	Procollagen Type I Alpha 1

PS	Phosphatidylserine
PTX	Paclitaxel
qRT-PCR	Real-Time Quantitative Reverse Transcription
R2	Coefficient of Determination
Rab	Ras-Associated Binding (Rab) Proteins
RB	Rose Bengal
RNA	Ribonucleic Acid
ROS	Reactive Oxygen Species
rRNAs	Ribosomal RNAs
RSD	Relative Standard Deviation
RSV	Resveratrol
SD	Standard Deviation
SEC	Size Exclusion Chromatography
siRNA	Small Interfering RNA
snoRNAs	Small Nucleolar RNAs
snRNAs	Small Nuclear RNAs
TEM	Transmission Electron Microscopy
TGFβ	Transforming Growth Factor Beta
TIM4	T Cell Immunoglobulin and Mucin Domain Containing 4
TIMP-1	Tissue Inhibitor of Metalloproteinases 1
TIMPs	Tissue Inhibitors of Metalloproteinases
TMB	3,3',5,5'-Tetramethylbenzidine
tRNAs	Transfer RNAs
TSG101	Tumor Susceptibility Gene 101
UC	Ultracentrifuge
UHPLC	Ultra-High-Performance Liquid Chromatography
v/v	Volume/Volume (Percentage Concentration by Volume)
VAN	Vancomycin
VEGF	Vascular Endothelial Growth Factor
VLDL	Very Low-Density Lipoprotein
VPS	Vacuolar Protein Sorting

vRNA	Vault RNA
w/v	Weight/Volume (Percentage Concentration by Weight)
XLogP3- AA	Calculated logP (octanol/water partition coefficient) values
5-FU	5-Fluorouracil

List of Tables

Table 1.1 Major classification of extracellular vesicles 11

Table 1.2 Composition of exosomes 15

Table 1.3 Current status of the clinical trials involving exosomes and wound healing 18

Table 2.1 Overview of common exosome isolation methods. 26

Table 2.2 Comparison of particle size, polydispersity index (PDI), and Zeta potential measured by DLS. Values represent the mean ±SD, n=3. 38

Table 2.3 Comparison of size distribution and particle concentration of exosomes measured by NTA. Values represent the mean ±SD, n=3. 41

Table 3.1 Drug lipophilicity and encapsulation methods into exosomes 63

Table 3.2 Sonication parameters for exosomes formulation optimization. 66

Table 3.3 Intra-assay precision and accuracy of PFD quantification method 71

Table 3.4 LOQ and LOD of PFD quantification method 72

Table 3.5 Short-term stability of PFD 72

Table 3.6 Summary of UHPLC method for quantification of PFD 73

Table 4.1 Optimal PCR reaction formulation for gene expression analysis 97

Table 4.2 Optimal PCR reaction program 97

Table 4.3 Optimal ELISA antibodies and antigens concentration 98

List of Figures

Figure 1.1 Anatomy of skin. Created with biorender.com..... 4

Figure 1.2 Mechanisms of exosomes biogenesis. Created with biorender.com..... 12

Figure 2.1 The mechanism of PEG precipitation and affinity isolation method. Created with biorender.com..... 32

Figure 2.2 Observation of potential exosome pellets. 37

Figure 2.3 Size distribution of exosomes analyzed by DLS...... 39

Figure 2.4 Characterization of exosomes by NTA. 40

Figure 2.5 Semi-quantitative dot blot antibody array (Exo-Check™) for the identification of common exosomal markers...... 42

Figure 2.6 Comparison of the purity of exosomes isolated from 20 mL of cell culture supernatant from fibroblasts using different methods...... 44

Figure 2.7 Characterization of exosomes by TEM...... 46

Figure 2.8 Characterization of exosomes by AFM..... 47

Figure 2.9 Impact of trehalose on the preservation of exosomes via lyophilization. 49

Figure 3.1 Post-loading drug encapsulation methods, including direct co-incubation, electroporation, sonication, permeabilization, freeze-thaw cycles, and extrusion method[103]. Created with biorender.com. 59

Figure 3.2 System suitability of UHPLC method for PFD quantification...... 71

Figure 3.3 Linearity of UHPLC method for PFD quantification. 71

Figure 3.4 Characterization of exosomes and sonicated exosomes. 74

Figure 3.5 PFD-loaded exosomes purified with exosomes spin column..... 76

Figure 3.6 PFD-loaded exosomes purified with Magcapture Exosome Isolation method.... 78

Figure 3.7 Comparison of particle recovery rates and EE% of PFD-loaded exosomes between the Magcapture Exosome Isolation method and the Exosomes Spin Column method. 79

Figure 3.8 Effects of sonication parameters on exosome formulation. 81

Figure 4.1 *In vivo* wound healing model using SKH-1 mice. 101

Figure 4.2 Selection of fluorescent dyes used for labeling exosomes *in vitro*. 104

Figure 4.3 *In vitro* time-dependent cellular uptake of exosomes by dermal fibroblasts. 106

Figure 4.4 *In vitro* dose-dependent cellular uptake of exosomes by dermal fibroblast at 24 hours. 108

Figure 4.5 *In vitro* cytotoxicity of (A) PFD, (B) Exosomes, and (C) PFD-exosomes. 110

Figure 4.6 *In vitro* scratch wound healing analysis of exosomes and PFD-exosomes. 113

Figure 4.7 Exosomes and PFD- exosomes affected the expression of genes associated with ECM remodelling by dermal fibroblasts *in vitro*. 115

Figure 4.8 Exosomes and PFD- exosomes affected the expression of proteins associated with collagen degradation by dermal fibroblasts *in vitro*. 117

Figure 4.9 Low-dosage exosome and PFD-exosome treatments for wound healing in SKH-1 mice. 120

Figure 4.10 Quantitative analysis of wound closure in low-dosage exosome and PFD-exosome Treatments *in vivo*. 121

Figure 4.11 High-dosage exosome and PFD-exosome treatments for wound healing in SKH-1 mice. 123

Figure 4.12 Quantitative analysis of wound closure in high-dosage exosome and PFD-exosome Treatments *in vivo*. 123

Figure 4.13 Histological analysis of wound skin sections collected on day 13 (Low dosage group). 126

Figure 4.14 Histological analysis of wound skin sections collected on day 13 (High dosage group). 128

Figure 5.1 Graphical result conclusion. 138

Chapter 1 Introduction

The first part of the introduction was adapted from the following review article:

Wang J, Chen D, Ho EA. Challenges in the development and establishment of exosome-based drug delivery systems. J Control Release. Published online October 12, 2020. doi:10.1016/j.jconrel.2020.10.020

Skin is the largest organ in the human body, making up 16% of total body weight and serving as the primary barrier against bacterial infection and environmental hazards. The wound healing process often results in scars that differ aesthetically, functionally, and morphologically from normal skin. Scarring that occurs after surgical procedures or traumatic injuries can have significant negative impacts on patients, leading to complications such as itchiness, pain, and physical dysfunction[1]. Patients with visible scars also suffer from psychosocial trauma with diminished self-esteem, anxiety, and depression[2]. In developed countries, over 100 million patients develop scars from surgical procedures each year[3], with an even larger number seeking scar reduction therapies. Management and treatment of these scars impose a significant financial burden on healthcare systems. In 2015, the annual cost for scar management was estimated at $20 billion in 2015[4], and the global market for scar therapy is projected to reach approximately $52.8 billion by 2030[5]. Significant efforts have been made to improve wound healing outcomes for patients, focusing on three main goals: 1) protecting wounds from external threats, such as bacterial infections and mechanical forces; 2) accelerating wound closure; and 3) minimizing scar formation.

1.1 Physiology of wound healing

1.1.1 Anatomy of skin

From the outside inwards, the anatomy of skin is composed of superficial epidermis, in-depth dermal layer and hypodermis (subcutaneous tissue) in Figure 1.1. The epidermal layer serves as a critical barrier, offering physical, chemical, and biochemical barrier and protect the skin from hazardous environmental threats. The epidermis is typically divided into five distinct layers: the stratum basale, stratum spinosum, stratum granulosum, stratum lucidum, and stratum corneum[6]. The predominant cell type in the epidermis is the keratinocyte, which makes up about 80-90% of

the cellular composition. These cells originate in the stratum basale and undergo progressive differentiation as they migrate toward the surface layer, the stratum corneum. During this process, keratinocytes produce keratin and other structural proteins that form the stratum corneum. The epidermis also includes melanocytes, which produce melanin for skin tone; Langerhans cells, which support immune defense against pathogens; and Merkel cells, which are involved in sensory perception[7]. The dermis layer provides the skin its strength and flexibility, consisting of two distinct parts: the papillary and reticular layers[8]. The papillary layer, located closest to the epidermis, contains numerous capillaries, lymphatic vessels, nerve endings, and sensory receptors. In contrast, the reticular layer is made up of dense connective tissue, including collagen, elastic, and reticular fibers, which provide the skin with elasticity, strength, and pliability. Fibroblasts are the predominant cells in the dermis, responsible for synthesizing and maintaining the extracellular matrix (ECM)[9]. The ECM is primarily composed of collagen and elastin fibers, which are embedded in a nonfibrous ground substance made up of proteoglycans and glycosaminoglycans. Together, collagen and elastic fibers contribute to the skin's strength and elasticity, offering crucial structural protection for the underlying muscles and organs. Hypodermis is the deepest layer of the skin, consisting of loose connective tissue, blood vessels, and nerves. This layer contains important cell types, including adipocytes, fibroblasts, and macrophages[10]. Adipocytes, or fat cells, play a crucial role in thermoregulation and insulation, while also storing nutrients and protecting the underlying tissues from injury.

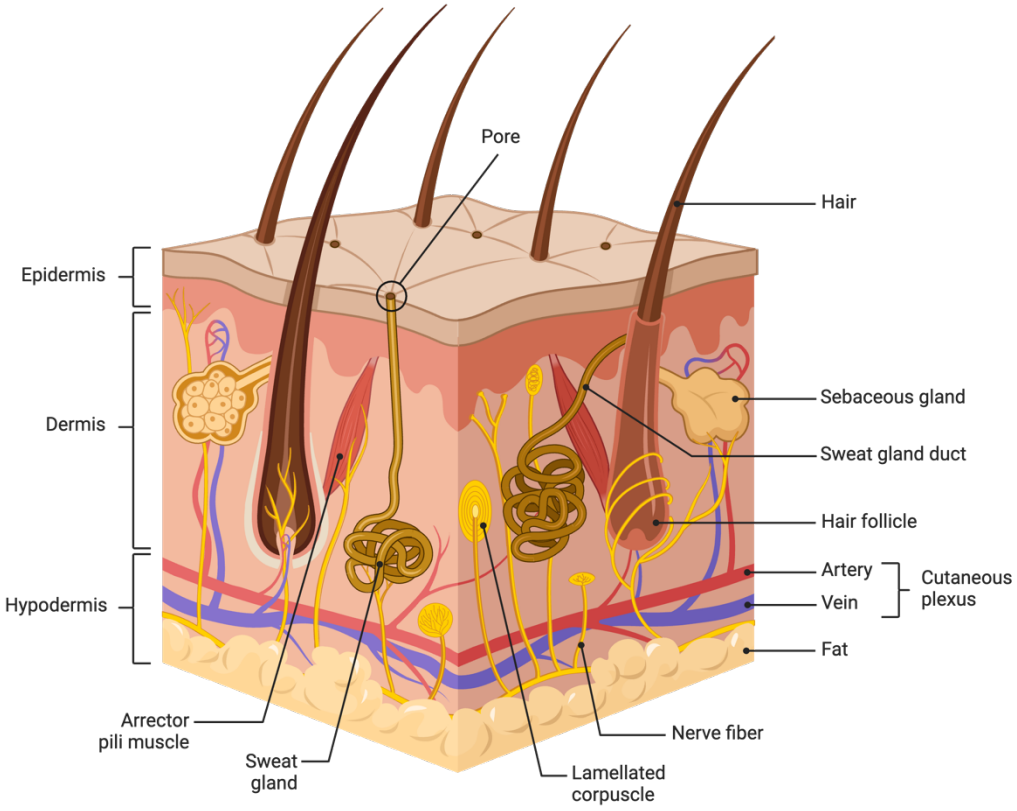


Figure 1.1 Anatomy of skin. Created with biorender.com

1.1.2 Wound healing process

Wounds can result from a variety of causes, including excisional injuries like surgical procedures, external factors such as pressure, burns, and cuts, as well as underlying conditions like diabetes or vascular diseases. These types of damage are categorized as either acute or chronic wounds based on their underlying causes and resulting consequences. Acute wounds commonly result from some form of trauma that could be blunt or penetrating in nature (such as surgical incisions, gunshot wounds, animal bites etc.), which generally heal over a short time frame. The time course of acute wound healing is usually from 5 to 10 days. Wound healing is a complicated

physiological process that is governed by a huge diversity of cellular and molecular events. Traditionally, the wound healing process can be classified into four over- lapping phases: hemostasis, inflammation, proliferation and remodeling[11]. Excessive inflammation, persistent infections, and biofilm formation can delay wound healing or contribute to the development of chronic wounds[12]. The severity and type of injury influence the final appearance of wound. An excessive healing response can lead to dermal fibrosis, resulting in hypertrophic scars or keloids[13].

1.1.2.1 Hemostasis

Hemostasis is the body's immediate response to stop bleeding when dermal tissue is wounded with vascular injury. Blood floods into the injury site, and the components within the blood, particularly platelets, interact with dermal collagen and other elements in the ECM. This interaction prompts the platelets to release factors that promote blood clotting. The blood clot typically consists of a network of fibrin fibers, platelets, and circulating clotting factors[14], which work together to seal the wound and prevent further blood loss. The blood clot and surrounding tissues act as reservoirs for cytokines and growth factors, such as transforming growth factor (TGF-β), platelet-derived growth factor (PDGF), fibroblast growth factor (FGF), and epidermal growth factor (EGF)[15]. These substances play crucial roles in initiating inflammatory responses and provide a framework for the migration of various cells essential for healing.

1.1.2.2 Inflammation

After bleeding is effectively managed, inflammatory cells move into the wound through chemotaxis and stimulate the inflammatory phase. This phase of wound healing mainly serves to defend against micro-organisms local infection, remove damaged tissue debris and prepare the wound environment for repair. In an early inflammatory phase, cytokines and growth factors released from the activated platelets can recruit inflammatory cell such as neutrophils to migrate

near the blood clot. Neutrophils can directly ingest foreign particles and produce antimicrobial substances (e.g lactoferrin, proteases, neutrophil elastase and cathepsin) for combating infections[16]. Monocytes are then attracted from the bloodstream to the wound site where they are activated to differentiate into macrophages, and the transition of monocytes and presence of macrophages mark the arrival of late inflammatory stage. Macrophages further contribute to the inflammation process by the phagocytosis of tissue debris, dead cells, and bacteria[17]. The inflammatory phase of wound healing persisted as long as necessary, ensuring the removal of excess bacteria and debris from the wound. However, prolonged inflammation can lead to significant tissue damage and hinder the subsequent proliferation phase, which result in formation of chronic wounds. Excessive inflammatory responses also contribute to the formation of exaggerated scars. This occurs because inflammatory cells release pro-inflammatory cytokines (IL-1, IL-6 TNF-α[18]), which stimulate the proliferation of fibroblasts and the production of the ECM[19]. As the ongoing inflammatory responses remain in equilibrium, the healing process gradually shifts towards the proliferative phase, aimed at repairing the wound. This transition occurs when macrophages begin to release enzymes and cytokines that trigger the migration and proliferation of keratinocytes, fibroblasts, and endothelial cells to wound bed.

1.1.2.3 Proliferation

Proliferation process of wound healing is the major event that contributes to wound healing and scar formation. This stage is characterized by re-establishment of fresh tissue which includes re- epithelialization (covering the wound surface) and angiogenesis (restoring the vascular network) and forming granulation tissue (filling the dermis). In the epidermal layer, keratinocytes start to migrate from the edges of the wound and proliferate into a complete sheet of cells, ensuring an adequate supply of cell population to encase the wound[20]. Keratinocytes produce proteins (keratins)

to rebuild the basement membrane[21]. Angiogenesis, the formation of new blood vessels, is a vital process in the development of granulation tissue. Insufficient angiogenesis can lead to ulceration and impaired healing. Newly formed capillaries ensure normal blood flow and provide sufficient oxygen and nutrients for the growth of new tissues and carry away all waste during repair[22]. To restore blood vessels, endothelial cells are stimulated by proangiogenic factors such as vascular endothelial growth factor (VEGF), PDGF, basic fibroblast growth factor (bFGF), and the serine protease thrombin, prompting them to proliferate and migrate towards the source of the angiogenic stimulus, where they then organize into small tubes at the dermal layer to form new capillaries and blood vessels[22].

In response to inflammatory mediators like fibronectin and growth factors such as PDGF, TGF-β, and bFGF, fibroblasts primarily migrate from the surrounding dermis to the wound site[15]. Once in the provisional wound matrix, these fibroblasts proliferate while simultaneously secreting ECM components. The ECM serves as a scaffold that supports cell adhesion, migration, growth, and differentiation during the wound healing process, effectively filling the wound gap. Both resident fibroblasts and fibroblasts migrated from bone marrow (also known as circulating fibrocytes) are activated by TGF-β1 to differentiate into myofibroblasts phenotype that is a type of highly contractile cells and responsible for production of abundant ECM molecules[23], notably collagen types I–VI and XVIII, glycoproteins, and proteoglycans for building up the structural integrity of and provide strength of granulation tissue. The new granulation tissue contains high content of collagens is characterized by pink, vascular, fibrous tissue which replace the clot at the wound site. Normal function of fibroblasts is an essential event during wound repair; however, fibroblasts over-activation, dysfunctional connective tissue metabolism, and excessive production

of several ECM components are the cause of all skin scarring including normal scars or pathological scars[24].

1.1.2.4 Remodeling

The final stage, remodeling, usually takes place over months to years, during which the majority of the cells involved in the previous healing process (macrophages, endothelial cells, and fibroblasts) undergo apoptosis[25]. New-established ECM in new tissue also alters, mediated by matrix metalloproteinases (MMPs) and tissue inhibitor of metalloproteinase (TIMPs)[26]. High levels of collagen type III and proteoglycans are gradually replaced by more robust type I collagen, and the orientation of collagen fibrils becomes more organized[11]. Cell fibrosis and excessive deposition of disordered ECM dominated by collagen lead to the formation of scar[27]. Following severe injury, certain components of the skin such as hair follicles and sweat glands are unable to regenerate, resulting in a healed skin that can only attain a maximum of 80% of its original tensile strength. The final outcome of the remodeling phase is new avascular and acellular tissue[28], which is less thick, firm and red than initially formed scar tissues.

1.2 Strategies for mitigating scar formation

Current strategies to reduce scar formation from excisional injuries can be categorized into two approaches: 1) interventions before the remodeling stage, known as pre-scarring interventions, and 2) therapies administered after the remodeling phase, referred to as post-scarring treatments.

1.2.1 Post-scarring treatments

Scar maturation can take years, leading patients to seek medical treatment only after scars develop into red, itchy, and raised tissue following surgery, trauma, or burns[29]. Therefore, the clinical reality postulate post-scarring therapies, which aim to revert collagen disposition and

reduce mature scar tissue. According to the latest International Clinical Recommendations on Scar Management, the only evidence-based treatments for improving scar quality are topical silicone applications and intralesional corticosteroid injections[30], compared to other accepted therapies like surgical excision and pressure garment therapy. Silicone gels and sheets are the gold standard and first-line option, offering a non-invasive and effective way to enhance scar color, thickness, and flexibility[31]. Major shortcomings lie in the poor adherence of medication and possible skin allergy, dermatitis, itch, or skin breakdown caused by silicone-based products[32]. Intralesional steroid injection, such as triamcinolone acetonide, also prevent scars by decreasing inflammation, inhibiting fibroblast proliferation, and by reducing collagen synthesis[33]. Patient compliance with corticosteroid injections is often low due to pain, high rates of scar recurrence (ranging from 9% to 50%), and side effects, which may include atrophy of surrounding skin, hypopigmentation, and telangiectasia.

1.2.2 Pre-scarring interventions and targets to mitigate scar formation

From a clinical point of view, earlier pre-scarring intervention hold greater promise than existing post-scarring therapies, as it is generally more difficult to alter ECM architecture and reverse mature scars than to prevent scar formation. Pre-scarring intervention focuses on the effective application of pharmaceutical agents, either locally or systemically, to influence the proliferation stage of wound healing. For instance, specific mediators have been identified to diminish fibroblast activation and the associated synthesis of ECM, as well as to disrupt the action of fibrogenic growth factors[34]. Given the complexity of fibrotic conditions, successful pre-scarring interventions require consideration of multiple signaling pathways and the use of novel multicargo-delivery therapies[35]. For example, the co-delivery of TGF-β inhibitor and histone deacetylase

inhibitor has been developed as a strategy to modulate skin fibrosis[36]. The development of advanced multi-delivery systems is crucial for achieving enhanced therapeutic effects.

1.3 Exosomes

The discovery of membranous vesicles can trace back to 50 years ago, although these vesicles were originally assumed to be cell wastes released via shedding of the plasma membrane. In 1983, exosomes were recognized by Pan and Johnstone[37] and Harding and Stahl[38] when studying on the transferrin receptor of reticulocyte. They found transferrin receptors are jettisoned from maturing blood reticulocytes into the extracellular space within small extracellular vesicles. Until 1989, Johnstone defined the name "exosome" for these extracellular vesicles (EVs). EVs carry various types of molecules, including proteins, lipids, and nucleic acids, as cargo. The key function of extracellular vesicles is molecular transfer ability from one cell to nearby or remote cells at a target tissue site. These cargos often consist of pathophysiological biomarkers and can influence the fate of recipient cells and tissues. Currently, extracellular vesicles are classified into three major categories: exosomes, microvesicles (MVs) and apoptotic bodies (summarized in Table 1.1). However, emerging subpopulation of extracellular vesicles such as migrasomes, autophagosome are identified and classified depend on their biogenesis, morphology and function. The largest EVs (1–5 μm) are apoptotic bodies that are formed during the late stages of apoptosis, which is a programmed cell death procedure. Typically, apoptotic bodies result from the fragmentation of cells and contain fragmented DNA. They facilitate the efficient removal of cellular debris by attracting phagocytes. MVs are vesicular structures shed by direct outward blebbing of the plasma membrane, and they deliver membrane protein, enzymes, growth factor receptors, cytokines, chemokines, lipids, and nucleic acids, including miRNAs, genomic DNA, and oncogenic genes[39]. MVs exhibit a considerable and diverse size range, in contrast to exosomes,

which typically maintain a more uniform size, falling within the range of 50 to 100 nm in diameter. Exosomes are distinct from other EVs due to their smaller size, their origin from endocytic compartments, and their unique set of markers and functions.

Table 1.1 Major classification of extracellular vesicles

Classification	Size	Origin
Exosomes	30-150 nm	Release by exocytosis of Multivesicular bodies (MVBs)
Microvesicles	100-1000 nm	Blebbing of plasma membrane/ Outward budding and pinching off from the plasma membrane
Apoptotic bodies	1-5 µm	Blebbing of apoptotic cells during cell shrinkage and programmed death
Migrasomes	500 - 3000 nm	Newly found organelles produced by migrating cells and grow on retraction fibers trailing behind the cells
Autophagosome	0.5- 1.5 µm	Formed during autophagy that sequesters and delivers cargoes for their degradation or recycling into the vacuole

1.3.1 Exosomes biogenesis

All cell types, from both plant and mammalian cells, and from embryonic stem to aged cells, produce exosomes[40]. Exosomes biogenesis begins with endocytosis, where plasma membrane fold inward and forms a cup-shaped structure that includes cell-surface proteins and soluble proteins from the extracellular milieu. This process forms early endosome, which may also, in some instances, directly fuse with an existing early endosome. Cargo intended for recycling will localize to the peripheral regions of the endosome and then either fuse with the Golgi network or the plasma membrane in the recycling endosome. Cargos not destined for recycling accumulate in the central vacuolar regions of the early endosome, leading to endosomal maturation. This process

transforms early endosomes into late endosomes and then into multivesicular bodies (MVBs). MVBs are formed through the inward invagination of the endosomal membrane, forming intraluminal vesicles (ILVs) within them. These ILVs eventually develop into exosomes. MVBs have two potential fates: they can fuse with lysosomes or autophagosomes for degradation, or they can merge with the plasma membrane to release ILVs as exosomes[41].

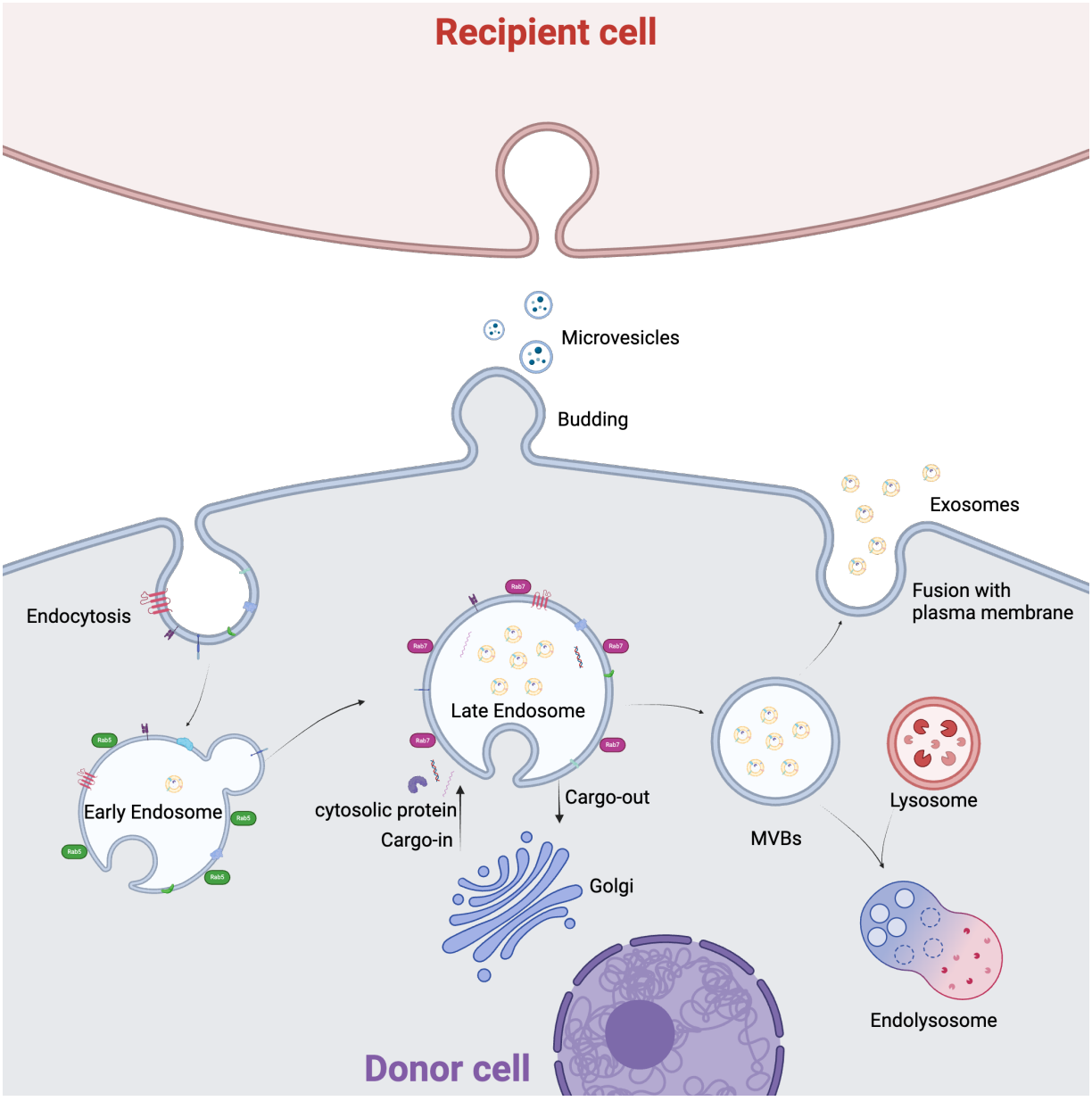


Figure 1.2 Mechanisms of exosomes biogenesis. Created with biorender.com

Exosome biogenesis is dependent on the site of biogenesis, membrane lipid composition and protein sorting. Overall, the mechanisms of exosomes biogenesis involve several types of proteins, including the ESCRT (endosomal sorting complexes required for transport) proteins, as well as accessory proteins like Rab, Sytenin-1, TSG101 (tumor susceptibility gene 101), ALIX (Programmed cell death 6-interacting protein), tetraspanins and syndecan-1[42]. Lipids including phospholipids, ceramides, sphingomyelinases also control exosomes biogenesis in a ESCRT-independent manner[43]. These proteins and lipids work together to attach to prospective exosome contents and facilitate the formation of ILVs that encapsulate these materials. The biogenesis of exosomes is influenced by various external factors such as cell type, cell density, serum conditions, and the presence or absence of cytokines and growth factors[44]. For instance, cancer cells tend to release more exosomes compared to non-cancer cells[45]. Serum deprivation stimulated the secretion of exosomes by the stem cells [46]. Additionally, the production and release of exosomes by stem cells can be enhanced by adding specific soluble cytokines directly to the culture medium[42].

1.3.2 Exosomes structure and composition

Exosomes are small, nano-sized vesicles with a lipid bilayer that encloses various biological molecules but do not contain cellular organelles. They lack proteins from the nucleus, mitochondria, endoplasmic reticulum, or Golgi complex. Instead, exosomal contents originate from the parent cells and include proteins, lipids, and nucleic acids that reflect the functions and metabolic states of these cells, potentially affecting the activities of recipient cells.[47] Exosomes from different cell origin typically have unique cargo compositions, although they often share certain proteins on their surfaces and within their cytosol. Individual EVs typically contain less than 100 total proteins, which is summarize in the Table 1.2. Proteins such as tetraspanins (CD9, CD63, and CD81) are involved in essential processes like cell communication, fusion, invasion,

motility, and signal transduction[44]. Additionally, ALIX, flotillin, and TSG101 are present in exosomes because they play a crucial role in their biogenesis[48]. Rab protein and annexin are crucial for the fusion and transport of vesicles, helping to mediate the docking of MVBs with the plasma membrane and regulating the secretion of exosomes[49]. Exosomes are also rich in specific membrane lipids, such as cholesterol (42.5% of lipids), sphingomyelin (12.5%), glycosphingolipids, phosphatidylserine, and ceramide, varying by cell type[43]. The nucleic acids within exosomes are packaged in a highly selective and non-random manner[50], influenced by the origin of the cells, tissues, and biological fluids. Some RNAs prominent in cells (such as rRNAs) are largely absent from their exosomes, whereas many different mRNAs and non-coding RNAs (primarily miRNAs[51] and tRFs) are often relatively over-represented[52]. Exosomes also contain various other RNA species, including mRNA fragments, snRNAs, snoRNAs, mitochondrial RNAs (mtRNAs), piRNAs, vault RNAs (vtRNAs), Y RNAs, circular RNAs (circRNAs), rRNA fragments, and long non-coding RNAs (lncRNAs).

Table 1.2 Composition of exosomes

Protein	Surface protein	Tetraspanins[53]	CD9, CD63, CD37, CD81, CD82, CD53
		Major histocompatibility complex (MHC)	MHC class I and class II proteins[54]
		Integrins	β2[55], β4[56] ,α4β1[57], α6β1[58], α6β4[59], αvβ3[60] , αvβ3[61] , αvβ6[62]
		Cell surface peptidases	Animopeptidase N[63], Dipeptidyl-peptidase IV[64], Glycosidase[65]
		Membrane trafficking proteins[66]	Annexins I, II, IV, V, VI, Rab 7 and Rab 11
		Glycoprotein	N-linked and O-linked glycoproteins
		Lipid raft-associated protein[70]	Ganglioside GM1, Src tyrosine kinase Lyn, and flotillin-1
		Signaling proteins[71]	GTPase HRas, Ras-related protein, Src, and RhoA
		Receptors	Epidermal growth factor receptor variant III [72]
	Cytosolic proteins	Hot shock protein (HSP) [9]	HSP27, HSP70, HSP90
		Cytoskeletal proteins[74]	Actin, myosin, tubulin, cofilin, moesin, Erzin, Radixin, Vimentin
		MVB- related proteins[75]	ALIX, TSG101, Clathrin, Vps (vacuolar protein sorting), Rab proteins
		Growth factors	TGFβ-1[76], VEGF-A[77], EGFR[78]
		Active enzymes[79]	
Nucleic acid	DNA		Double-stranded DNA[80,81], single-stranded DNA, mitochondrial DNA
	RNA	Coding RNAs	mRNA[82]
		Regulatory noncoding RNAs	miRNAs, lncRNAs[83,84], circRNAs[85], piwi-interacting RNAs (piRNAs)
		Housekeeping noncoding RNAs[86]	ribosomal RNAs (rRNAs), transfer RNAs (tRNAs), small nuclear RNAs (snRNAs), small nucleolar RNAs (snoRNAs)
Lipid[43]			Ceramide, cholesterol, sphingomyelin, glycosphingolipids, phosphatidylethanolamines (PE), phosphatidylcholine (PC), phosphatidylserine (PS), phosphatidylinositol (PI)

1.3.3 Exosomes function and medical application

Exosomes participate in intercellular communication and modulate different signaling pathways. Once delivered to target cells, exosomes regulate the behaviour and morphology of recipient cells, which may result in either normal physiology or pathogenesis depending on the origin of exosomes. This discovery of exosomes paves the way for their medical applications, including disease diagnosis, exosome-based therapies, drug delivery systems, and cancer vaccines[87]. Firstly, exosomes carry molecules originated from their parent cells, which can be detected in biological fluids such as blood, urine, or cerebrospinal fluid[88]. These cargos can serve as diagnostic markers for different diseases. In terms of therapy, exosome-based treatments harness the natural properties of exosomes to deliver bioactive substances and influence disease mechanisms. Exosomes therapies, as a cell-free option, offer same therapeutic and clinical benefits as cell therapy[89]. For example, known exosomes from many native stem cells have been shown to recover adversarial conditions and damaged tissues[87]. Notably, exosomes are easier to store at ultra-low temperatures compared to cells, which require complex handling for cryopreservation and thawing. Exosomes offer a more controlled approach to dosage through various administration methods, such as topical applications and injections. This versatility enhances their usability in different treatment contexts[90]. Exosomes also hold promise as drug delivery systems, as their natural ability to cross biological barriers makes them effective carriers for therapeutic molecules. When compared to synthetic nanoparticles, exosomes offer superior stability and biocompatibility with low immune-rejection[91]. Lastly, Exosomes are also being explored as components of cancer vaccines, leveraging their ability to present tumor-associated antigens and stimulate an immune response.

1.3.3.1 Therapeutic application of exosomes in wound healing

As a stand-alone therapy, exosomes exhibit beneficial therapeutic outcomes in improving wound healing[92]. Primarily derived from human adult stem cell lines, exosome administration has been shown in nearly all studies to positively impact wound healing. In rodent models, these exosomes consistently accelerate healing and stimulate angiogenesis[51]. Other significant benefit of exosomes is their ability to optimize collagen deposition[93], enhance cell viability in the wound bed[94] and reduce fibrogenesis. Exosomes origin from stem cells, particularly from human adipose-derived stem cells (ADSCs) and human umbilical cord mesenchymal stem cells (hUCMSCs) were found to enhance wound healing. For example, local injections of ADSCs- exosomes reduce the healing time and reduce scar formation by inhibiting collagen synthesis in rodent models[51]. ADSCs that express miR-192-5p can effectively reduce hypertrophic scar fibrosis by modulating the Smad signaling pathway. Their positive impact on wound healing is attributed to reduced collagen deposition, prevention of fibroblast differentiation into myofibroblasts, and reduction in the formation of hypertrophic scars[95]. Additionally, exosomes from hUCMSCs have been found to increase wound healing rates, enhancing angiogenesis [96]and minimize scar formation in animal studies[97]. Exosomes derived from non-stem cells such as human amniotic epithelial cells accelerate wound healing by stimulating the proliferation and migration of fibroblasts[98]. Furthermore, fibrocyte-derived exosomes are rich in miR-21, which plays a crucial role in increasing collagen release from fibroblasts, enhancing the deposition of mature collagen fibrils, and promoting wound contraction in the early stages of healing[99]. To achieve sustained release and maintain the long-term stability and bioactivity of exosomes, wound dressings that incorporate exosomes are being developed. For example, exosomes from hUCMSCs incorporated into Pluronic F127 gel promote diabetic wound healing[100]. Human umbilical vein endothelial cells (hUVECs) exosomes have also

demonstrated improved effects in promoting re-epithelialization, collagen deposition, and angiogenesis when incorporated into gelatin methacryloyl hydrogels used as wound dressings[101]. Furthermore, hydrogel wound dressings that combine exosomes with antimicrobial peptides have been found to facilitate scarless healing. This process is mediated by exosomal miR-21-5p, offering a safe and effective cell-free approach for healing deep second-degree burn wounds[102].

Current clinical trials (searched from https://clinicaltrials.gov/) on exosomes for wound healing explore their efficacy, safety, and regenerative potential using sources like adipose tissue, mesenchymal stem cells (MSC), plasma, and platelet-derived extracellular vesicles. These trials (summarized in Table 1.3) show promising results in enhancing wound healing and skin regeneration, with topical applications, injections, and personalized therapies being assessed across various phases.

Table 1.3 Current status of the clinical trials involving exosomes and wound healing

Clinical Trial Number	Type	Objectives	Collection Method	Administration of Exosomes	Monitoring Method
NCT05475418	One-arm pilot study	Evaluate the efficacy of adipose tissue-derived exosome dressings in promoting wound healing.	200-300ml of adipose tissue collected, extracellular vesicles retained after homogenization and filter screening	Exosomes are mixed with sterile hydrogel and covered with an inert dressing.	Wound area measurements and photographic documentation.
NCT02565264	Open prospective clinical trial	Assess the effects of autologous exosome-rich plasma on healing in patients with intractable cutaneous ulcers.	Participants' own plasma	Participants receive daily treatments of autologous exosome-rich plasma for 28 days.	Changes in wound dimensions (length, width, depth).
NCT05243368	Pilot study	Develop a therapeutic approach to accelerate healing of chronic skin ulcers in diabetic patients.	Extracted from MSCs	Personalized nutritional supplementation combined with mesenchymal stem cell (MSC)-derived exosome application.	Wound healing evaluation (method not specified).

1.3.3.2 Exosomes as drug delivery system to enhance wound healing

Introducing a drug delivery system is essentially important for improving therapeutic outcomes of drugs in the context of wound healing. One reason is that the increased expression of degradative enzymes in wound bed and impairs the bioactivity of drugs that are administrated topically[35]. On the other hand, the rapid dilution in wound fluid fails to localize drugs at the wound site and achieve their bioavailability[36]. Using exosomes as drug carrier is important to improve the drug accumulation and enhancing drug stability during healing processs[103]. As exosomes protect their cargo from enzymatic degradation during transit through the extracellular environment[42], exosomes may serve as carriers for efficiently deliver of both hydrophobic and hydrophilic drugs into wound sites. For example, pioglitazone as a compound for treatment for diabetes, and pioglitazone-treated mesenchymal stem cell (MSC) generate exosomes accelerated diabetic wound healing by promoting the angiogenic function of HUVECs through activation of the PI3K/AKT/eNOS pathway[104]. Atorvastatin was delivered intracellularly by MSC-exosomes, which accelerated diabetic wound repair by enhancing angiogenesis through the inhibition of PTEN and subsequent stimulation of the PTEN/AKT/eNOS pathway[105]. Exosomes have natural superior ability to protect internal cargo and the potential to deliver it to specific cell types, which makes suitable for delivery small molecule and genes that have intracellular targets.

Chapter 2 High-Purity Exosome Isolation from *In Vitro* Cultured Human Dermal Fibroblasts and Characterization Techniques

2.1 Overview

This chapter presented a comprehensive workflow for the production, isolation, and characterization of exosomes derived from human dermal fibroblasts cultured *in vitro* under static conditions. Two commonly used isolation methods, PEG precipitation and affinity-based isolation, were compared and evaluated to identify an efficient technique capable of yielding exosomes with high purity and consistency. Various quality control analyses were performed to assess the morphological, biophysical, and physicochemical properties of the isolated particles. Affinity-based isolation demonstrated superior efficiency in producing highly pure and well-dispersed exosomes. Biophysical characterization using transmission electron microscopy (TEM) and atomic force microscopy (AFM), alongside molecular characterization via antibody array and enzyme-linked immunosorbent assay (ELISA), conclusively confirmed the isolation of human dermal fibroblasts exosomes from conditioned media *in vitro*. This study provided a valuable framework for future studies related to developing exosomes as a cellular product, offering optimized strategies for the isolation, characterization, and storage of exosomes.

Keywords: Exosomes, isolation methods, Exosomes characterization, Exosomes storage

2.2 Introduction

Achieving a pure isolate of exosomes without other components remains a challenge with current isolation technologies. Therefore, exosome isolation is technically defined as the process of enriching exosomes from various biological macromolecules, which can include proteins, protein aggregates, lipoproteins, other EVs, and cells. The ideal isolation method should ensure high consistency, yield, purity, and scalability while preserving the vesicular structure and molecular integrity of the exosomes. However, the complex nature of biological fluids and *in vitro* cell cultures means that obtaining pure exosomes often involves trade-offs regarding cost, yield, scalability, and therapeutic potential. Each isolation method has its specific advantages based on the application and source of the exosomes, as summarized in Table 2.1. Currently, most research on exosome-based drug delivery operates at relatively low levels of purity, which may hinder clinical translation[106]. For instance, lipoproteins frequently co-isolate with exosomes[107]. The impact of these non-exosome macromolecules on the effectiveness of exosome-based drug delivery remains unclear. Despite these challenges, we posit that higher purity of exosomes is essential for maintaining research integrity, ensuring clinical safety, and enhancing clinical efficacy.

Differential ultracentrifugation (UC) is the most widely-used method for isolating exosomes[37] in most literature and is still considered the gold standard due to its simplicity and high processing capacity. By stepwise increase of centrifugation speed, unwanted contaminants (cells, cell debris, microvesicles /apoptotic bodies) are removed based on their density, size and shape at each stage. Exosomes derived from UC exhibit a high yield, but their purity is frequently compromised when isolated from biological fluids containing serum components. The presence of protein aggregates and lipoproteins can result in their co-isolation with exosomes, which negatively impacts purity[108]. From cell culture (using media with 10% exosome-depleted serum,

one group estimated that 20% of their isolate was not exosomes[108]. If using a prolonged UC protocol (~4 hours) there is further risk of contamination by soluble proteins[109]. High-speed centrifugation may cause damage to exosome membranes and reduce their biological activity[110].

Density gradient ultracentrifugation (DG-UC) is based on the principle of setting up an increasing density gradient media (such as sucrose and iodixanol)[110,111] from the top of the tube to bottom. After centrifugation, exosomes will settle in the layer that corresponds to their density, whereas impurities of different densities will be allocated into distinct layers. Among physical-based exosome isolation methods, DG-UC is one of the best in terms of purity, yield, and preservation of vesicular structure. However, high-density lipoprotein (HDL) and low-density lipoprotein (LDL) contamination of the exosome-containing fraction has been observed[112]. One group estimated that their exosomes were co-isolated into the same fraction as HDL, at a ratio of 1:100 (exosome: HDL)[113]. With an optimized protocol, one group was able to minimize lipoproteins through use of extended DG-UC[114]. Nonetheless, the clinical application is limited by the prerequisite for preliminary sample preparation, arduous operation, and a longer centrifugation time (>16 h).

Size exclusion chromatography (SEC), alternatively referred to as gel filtration chromatography or gel permeation chromatography, is a chromatographic method that uses a column with porous beads to retain particles smaller than the pore size, while quickly flushing out particles larger than the pore upon gravity or low-speed centrifugation. Exosomes can be separated from proteins based on their size differences, since exosomes are 40-100 nm, whereas most proteins are smaller than 10 nm. After initially eliminating larger debris via centrifugation, SEC with different types of beads is subsequently employed to harvest exosomes of appropriate size. Sepharose CL-4B, Sephacryl S-400, and Sepharose CL-2B are the major types of beads for

isolating exosomes[115–117]. The apparent pore size distribution of these SEC beads are 42, 31, and 75 nm, respectively[118]. Nonetheless, the sizes of larger protein complexes such as LDL, VLDL (very low-density lipoprotein), and chylomicrons overlap with those of smaller exosomes. Therefore, selecting the appropriate bead size entails a trade-off using larger bead sizes can eliminate more lipoproteins but may also discard smaller exosomes, whereas smaller bead sizes can enable the isolation of smaller exosomes while retaining lipoproteins. SEC also requires that the input sample volume be much smaller than the column volume, otherwise the sample will elute unevenly and decrease separation efficiency[119]. Furthermore, the elution process will invariably lead to a sample dilution due to diffusion and may need to be concentrated post-isolation by another method, leading to decreased yield. SEC does, however, have several advantages as the exosomes are not subject to any harsh physical interaction, the vesicular structure is well preserved[116]. SEC might be a possible option for large scale processing of exosomes, due to the low cost and speed of isolation.

Filtration describes a broad variety of techniques that use membranes with specific pore sizes to selectively retain or elute particles of a certain size. In direct flow filtration, the membranes are positioned at an angle perpendicular to the flow direction. Rapid accumulation of particles on membrane may result in clogging of exosomes on membrane surface and lead to a low recovery rate[120]. Therefore, direct flow filtration is more suitable for handling small-scale liquids. In tangential flow filtration, the flow is setup parallel to the filter membrane. In one example, the pressure was carefully controlled to minimize exosome loss through membranes due to excessive force[120]. Continuous recycling of the retentate to pass over the membrane continuously greatly improves isolation efficiency when compared to direct flow filtration. In another study, tangential flow filtration was superior to UC in scalability and time consumption (~1 hour)[121].

Precipitation has been employed in exosome isolation due to its simplicity, scalability, low cost, and the effectivity and reproducibility demonstrated in previous studies[122,123]. The principle of using polymer precipitation is borrowed from nucleic and virus precipitation using PEG (polyethylene glycol). PEG is a hydrophilic polymer that can absorb water molecules from the surrounding less soluble particles, thereby forcing them to sediment under low-speed centrifugation. Several findings have shown that PEG could form a network to entrap exosomes and form aggregates[122–124]. PEG precipitation it often results in exosome aggregation and contamination with non-exosomal proteins, lipoproteins, and other cellular debris[125]. Nevertheless, this method is the easiest to commercialize due to the minimized sample handling.

Affinity- based separation show great promise for enrichment of specific subtypes of exosomes. This method describes a technique in which exosome capture molecules are attached to an easily separatable carrier (eg. magnetic beads, membranes and solid surfaces). When the capture molecule (such as proteins, antibodies, and aptamers) interacts with the exosomes' lipid or antigen, the carrier selectively binds to exosomes, resulting in the formation of a complex that can be separated from the rest of the sample. Binding is crucial for the subsequent applications of exosomes. For instance, utilizing an antibody as the capture molecule (such as against CD63) enables the isolation of exosomes with a high degree of purity, making it advantageous for proteomics, lipidomics, or RNAomics[126]. Due to the harsh conditions that are required for breaking the interaction between an antibody and an antigen, a more easily reversible reaction (e.g. Tim4-phosphatidylserine), pure exosomes in vesicular form can be recovered, although with limited yield[31]. In recent years, there has been expanding use of bulk magnetic isolation in biotechnology[127]. Thus, magnetic exosome isolation might be a possible option in upscaling exosome processing.

Table 2.1 Overview of common exosome isolation methods.

Isolation Method	Yield	Purity	Advantages	Disadvantages	Primary applications	References
UC	*****	**	1)Yield can be maximized with pure samples 2)Well established method 3)Simple	1)Difficult to upscale 2)Non-exosome contamination	1)Reliable initial method for high-yield pure sample collection 2)Sample pre-processing 3)Sample concentration	108,109,112,115,128,129
DG-UC	*****	****	1) Yield can be maximized with pure samples 2)Preserves vesicular integrity 3)Relatively high purity	1)Difficult to upscale	1)Isolates relatively pure exosomes for high-yield collection.	110,114,129
SEC	***	***	1)High upscale potential	1)Non-exosome contamination	1)Large-scale isolation	110,115,117,130
Direct Flow Filtration	**	**	1)High yield 2)High upscale potential	1)Membrane clogging 2)Membrane leakage	1)Sample pre-processing 2)Sample concentration 3)Buffer exchange	110,120
Tangential Flow Filtration	*****	****	1)High upscale potential	1) Limited understanding of the optimal setup	1)Large-scale isolation 2)Sample concentration 3)Buffer exchange	120,121,131
Precipitation	*****	*	1) Inexpensive 2)Commercially viable	1)Vey low purity	1)For high yield collection 2)Large-scale isolation	122–124
Affinity-based separation	*	*****	Fast isolation and high purity	1)Low yield	1) High purity exosomes isolation	126

		2) Expensive and difficult to upscale	2) Separation of specific exosome subgroups and high purity

*= lowest yield/purity; *****=highest yield/purity

To evaluate the efficacy of exosomes isolation methods, both external characterization (physical) methods and internal characterization (compositional/biochemical) methods should be employed to profile exosomes. External characterization refers to the detection of morphology and particle size, and the inclusion characterization method is to confirm the identity of exosomes by analyzing their cargo. These methods together provide insights into their structure, morphology, size distribution, cargo composition and biophysical properties, thereby facilitating a comprehensive understanding of exosomes.

This chapter aims to develop and optimize a comprehensive workflow for the production, isolation, and characterization of exosomes derived from human dermal fibroblasts cultured *in vitro* under static conditions. We specifically focus on comparing two widely used isolation methods, PEG precipitation and affinity-based isolation, to determine which method yields exosomes with the highest purity and consistency. Various characterization including morphological, biophysical, and physicochemical assessments, were conducted to thoroughly characterize the isolated exosomes.

2.3 Material and methods

2.3.1 Dermal fibroblasts cell culture and subculture

The immortalized BJ fibroblast cells (ATCC®, CRL-2522™) were cultured in Eagle's Minimum Essential Medium (EMEM, 320-005-CL) supplemented with 10% fetal bovine serum (FBS, Gibco Life Technologies, Canada) and 1% penicillin/streptomycin at 37 °C in 5% CO_2 in tissue culture flask (Falcon™ Tissue Culture Treated Flasks). Cell morphology was checked daily to ensure healthy cell growth and monitor cell confluency. Once achieving 90% of confluence, the supernatant was removed. The cells were rinsed with phosphate-buffered saline (PBS) followed by the addition of 0.05% (w/v) Trypsin- 0.53 mM EDTA solution and incubate at 37 °C in 5% CO_2 to remove all traces of serum that contains trypsin inhibitor. The cells were observed under the microscope to ensure the cell layer is dispersed (usually within 5 to 15 minutes). Complete growth medium was the added to the flasks to suspend the cells, and the cells were then transferred into a centrifugation tube. Trypsin- EDTA was removed by gentle centrifugation for 5 minutes at 150 × g (Thermo Fisher, Sorvall Legend Centrifuge). The supernatant was discarded, and the cells were resuspended in complete growth medium and cultured in new tissue culture flasks or plates at 37 °C in 5% CO_2.

2.3.2 Dermal fibroblasts freezing and thawing

Cells were gently detached from tissue culture flask with 0.05% (w/v) Trypsin- 0.53 mM EDTA solution and resuspended in complete growth medium. Cell suspension was centrifuged at 150 × g for 5 minutes, and the supernatant was decanted without disturbing the cell pellet. Cell pellet was evenly resuspended in complete growth medium described above supplemented with 5% (v/v) DMSO (dimethylsulfoxide) and transferred to cryogenic storage vials. The cryovials

containing the cells was placed in an isopropanol chamber and store them at –80°C overnight. Then the frozen cells were transferred to liquid nitrogen for long term storage. Cells were thawed by gentle agitation the cryovial in a 37°C water bath. Thawing should be rapid (approximately 2 minutes). The cryovial was removed from water bath as soon as the contents are thawed. Cells were transferred to a sterile centrifuge tube containing 9 mL of complete growth medium. The cryoprotectant agent (DMSO) was removed by gentle centrifugation for 10 minutes at 125 × g. Cells were resuspended in complete growth medium and transferred to tissue culture flasks.

2.3.3 Harvest of cell culture supernatant contains exosomes from static plate monolayer culture

All cell culture supernatants were harvested for human dermal fibroblasts within passage 20. Once achieving 80% of confluence, the supernatant was removed, and EMEM supplemented with 10% exosome-depleted FBS (Gibco Life Technologies, Canada) and 1% penicillin/streptomycin was added to the cells and cultured for 2 days before harvesting the cell culture supernatant. To obtain human dermal fibroblasts-derived exosomes, the cell culture supernatant was filtered with a 0.22 μm syringe filter three times to remove microvesicles. The supernatant was centrifuged at 500g and 3000g for 10min, respectively, to remove intact cells and cell debris. The supernatant was condensed with a centrifuge column (Amicon® Ultra Centrifugal Filter, 100 kDa MWCO) before purification.

2.3.4 Isolation of exosomes

Cell media supernatant was then harvested after exposure to exosomes-depleted FBS media. After collection, the supernatant was processed as indicated in Figure 2.1. The centrifugation at 500 ×g 10 min was to remove cells. The second centrifugation step (10 min at 3,000 ×g) removes cell debris. The filtration step further removed larger apoptotic bodies and MVs (200–500 nm).

Finally, the supernatant was condensed 50 times using Amicon® Ultra Centrifugal Filter, (10 kDa MWCO) before further isolation. As discussed, the chosen exosome isolation method is very dependent on downstream applications and intended uses. Two separate isolation methods were evaluated in this study:

2.3.4.1 PEG precipitation methods

60% (w/v) PEG 6000 solution was added into cell medium supernatant to achieve a final concentration of 15% (w/v), as modified from previous literature[123]. After incubating the mixture overnight at 4 °C, the mixture was centrifuged at 3000g, 4°C for 30min to harvest the pellets. The supernatant was discarded as much as possible, and the pellets were resuspended in 1.2 mL of PBS. Then, 400 µL of 60% (w/v) PEG was added to bring the concentration to 15%. The mixture was again incubated mixture overnight at 4 °C and then centrifuged at 3000g, 4°C for 30min to harvest the pellets.

2.3.4.2 Affinity method

For the affinity method, MagCapture Exosome Isolation Kit PS (Fujifilm WAKO Pure Chemical Corporation, Japan) was used based on the manufacturer's instructions. Briefly, exosomes were isolated by magnetic beads coated with Tim4 (T cell immunoglobulin and mucin domain containing 4) protein, which specifically binds the phosphatidylserine (PS) displayed on the surface of exosomes. As the binding process is Ca^{2+}-dependent, intact exosomes were eluted from the beads by adding a Ca^{2+}chelator, EDTA.

2.3.4.2.1 Immobilization of Exosome Capture

60µL of Biotin Capture Magnetic Beads and 500µL of Exosome Capture Immobilizing Buffer, and spined on a vortex mixer, into a new 1.5 mL reaction tube. The tube was then placed

on the magnetic stand for 1 min to separate the beads from the solution. The solution was then removed and replaced with 500μL of Exosome Capture Immobilizing Buffer and 10μL of Biotin-labeled Exosome Capture. Reaction tube was vortexed, and the beads were mixed for 10 min at 4 ℃ with a rotator. The beads were then placed on the magnetic stand for 1 min to separate the beads from the solution, and the supernatant was removed. 500μL of Exosome Capture Immobilizing Buffer was added into the 1.5 mL Reaction Tube to wash the beads. The beads were again placed on magnetic stand for 1 min to separate the beads from the solution, and the supernatant was removed. After repeated washing of the beads for 2 times, the Exosome Capture-immobilized beads were then ready to be subject to affinity isolation of exosomes.

2.3.4.2.2 PS affinity reaction

2μL Exosome Binding Enhancer was added into 1mL condensed cell media supernatant and mixed by vertexing. The mixture was transferred to a 1.5mL Reaction Tube containing Exosome Capture-immobilized beads. The beads and the condensed cell media supernatant were mixed by vertexing on a rotator for 3 hours at room temperature. The beads were then placed on the magnetic stand for 1 min to separate the beads from the solution, and the supernatant was removed. The bead was wash for 3 times with 1 mL of Exosome Capture Washing Buffer. The beads were placed on magnetic stand for 1 min to separate the beads from the solution, and the supernatant was removed as much as possible.

2.3.4.2.3 Elution of Extracellular Vesicles

50μL of Exosome Elution Buffer (1×) was added to the beads and mix by vertexing. The beads were then spined down and placed on the magnetic stand for 10 min to separate the beads from the solution. The supernatant was transferred to a new 1.5 mL microcentrifuge tube. 50μL of Exosome Elution Buffer (1×) was added into the 1.5 mL Reaction Tube again beads and mix by

vertexing. The beads were then spined down and placed on the magnetic stand for 10 min to separate the beads from the solution. The supernatant was combined to the supernatant collected form last step to obtain 100μL exosomes.

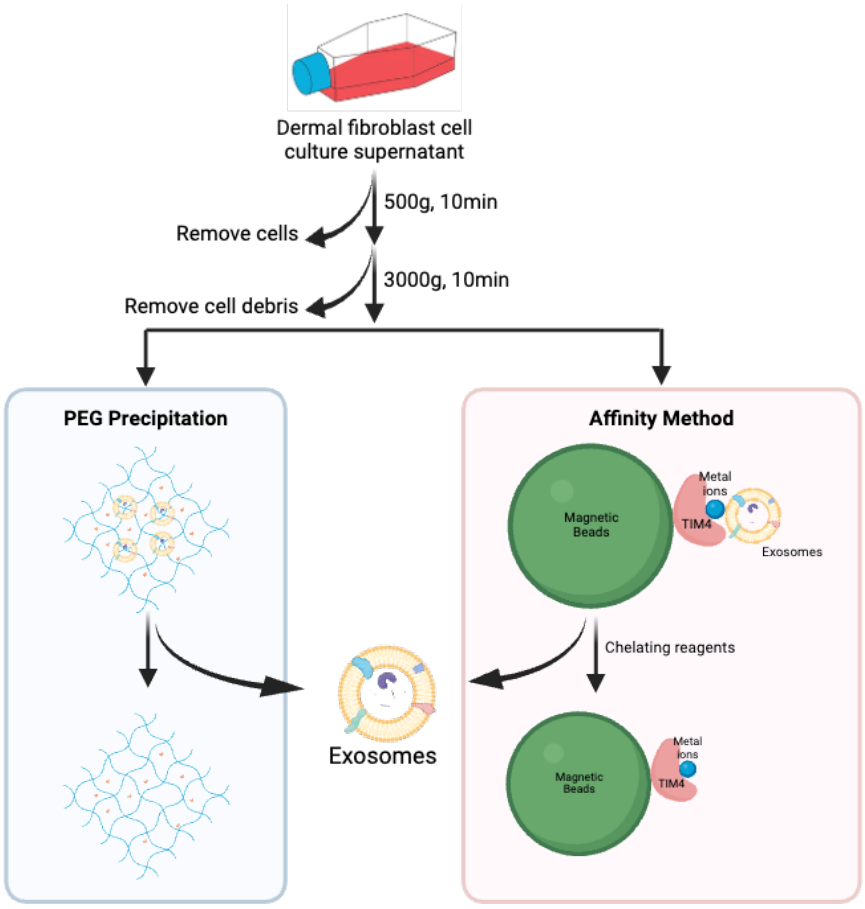


Figure 2.1 The mechanism of PEG precipitation and affinity isolation method. Created with biorender.com

2.3.5 Protein content analysis of exosomes isolate

2.3.5.1 Exosomes marker identification

Exo-Check™ exosome antibody array (System Biosciences) was a semi-quantitive dot blot for confirmation the identity of exosomes. This array is pre-printed with eight positive markers including CD63, CD81, epithelial cell adhesion molecule (EpCAM), annexin A5 (ANXA5), tumor susceptibility gene 101 (TSG101), flotillin-1 (FLOT1), intercellular adhesion molecule 1 (ICAM), programmed cell death 6 interacting protein (ALIX). An empty spot is included and serves as a blank control. 50 µg exosomes isolate were firstly lysed with 10% (v/v) lysis buffer and then labeled with 1 µl of labeling reagent according to the manufacturer's instruction. After 30 min constant mixing at room temperature, the excess labeling reagent was removed using column. Membranes were immersed in the mixture of labeled exosome lysate and 5 mL blocking buffer at 4 °C overnight on a shaker. The membrane was washed twice. 5 ml detection buffer was then added to the membrane and incubated for 30 min at room temperature on a shaker. The membrane was washed and developed with WesternBright Sirius HRP (horseradish peroxidase) substrate (Advansta, Menlo Park, CA, USA) and imaged by iBright Imaging Systems (Invitrogen, Thermo Fisher).

2.3.5.2 CD63 Enzyme-linked immunosorbent assay (ELISA)

Exosome-specific marker, CD63, was verified and quantified by ELISA. The content of CD63 was evaluated using an in-house indirect ELISA assay. Firstly, clear polystyrene microplates (R&D system, DY 990) were coated with 100 µL of human CD63 protein and exosomes in 1X PBS and incubated overnight at 4 °C. The next day, wells were washed three times with 100 µL of 1x wash buffer (R&D system, WA126). To inhibit the non-specific binding, the plate was blocked by 1% BSA at room temperature for 2h. Plates were washed as before and added with 100 µL anti-

CD63 antibody (Sinobiological, 11271-MM10), prediluted with 1:1000. The plate was incubated overnight at 4 °C. Plates were washed as before, and 1 μg/mL goat anti-mouse IgG secondary antibody (HRP conjugated, Sinobiological, SSA007) was added to each well and incubated at room temperature for 2h. 100 μL of TMB substrate (Abcam, ab171524) was used as HRP substrate. The reaction was then stopped with stop solution (Abcam, ab171529). Optical densities were measured on a microplate reader (Varioskan LUX Multimode Microplate Reader, Thermo Fisher) at 450 nm.

2.3.5.3 Total protein quantification

The total protein content of exosomes sample was measured by bicinchoninic acid (BCA) assay (QuantiPro™ BCA Assay Kit, Sigma).

2.3.6 Characterization of exosomes isolate

2.3.6.1 Dynamic Light Scattering (DLS) Analysis

Zetasizer (Malvern, UK) was used to determine the hydrodynamic diameter and zeta potential of particles. All exosome samples were diluted in 1mL PBS and transferred to cuvettes for size measurement and capillary zeta cell for zeta potential measurement. The peak corresponds to the intensity and size at which the most abundant particles were detected.

2.3.6.2 Nanoparticle tracking analysis (NanoSight™)

Size distribution and exosomes concentration were measured by tracking the Brownian motion of individual nanoparticles using a NanoSight NS300 system (Malvern, UK) under scatter mode. Exosomes were diluted to appropriate concentration (10^8~10^9 particles/ ml) for NTA analysis. 1ml liquid samples were taken by a 1ml syringe and inject into the sample chamber of NTA fitted with green laser (532nm). Camera focus was manually adjusted to make the particles

appear as sharp individual dots. All samples were counted five times, each collecting 60-second videos with a minimum valid tracking of 200 tracks per video. All analysis were performed using NanoSight NS300 NTA 3.4 software.

2.3.6.3 Transmission electron microscopy (TEM)

The morphology of exosomes was characterized by TEM was used to verify the presence and observe the morphology of exosomes in the purified samples. The exosomes suspensions were fixed on 200-mesh formvar and carbon-coated copper grids (Electron Microscopy Science) using 2.5% (v/v) glutaraldehyde (Electron Microscopy Science) as a fixative agent. Then, the grids were transferred onto drops of UranyLess (Electron Microscopy Science) for negative staining. Each grid was studied using transmission electron microscope (Libra® 200MC TEM, Zeiss).

2.3.6.4 Atomic force microscopy (AFM)

AFM (Asylum Cypher and BIO-3D) was also used for characterizing exosomes. Briefly, exosomes suspensions were diluted in deionized water and added to clean silica wafers and air-dried overnight. Silicon probes coated with aluminum was used for imaging in tapping mode. Topographic height and phase images were captured at room temperature with a scan rate of 0.9965 Hz.

2.3.7 Preservation of exosomes at room temperature using lyophilization

Freshly prepared exosomes were rapidly frozen at -80°C, either in the presence or absence of trehalose. The samples were then lyophilized overnight using a benchtop freeze dryer (Labconco, FreeZone) and stored at -4°C until use. Before analysis, the lyophilized exosomes were rehydrated with water and vortexed immediately.

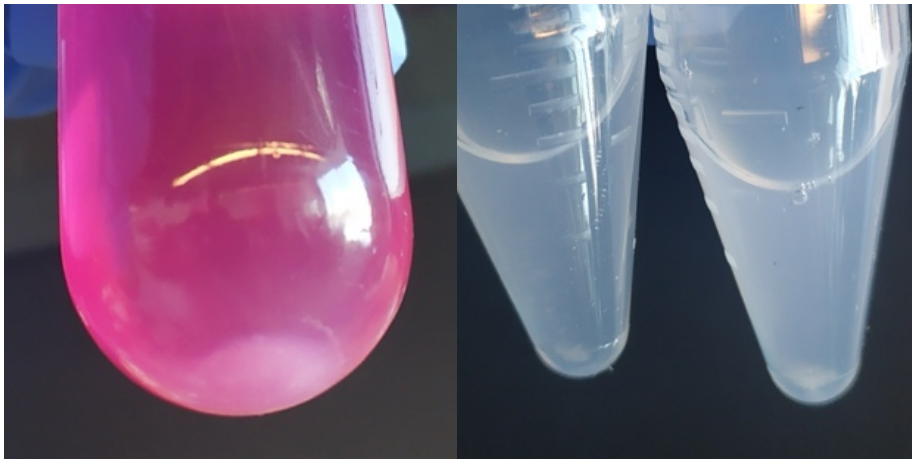
2.4 Results

2.4.1 Comparative analysis of exosome isolation methods from static cell-cultured human dermal fibroblasts

In this study, we utilized a static cell culture system employing tissue culture flasks to harvest exosomes produced by human dermal fibroblasts *in vitro*, a method known for its accessibility and requiring less skilled labor. Commercial FBS, commonly used in cell biology experiments for nutrient and growth factor supplementation, still contains numerous exosomes. Therefore, the exosome-containing components of the culture medium, such as FBS, were depleted of exosomes before being used for cell cultures. We found the depletion of exosomes from FBS did not induce significant cell death or reduce growth rate.

The performance of two exosome isolation methods was evaluated and the yield, purity, and quantity of exosomes was compared. In this study, we adapted the isolation by Weng et al[123] using PEG with molecular weight of 10 kDa and 15% of final concentration for exosome isolation. The expected pellets were formed and observed after centrifugation as shown in Figure 2.2 A. For the affinity isolation method, exosomes were isolated by magnetic beads coated with Tim4 (T cell immunoglobulin and mucin domain containing 4) protein, which specifically binds the phosphatidylserine (PS) displayed on the surface of exosomes. As the binding process is Ca^{+}-dependent, intact exosomes are expected to be easily eluted from the beads by adding a chelator, EDTA. We did not observe any visible pellets in the affinity isolation process, and the harvest exosomes are transparent and suspended in PBS as shown in Figure 2.2 B.

A.



B.

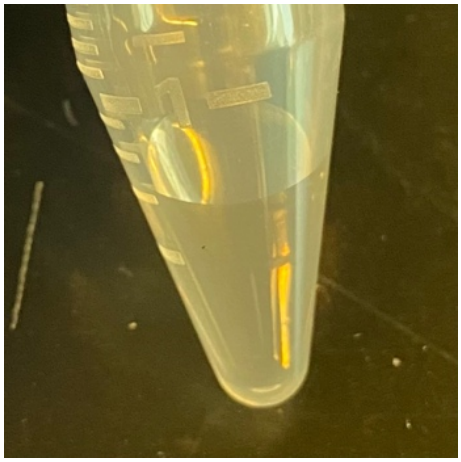


Figure 2.2 Observation of potential exosome pellets. (A) Exosome pellets were precipitated from cell culture supernatant using 15% PEG and from PBS using 15% PEG. A very thin, barely visible grayish film was observed at each step. (B) Exosomes isolated using the affinity isolation method showed no visible pellet or film.

The size distribution of the enriched vesicles was analyzed by DLS. Exosome isolate showed different size distribution patterns based on different isolation methods (Table 2.2). The polydispersity index (PDI) of exosomes harvested by PEG precipitation was higher (0.467±0.039)

than those harvested with affinity method (0.323±0.049), indicating the exosome isolate are inevitably heterogeneous particle distribution system regardless of the isolation methods. PS capture exosomes were relatively more homogenous than PEG-precipitated exosomes. As can be observed in the graph of size distribution by intensity, exosomes isolated by PEG were around 69.81± 4.27nm with two peaks, around 46 nm and 210 nm (Figure 2.3), respectively. The size distribution shifting to higher values could possibly be due to the clumping or aggregation of exosomes induced by PEG[122]. Exosomes captured by the affinity method were larger at 268.43± 8.60nm, showing one distinct peak. Exosomes isolated with both methods displayed a negative charge due to the nature of cell plasma membrane that carry a net negative surface charge due to the nature of molecules expressed at their surfaces under physiological condition[132]. A higher magnitude of zeta potential (-10.725± 1.084mV) was exhibited in affinity-isolated exosomes, suggesting exosomes isolated by this method were more stable.

Table 2.2 Comparison of particle size, polydispersity index (PDI), and Zeta potential measured by DLS. Values represent the mean ±SD, n=3.

	Size (nm)	PDI	Zeta potential (mV)
Exosomes isolated by PEG precipitation	69.81±4.27	0.467±0.039	-7.769±0.655
Exosomes isolated by affinity method	268.43±8.60	0.323±0.049	-10.725±1.084

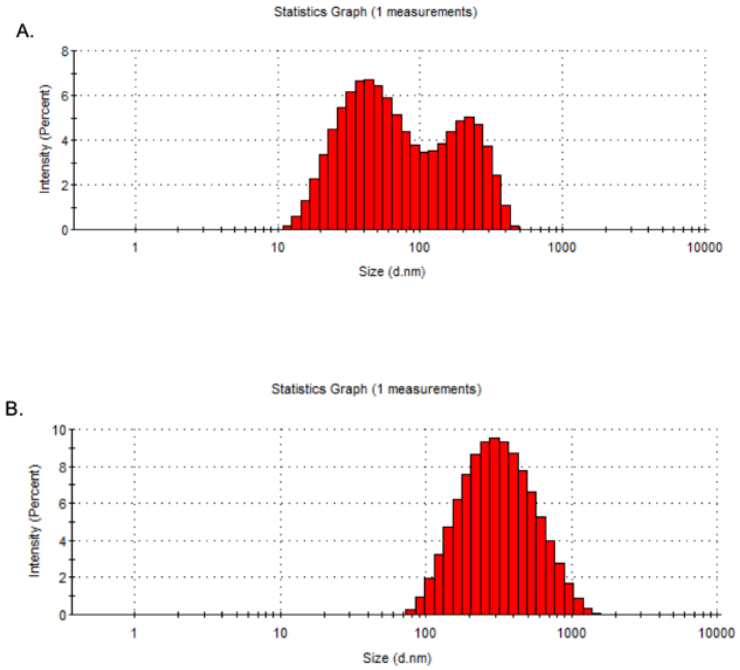


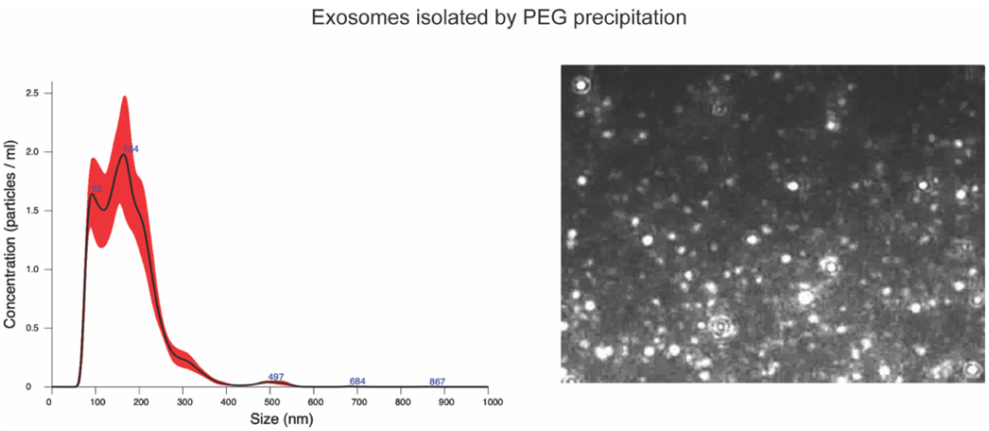
Figure 2.3 Size distribution of exosomes analyzed by DLS.

(A) Results from the PEG precipitation method. (B) Results from the affinity method.

Further characterization with NTA was employed to determine the exosomes' particle concentration, size mode, and parameter D90 (the diameter of which 90% of the particles diameter are below this value), as shown in Table 2.3. A similar distribution pattern was shown with two peaks (92nm and 184 nm, respectively) as the size results from DLS for the PEG precipitation method. Affinity-isolated exosomes showed mono-distribution at 106nm. We also observed D90 was significantly higher in exosomes isolated with PEG (255.8 nm) compared to affinity method (174.5 nm). Both isolation methods could harvest 10^9 particles/ml of exosomes; however, PEG gave twice the number of particles than the affinity method per 20mL conditioned media. Although DLS and NTA both measure the hydrodynamic diameter of nanoparticles, the size of exosomes measured by DLS and NTA show differences here. This can be explained by one of the artifacts of

DLS that DLS is less reliable and accurate when the suspension system is polydisperse[133]. The size distribution profile is likely to be interfered by the large particle's population since they scatter more light than smaller particle. In summary, the DLS analysis and NTA analysis both directed to the conclusion that PEG could enrich a larger population of vesicles. However, it also inevitably harvests a heterogeneous population of particles compared to the affinity method. In contrast, the affinity method yields fewer vesicles, but with a more homogeneous population.

A.



B.

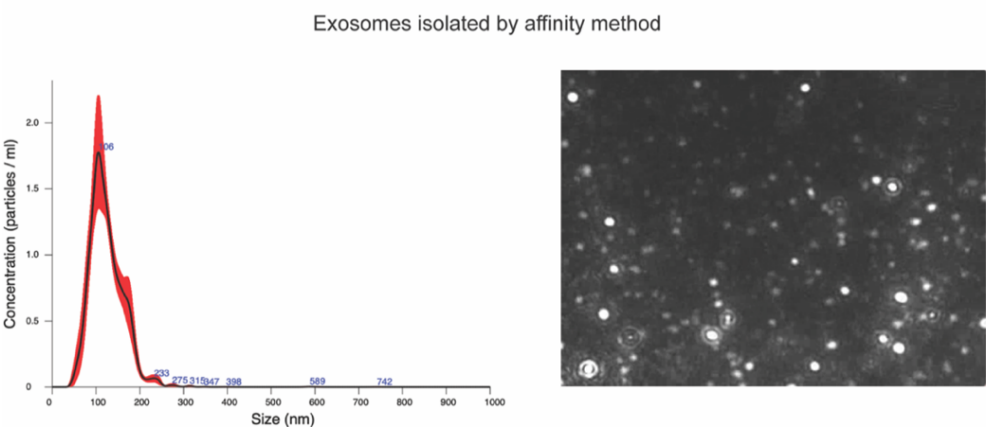


Figure 2.4 Characterization of exosomes by NTA. (A) Size distribution of exosomes isolated using the PEG method, along with NTA video frames showing exosome particles in PBS. (B) Size distribution of exosomes isolated using the affinity method, accompanied by NTA video frames of exosome particles in PBS.

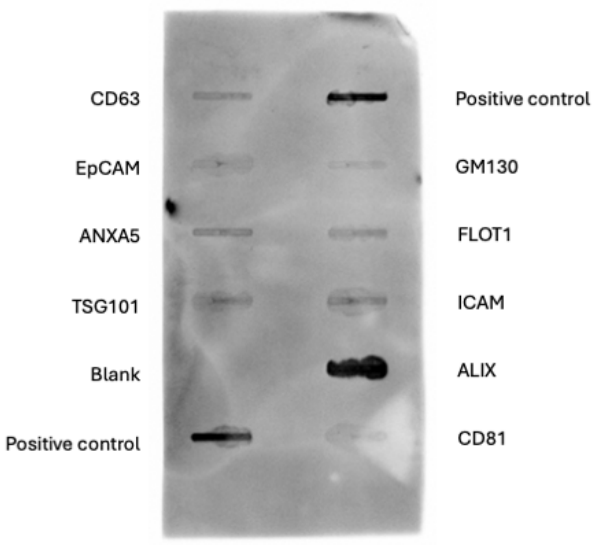
Table 2.3 Comparison of size distribution and particle concentration of exosomes measured by NTA. Values represent the mean ±SD, n=3.

	Size mode (nm)	D90 (nm)	Concentration (particles/ml)
Exosomes isolated by PEG precipitation	171.8±2.0	255.8	$2.96x10^9±5.35x10^8$
Exosomes isolated by affinity method	125.8±3.2	174.5	$1.36x10^9±1.95x10^8$

To validate the exosome nature of isolated particles and compare the quality of exosomes enriched by both isolation method, samples were lysed and the expression of the exosomal surface biomarkers was evaluated by a semi-quantitative dot blot antibody array. We found the absence of cellular contamination marker GM130 (a cis-Golgi marker) from exosomes isolated with both methods, indicating both methods are lack of any cellular contamination. CD81, a tetraspanin involved in exosome biogenesis, was barely detectable in both PEG-precipitated and affinity-isolated exosomes. CD63 is detectable for both methods of isolation but shows low expression. ALIX was highly expressed with both isolation methods. Other exosomal-associated markers including EpCAM, ANXA5, FLOT1, TSG101 and ICAM were more abundant in affinity-isolated exosomes, compared to PEG-precipitation. Here, we successfully characterized at least one protein from each category of transmembrane (CD63), cytosolic (TSG 101), and intracellular proteins (ALIX) for both methods of isolation[134], which meet the requirements of Minimal Information for Studies of Extracellular Vesicles (MISEV). However, with the same total protein amount in the

exosome isolate, the affinity method yielded a particle population with higher exosomal marker expression.

A.



B.

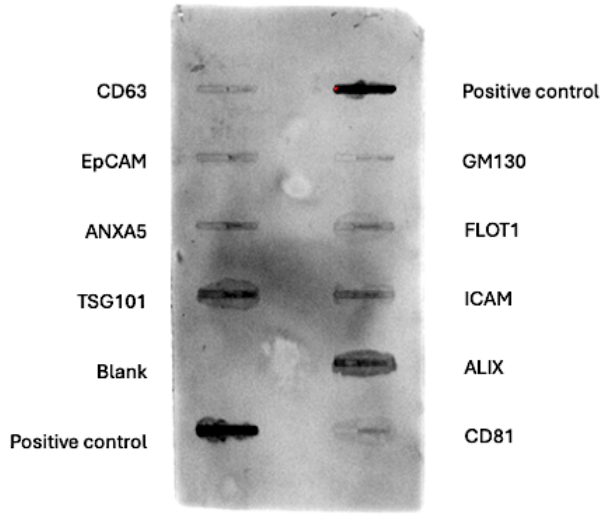


Figure 2.5 Semi-quantitative dot blot antibody array (Exo-Check™) for the identification of common exosomal markers. (A) Exosomes isolated using the PEG method. (B) Exosomes isolated using the affinity method.

Purity of exosomes is also a critical criterion for the quality control of exosomes. Particle-to-protein, protein-to-lipid, or RNA-to-particle ratios are usually utilized to evaluate exosome purity after isolation. Therefore, we further conducted a series of protein and particle quantification assays including an in-house indirect CD63 ELISA assay, BCA assay and nanoparticle tracking analysis to critically compared the purity of exosomes (Figure 2.6). Our result indicated the presence of CD63 was 12 times more in PEG-precipitated exosomes than the affinity-captured ones. Although PEG precipitation produced a higher exosome yield, a higher amount of total protein was given simultaneously. This suggests PEG gathered a significant larger amount of protein contaminants together with the exosomes. The ratio of particle number to total protein content (particles /μg protein) has been widely employed as a parameter to evaluate the purity of exosome preparations. A relatively higher ratio is believed to indicate less contaminants and higher purity. Vesicle preparation with $<10^8$ particles / μg protein is arbitrarily considered unpure[135]. Our results proved that affinity method can efficiently produce $6.15x10^9$ particles / μg protein, which is approximately 85 times fold higher that PEG precipitation. Similar results were also seen from the ratio of CD63 content to total protein content (ng/ μg), affinity captured exosomes was 15 times significantly higher than the PEG method. In summary, the affinity isolation showed a lower yield and recovery of exosomes, but a higher exosomes purity than PEG precipitation. Given that the further application of human dermal fibroblasts-derived exosomes involves the exosome-mediated transfer of cargo, which requires high sample purity to achieve specific effects, we have selected the affinity isolation method for all following studies.

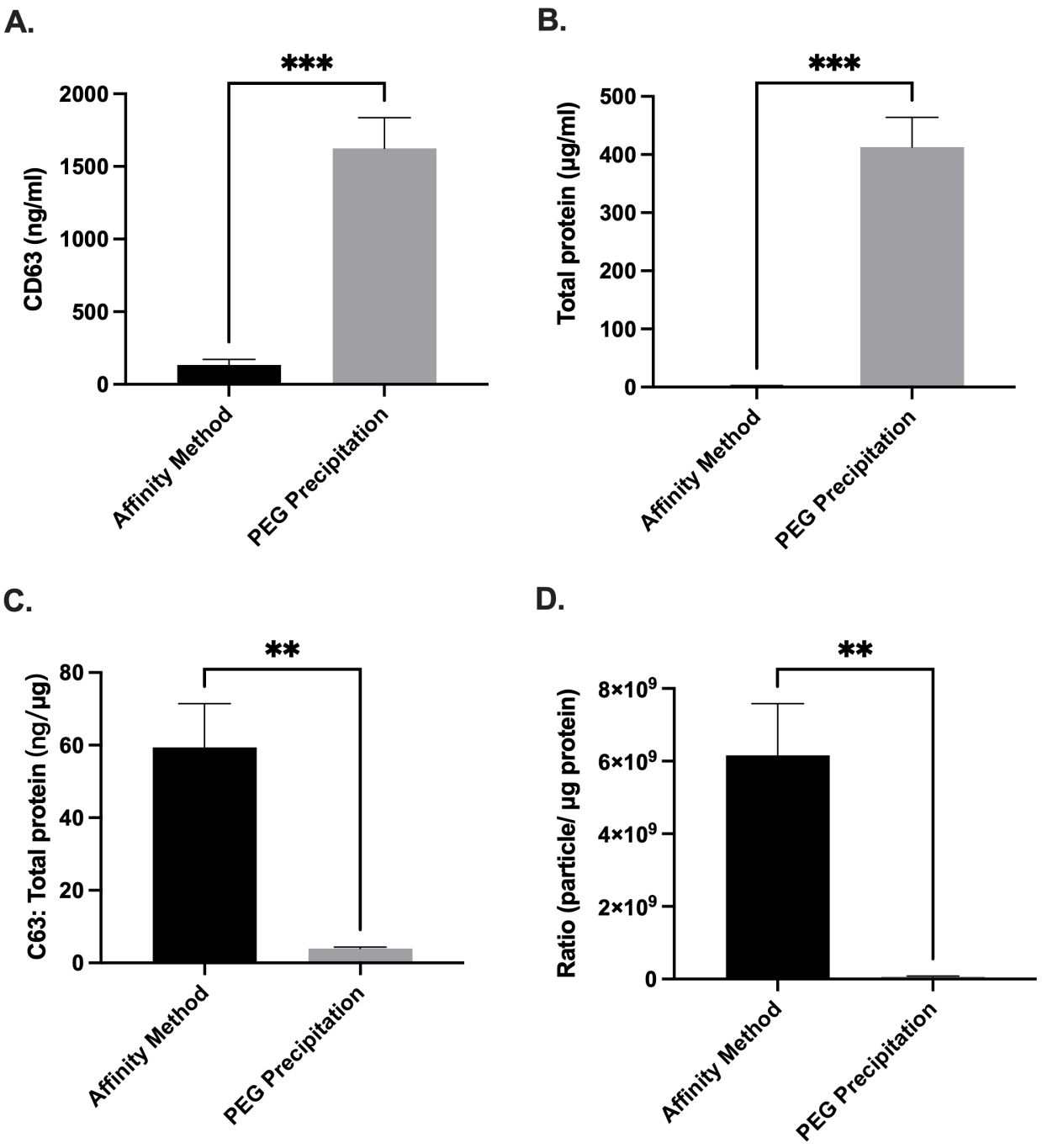


Figure 2.6 Comparison of the purity of exosomes isolated from 20 mL of cell culture supernatant from fibroblasts using different methods. (A) CD63 content measured by ELISA. (B) Total protein content determined by the BCA assay. (C and D) Purity of exosome suspensions. Values represent the mean ±SD, n=3. A t-test was performed. P value $\leqslant$ 0.05 was considered to be statistically significant. *, **, and *** stood for $P < 0.05$, $P < 0.001$, and $P < 0.0001$ respectively.

2.4.2 Morphological characterization of exosomes isolated via affinity method

While the presence of exosomal markers suggests the expected protein components of exosomes reported by literature[134], further biophysical evidence is needed to confidently conclude that the isolated vesicles are exosomes. The morphology of exosomes isolated by affinity method was observed by TEM. Most particles were intact and have a spherical morphology. The observed structures had a range of diameters (10 – 100 nm), but all showed distinct membranes (observed as black borders). No cup-shape vesicles were observed under TEM. TEM also reveals the presence of smaller particles that cannot be detected with DLS and NTA. We speculate the smaller particles (<30nm) could possibly be lipoproteins which are a common contaminant co-isolated with exosomes since it is an essential component in cell culture media supplemented with FBS. It is also important to consider that TEM dehydration and fixation processes may introduce artifacts, leading to exosomes size measurements that are smaller than the actual particle size.

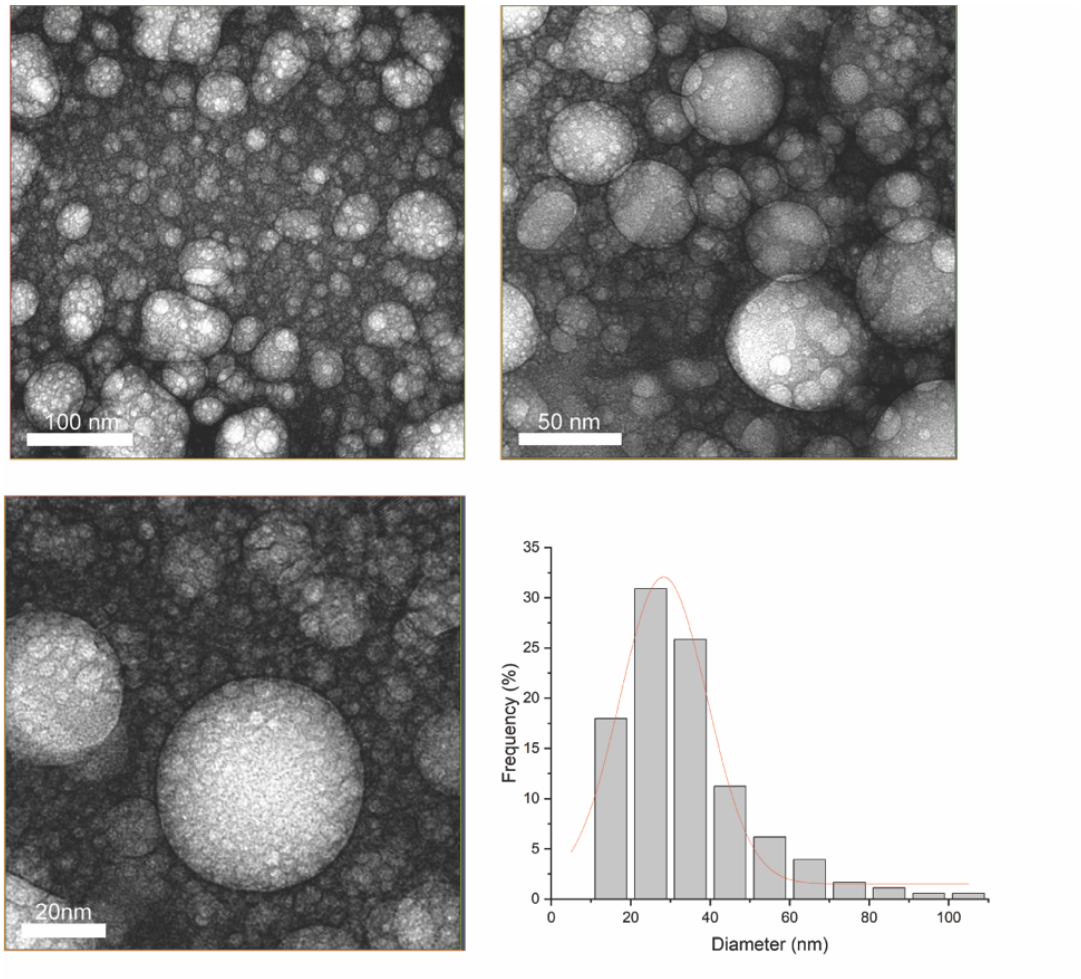


Figure 2.7 Characterization of exosomes by TEM. Morphological analysis of exosomes isolated using the affinity method, captured with a Zeiss Libra 200MC TEM. Magnifications used are 200,000x, 100,000x, and 50,000x, respectively. Particle analysis is also included.

Both AFM phase and height images reveal a fairly homogeneous and nearly spherical structure of exosomes without apparent aggregation. (Figure 2.8). The diameter measured by the phases image was approximate 80-300 nm and the height of exosome particles ranged from around 6 to 8nm, indicating the possibility that exosomes were adsorbed and flatten onto the silica wafers. The interaction between exosomes and supporting substrate causes the deformation of exosomes

and modifies the shape of the exosomes. Therefore, the height measurement of exosomes was smaller than the phase diameter. In general, the height values typically fall within the range reported in the literature and align with the dimensions of solid surface-supported membrane vesicles observed under liquid conditions[136].

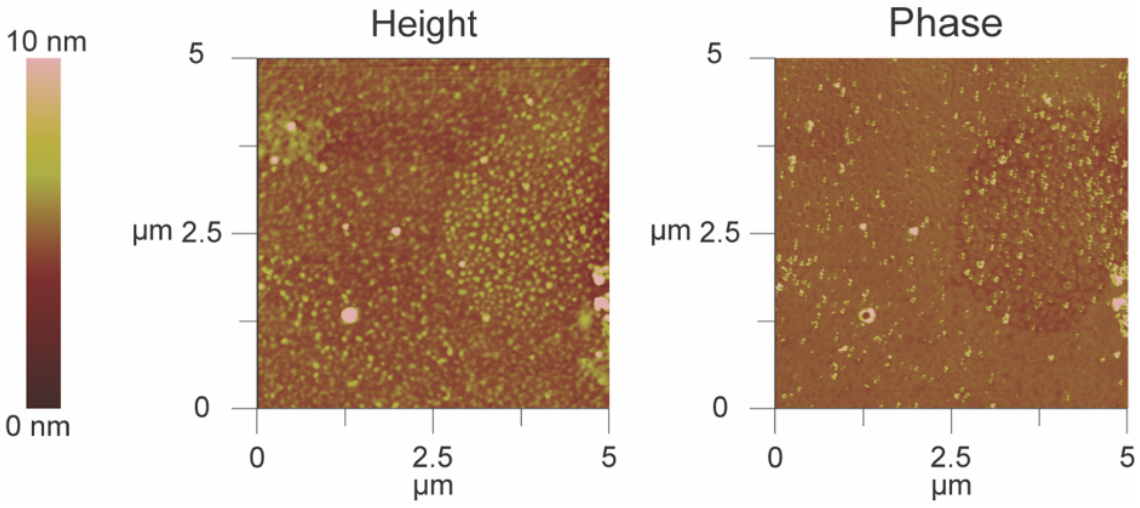


Figure 2.8 Characterization of exosomes by AFM

2.4.3 Room temperature preservation of exosomes through lyophilization

Exosomes are recommended to be stored at −80 °C[137,138]; however, this temperature is not suitable for their handling or transportation. Lyophilization has been used for long-term preservation of various biological materials at room temperature. In this study, a room temperature exosome preservation method was employed with lyophilization. We also compared the properties of lyophilized exosomes with those stored at -80°C and assessed the impact of the cryoprotectant trehalose on their physical properties. The exosome particle number decreased to 90% after lyophilization, and the addition of trehalose could sufficiently maintain the exosome particle concentration under lyophilization. After lyophilization with or without the presence of trehalose,

all samples showed fine size distribution. However, the introduction of trehalose increases the size of exosomes dramatically from 114.2±1.8 nm to 175.1±3.8 nm. Freeze-dried exosomes also showed a size increase to 143.8±2.1 nm. In general, exosomes that went through different storage conditions still displayed negative particle charges, indicating the stability of exosomes under lyophilization with or without the presence of trehalose.

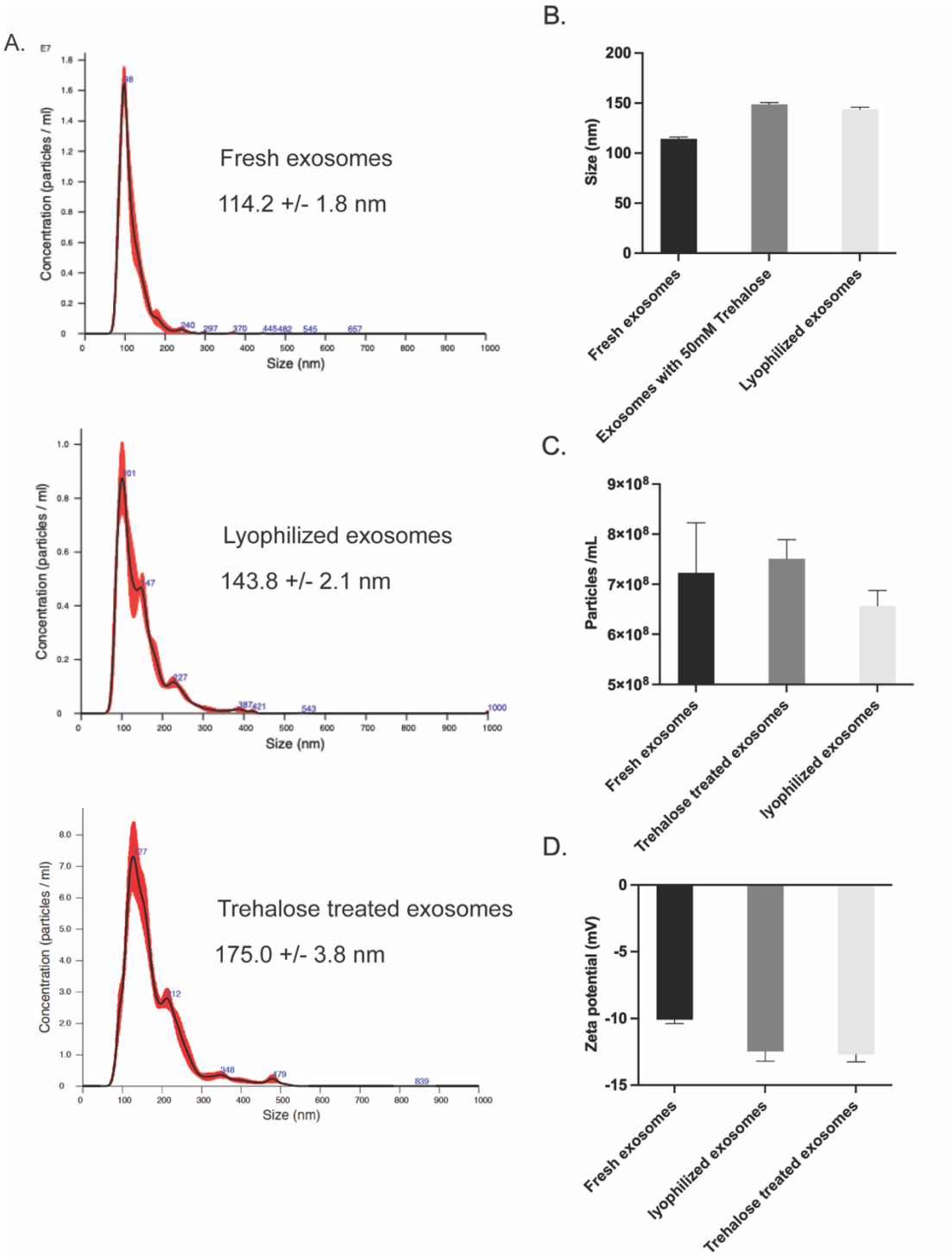


Figure 2.9 Impact of trehalose on the preservation of exosomes via lyophilization. (A) Size distribution of exosomes as characterized by NTA. (B) Size of exosomes characterized by NTA. (C) Particle concentration of exosomes as determined by NTA. (D) Zeta potential of exosomes as measured by DLS. Values represent the mean ±SD, n=5.

2.5 Discussion

Isolating exosomes from the complex and heterogeneous extracellular fluid remains a challenge, often leading to confusion and potential misinterpretations in the scientific community due to inadequate purification methods. This chapter focuses on developing a method for harvesting and isolating exosomes derived from human dermal fibroblasts in static cell culture. We evaluate the efficacy of different isolation methods in terms of yield, purity, and quantity to identify a technique that produces high-quality exosomes for downstream applications. Additionally, we conduct biophysical characterization to assess the size, morphology, and exosomal markers of the isolated exosomes.

All mammalian cells cultured *in vitro* produce EVs in the extracellular environment of their culture medium. Monolayer or multilayer cultured cells serve as significant sources of exogenous exosomes due to their high accessibility in laboratories[139]. The human dermal fibroblast cultured in this study is considered allogeneic cells and has been utilized in medical applications such as biological dressing or preparing the wound bed before applying a permanent graft, particularly for large wounds[140]. To ensure that the exosomes are derived from genetically stable and non-senescent dermal fibroblasts, we cultured human dermal fibroblasts in monolayer or multilayer flasks and collected the supernatant produced by fibroblasts within passage 20[140]. The supernatants collected were used for exosome isolation. This study evaluated two methods: PEG precipitation and the affinity method, focusing on yield, purity, and quality. PEG precipitation utilizes a hydrophilic polymer that absorbs water, allowing less soluble particles to settle during low-speed centrifugation. While this method is simple and cost-effective, it can lead to contamination from non-exosomal proteins. In contrast, the immunoaffinity method uses magnetic beads coated with TIM4, which specifically binds to phosphatidylserine found on exosomes. Although it yields fewer

particles, this method produces a high-purity exosome isolate, effectively separating exosomes from contaminants.

Following on exosomes isolation, we first confirmed the presence of external (CD63, EpCAM, ANXA5, and ICAM) and internal (TSG101, ALIX, and FLOT1) exosomal protein markers in exosomes isolated by both methods using a semi-quantitative antibody array. The results indicated exosomes are contained in the enriched particle population. The affinity method produced exosome isolate with higher expression of exosomal protein markers, despite containing the same total protein as PEG-precipitated exosomes. Our protein and ELISA analysis also indicated PEG precipitation produced significantly higher exosome yield (particle number, CD63 content, and total protein content) than the affinity method. However, we observed PEG precipitation significantly compromises exosome purity by introducing non-exosomal proteins. A post-processing step is still necessary to remove these contaminants after precipitation. Affinity-based isolation yielded fewer exosomes but with higher purity compared to PEG. The reason for the low yield is likely due to the multiple washing steps during the affinity isolation, which may have resulted in inefficient capture and loss of exosomes[113]. In summary, the protein content analysis of exosome isolate aligns with previous findings, indicating that PEG precipitation resulted in a higher exosome yield but lower exosomes purity as compared to the affinity method[125].

To ensure a consistent and reproducible isolation of exosomes, it is important to control the biophysical properties (size distribution and particle concentration) of each exosomes' isolate. DLS and NTA are both promising techniques for exosomes' hydrodynamic particle size analysis. Illuminated by laser, DLS records the fluctuations of the light intensity scattered by particle Brownian motion, and hydrodynamics can be calculated and determined via the Stokes-Einstein equation. DLS offers simplicity of operation and low cost of measurements. However, in the case

of the characterization of exosomes, DLS overestimates total particle count and is regarded less reliable when the particle population is polydisperse[133]. As the larger particle subpopulation scatters more light, the particle size distribution profile can be strongly compromised by larger particles, especially for measuring polydisperse particles such as exosomes. In addition, DLS is believed to be an ideal technique for measuring high-concentration nanoparticles (10^8~10^{12} particles/ml)[141]. NTA is a high resolution method for real-time visualization and analysis of polydisperse samples[142], especially for exosomes. Our results showed discrepancies between NTA and DLS particle size characterization methods. Despite this, both methods indicated that the affinity method yields fewer but well-dispersed vesicles. Comparatively, PEG precipitation led to a more heterogeneous population of particles. The diverse particle population could be lipoproteins, aggregated exosomes, other protein aggregates (hundred nanometers) or other non-exosomal particles. Hence, we conclude that PEG precipitation is not suitable for the efficient isolation of exosomes due to concerns regarding exosome purity and the yield of heterogeneous vesicles. Instead, exosomes enriched by the affinity method were used for downstream applications, representing a superior isolation technique for generating high-quality exosomes.

Further characterization was conducted to confirm the morphology of exosomes isolated with affinity method under TEM and AFM. The morphology of the exosome-like structures was similar to previous reports of common exosomal shapes observed under TEM. Exosomes appeared as isolated vesicles with characteristic rounded morphology with no information about their substructural details under AFM, in line with previous reports for exosomes isolate from other cell sources[136].

Lyophilization can prolong the shelf life of exosomes, allowing freeze-dried EV to be stored at room temperature, which significantly reduces storage costs and complexity for off-the-

shelf use. Our investigation into the lyophilization method revealed that directly lyophilizing exosomes resulted in changes to particle number and size distribution. We found that adding 12.5 mM trehalose—a natural, non-toxic sugar commonly used as a protein stabilizer and cryoprotectant—helped preserve the number of exosomes. These findings are consistent with previous studies showing that trehalose effectively maintains the colloidal stability of extracellular vesicles (EVs), prevents ice crystal formation within the particles, and improves EV recovery rates[143].

2.6 Conclusion

In this chapter, we developed a comprehensive workflow for harvesting, isolating, and characterizing exosomes derived from human dermal fibroblasts cultured *in vitro* under static conditions. We compared two commonly used isolation methods—PEG precipitation and affinity isolation—to identify an efficient technique that yields exosomes with high purity and consistency. To ensure the quality of the isolated exosomes, we conducted various characterization analyses to confirm their morphological, biophysical, and physicochemical properties. Our findings indicated that affinity isolation produces exosomes with high purity and good dispersion. The biophysical characterization techniques, including TEM and AFM, alongside molecular techniques such as antibody arrays and ELISA, successfully verified the isolation of high purity exosomes from the conditioned media of *in vitro* cultures. We also identified trehalose as a useful stabilizer and cryoprotectant that helps preserve exosomes during lyophilization. This study offers valuable insights and optimized strategies for future research on exosomes, focusing on their isolation, characterization, and storage.

Chapter 3 Active Drug Encapsulation and Formulation Optimization for Utilizing Exosomes as Drug Carriers

3.1 Overview

Exosomes are increasingly favoured as cargo carriers due to their high biocompatibility, stability, and low immunogenicity. Their lipid bilayer membrane protects the cargo from degradation, making them desirable for drug delivery. However, achieving efficient drug encapsulation in exosomes remains challenging. This chapter aims to develop a method for encapsulating pirfenidone (PFD) into exosomes. We systematically optimized the active drug loading method using sonication to enhance drug encapsulation efficiency (EE%), loading efficiency (LE%), and overall exosome yield. Additionally, we explored various techniques to remove excess drug after encapsulation to improve yield. Human dermal fibroblast exosomes were successfully loaded with PFD, achieving an EE of 11.136% ± 1.267%, an LE of 10.012% ± 1.026%, and the highest particle recovery rate of 64.213% ± 8.49%. It is crucial to carefully control sonication to maintain the integrity of the exosomes. This study provides valuable insights into using exosomes as effective carriers for drug loading while preserving their membrane integrity.

Keywords: Exosomes, drug delivery, pirfenidone, formulation optimization

3.2 Introduction

The use of exosomes loaded with therapeutic substances including but not limited to chemical molecules, nucleic acids, and proteins[144] has shown promising therapeutic outcomes, and this delivery system can mitigate the adverse effects of drugs while preserving their pharmacological activities. The structure of exosomes theoretically enables exosomes to encapsulate hydrophilic drugs in the core and hydrophobic molecules into the lipid bilayer. However, many studies have demonstrated a common challenge: the low capacity of exosomes to transport therapeutic substances, which hinders their application in drug delivery. Two approaches are currently available for incorporating cargos into exosomes: 1) pre-loading before exosomes isolation and 2) post-loading after exosomes isolation. The choice of method depends on the specific drug and its properties, as well as the desired release mechanism.

Therapeutic molecules can be integrated into exosomes during their biogenesis. Preloading occurs when cells are cultured with the drug of interest. In this process, the drug is naturally incorporated into the exosomes as they generate, and the drug-loaded exosomes are then released into the medium and isolated. However, pre-loading is only effective for lipophilic drugs that can easily cross cell and vesicle membranes. Exosomes carrying therapeutic genes, such as miRNA, siRNA, and mRNA, can be generated by transfecting the exosomes producing cells via liposomes, electroporation, or viral infection. For example, cationic polymers such as polyethylenimine (PEI) have been used to develop nanoparticles for non-viral transfection. For example, Trivedi et al. transfected microRNA-125b and wt-p53 into SK-LU-1 lung cancer cells using hyaluronic acid-polyethyleneimine (HA-PEI) / hyaluronic acid-polyethylene glycol (HA-PEG) conjugate nanoparticles[145]. This resulted in an increased expression of these molecules in the exosomes derived from the modified cells. Peptides and proteins can also be displayed on the surface of

exosomes through transfection. Ran et al. achieved this by engineering exosomes from murine NIH3T3 fibroblasts by incorporating the inhibitory domain of the propeptide into the CD63 surface marker using lentivirus[146]. These engineered exosomes specifically bound to mature myostatin in serum from wild-type mice, unlike exosomes from unmodified or empty plasmid-transfected cells. Cells can also produce drug-encapsulated exosomes when exposed to small molecules. Pascucci et al. exposed high doses of paclitaxel (PTX) to murine stromal cell line SR4987 and produced PTX-loaded exosomes that showed an obvious anti-proliferative effect on the human pancreatic cell line CFPAC-1[147]. Although these are promising examples of pre-loading therapeutic compounds into exosomes, achieving consistent drug loading with this method remains challenging. Additionally, the precise mechanism of how therapeutic cargos are encapsulated during exosome biogenesis is not yet fully understood.

Another approach is post-loading, where the drug is directly introduced into isolated exosomes. Methods such as direct co-incubation, sonication, electroporation, freeze-thaw cycles, and extrusion are used to incorporate therapeutic molecules after exosomes have been harvested and isolated. These techniques typically achieve higher encapsulation than pre-loading and offer more precise control over the amount of drug loaded. (Figure 3.1). Direct co-incubation of exosomes and drug is a straightforward method for passive drug loading. However, this approach generally results in a lower loading capacity. For example, PTX was loaded into bovine milk-derived exosomes by mixing the PTX solution with exosome dispersion and incubating at room temperature[148]. PTX-loaded exosomes showed a practical loading efficiency of ~8%. Similarly, doxorubicin (DOX) achieved a loading efficiency of only 11.73% when encapsulated in HEK-293T cell exosomes[149]. An antibiotic linezolid showed a loading capacity of 5.06%±0.45% in macrophage-derived exosomes[150]. In the absence of additional mechanical or electrical forces,

drug diffusion into exosomes during co-incubation is influenced solely by the drug's hydrophobicity [151,152], molecular size[151,153], and charge[154]. The tightly packed lipid structure of the exosome membrane hinders drug molecules from diffusing across the hydrophobic bilayer and entering the exosomes.

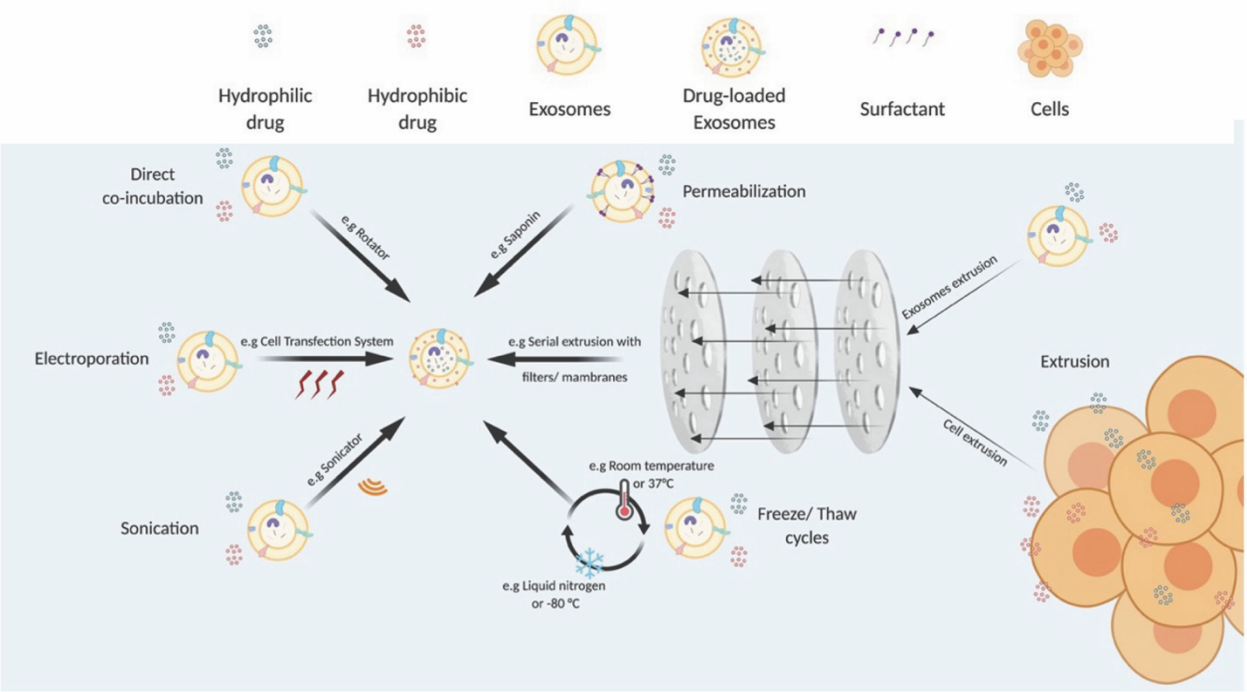


Figure 3.1 Post-loading drug encapsulation methods, including direct co-incubation, electroporation, sonication, permeabilization, freeze-thaw cycles, and extrusion method[106]. Created with biorender.com.

To further improve drug encapsulation, active loading techniques are often employed to enhance drug encapsulation, which include electroporation, sonication, permeabilization, extrusion and freeze-thaw cycles[155] etc. Electroporation technique is primarily employed in introducing extracellular genes to living cells, applies electric pulses that disrupt cell membranes and create pores for cargo entry[156]. Electroporation also disrupts the exosomal membrane and

allow for drug incorporation into exosomes. For instance, Liang et al. used electroporation to simultaneously package the anticancer drug 5-FU and the miR-21i inhibitor into engineered exosomes[157]. However, a significant challenge with this method is the tendency to form aggregates of nucleic acids and exosomes during the encapsulation[158]. An EE of 19.34% was achieved when loading hexyl 5-aminolevulinate hydrochloride into macrophage-derived exosomes[159]**.** Kim et al. evaluated different methods for loading PTX into macrophage exosomes and found that electroporation achieved a loading efficiency of 5.3%, compared to 28.29% with sonication and 1.44% with direct co-incubation at room temperature[160]. Recent studies also suggest that rapid freezing and thawing of exosomes—using liquid nitrogen or -80 °C followed by thawing at room temperature—can facilitate drug incorporation. The rationale for this method is that slight disruption of the lipid bilayer of exosomes after limited cycles of freeze and thaw enable drug molecules to diffuse into the exosomes. The biological activity of the original exosomes is also maintained during this process. In a study by Haney et al[154], catalase was loaded into macrophage-derived exosomes for targeted delivery to the brain in Parkinson's disease. The freeze-thaw cycle method achieved a loading efficiency of 14.7 ± 1.1%, significantly higher than the 4.9 ± 0.5% efficiency from direct incubation, but less effective than sonication and extrusion methods. Hajipour et al. used the freeze-thaw cycle to load human chorionic gonadotropin (hCG) into exosomes, achieving an encapsulation rate of 14.02 ± 5.46% and a loading capacity of 245.06 ± 95.66 IU/mg[161]. These results were lower than those obtained using sonication, which achieved 40.55 ± 4.21% encapsulation and 710.05 ± 73.74 IU/mg under the same conditions. Saponin is a surfactant that increases cell membrane permeability by interacting with membrane cholesterol to create pores while preserving the lipid bilayer's integrity[162]. This property also improves the permeabilization of exosome membranes and improve drug encapsulation without affecting

exosome morphology. Using a 0.01% saponin significantly improved hydrophilic compound, porphyrin, loading into extracellular vesicles compared to methods such as direct incubation, electroporation, and extrusion[152]. Saponin treatment increased catalase loading efficiency more than three-fold, achieving 18.5% compared to 4.9% with co-incubation[154]. However, saponin's potential to cause hemolysis raises concerns about its use in intravenous injections[163]. Extrusion techniques create exosome-like nanoparticles by serially passing donor cells or purified exosomes through filters with specific pore sizes under controlled temperature and pressure. This process breaks down the cells or exosomes into free lipids and proteins, which then reassemble into new vesicles[164]. Extrusion through a lipid extruder (200 nm pore size) under a controlled temperature, effectively encapsulated catalase into exosomes, achieving a loading efficiency of 22.2 ± 3.1%. This result is comparable to the 26.1 ± 1.2% efficiency obtained through sonication[154]. By mixing PTX with the exosomes and passing the solution through a lipid extruder with a 100 nm pore size, a PTX loading efficiency of 14.23 ± 0.25% was achieved, which was significantly higher than the 6.87 ± 0.4% efficiency obtained using conventional freeze-thaw methods[165]. The disadvantage of the extrusion method is that extrusion appears to induce changes in the exosomes physical properties (including zeta potential and protein composition)[163]. Specifically, when porphyrins were loaded into breast cancer cells exosomes through repeated and intensive extrusion—31 times through a 400 nm polycarbonate membrane at 42°C—a significant decrease in the zeta potential of the exosomes was observed and caused cytotoxicity[152].

Among the various active encapsulation methods, sonication is notable for its high drug-loading efficiency and controllability. This technique applies mechanical shear force that temporarily disrupts exosomal membranes, facilitating drug permeation[154,160]. After sonication, exosomes must be restored by incubating the mixture at a specific temperature for at least an hour

to preserve their protein content[154,166,167]. For hydrophilic compounds such as gemcitabine (GEM), sonication significantly improved loading capacity from 2.79 ± 0.72% to 11.68 ± 3.68% compared to direct incubation[168]. Similarly, the sonication method achieved the highest practical drug loading efficiency at 21.5 ± 2.4% of 5- Fluorouracil into exosomes, outperforming the incubation method (10.8 ± 1.2%)[169]. For hydrophobic compounds like PTX, sonication achieved an EE of 28.29% ± 1.38%, significantly higher than the co-incubation (1.44% ± 0.38%) and electroporation methods (5.3% ± 0.48%)[160]. Another study reported that sonication increased PTX loading efficiency nearly 10-fold, from 4.2% to 36.8%[170]. Berberine also showed higher loading when using sonication, with content in exosomes reaching 17.13 ± 1.64%, compared to 5.00 ± 0.70% with the incubation method[171]. Yerneni et al. demonstrated that mild sonication could sequentially load albumin and curcumin into exosomes, achieving loading efficiencies of about 38% for albumin and 56% for curcumin, resulting in exosomes with enhanced stability and anti-inflammatory properties[172]. However, a drawback of sonication is the potential reformation or deformation of exosomes, which may disrupt their integrity. Despite this, sonication remains an effective method for developing novel exosome drug delivery systems, offering strong potential for optimizing drug delivery.

Table 3.1 Drug lipophilicity and encapsulation methods into exosomes

Drug	Partition Coefficient (logP)	Loading Method	Loading Efficiency
Paclitaxel (PTX)[148,160]	~3.0 to 3.2 (XLogP3-AA = 2.5)	Sonication	19.55 ± 2.48%~28.29 ± 2.48%
		Electroporation	5.3± 0.48%
		Incubation	1.44 ± 0.38%~8%
Resveratrol (RSV)[173]	~3.09 (XLogP3-AA = 3.1)	Incubation	15 μM
		Sonication / Electroporation	<2 μM
Erastin (Er)[174]	~2.5 to 3.0 (XLogP3-AA=4.8)	Sonication	Not provided
Rose Bengal (RB)[174]	~2.7 (XLogP3-AA=8.5)	Sonication	Not provided
Berberine (Ber)[171]	NA (XLogP3-AA = 3.6)	Sonication	17.13 ± 1.64%
		Incubation	5.00 ± 0.70%
Curcumin (CUR)[172,173]	~2.3-3.2 (XLogP3-AA = 3.2)	Incubation	2 μM
		Sonication / Electroporation	<2 μM
		Sonication	~56%
Doxorubicin (DOX)[149]	~1.7 to 1.8 (XLogP3-AA = 1.3)	Incubation	11.73%
5-Fluorouracil (5-FU)[169]	~0.9 (XLogP3-AA = -0.9)	Sonication	21.5 ± 2.4%
		Triton X-100	13.7 ± 3.1%
		Incubation	10.8 ± 1.2%
Vancomycin (VAN)[175]	~-0.5 (XLogP3-AA = -2.6)	Sonication	22.15% ± 3.21%
Aspirin (ASA)[176]	~-1.15 (XLogP3-AA=1.2)	Sonication	~20%
Gemcitabine (GEM)[176]	~-1.5 (XLogP3-AA= -0.27)	Sonication	11.68 ± 3.68%
		Incubation	2.79 ± 0.72%
Methotrexate (MTX)[177]	−1.85 (XLogP3-AA=-1.8)	Freeze-Thaw	64.54 ± 1.54%
		Sonication	55.52 ± 1.91%

This chapter focuses on developing a method to encapsulate PFD in exosomes. We optimized the active drug loading process using sonication to improve drug encapsulation efficiency (EE%), loading efficiency (LE%), and the overall yield of exosomes. Furthermore, we

examined different techniques for removing excess drug after encapsulation to enhance the final yield and drug encapsulation.

3.3 Material and methods

3.1.1 Development and Validation of UHPLC Method for Quantification of Pirfenidone (PFD)

Pirfenidone (PFD) was purchased from TCI America (P1871), and analytical grade acetonitrile and acetic acid were purchased from Sigma Aldrich. High purity water was obtained from Millipore Milli-Q Plus water purification system (Millipore). Chromatography analysis was performed on ACQUITY UHPLC H-Class PLUS System (Waters Corporation, USA) equipped with a photo diode array (PDA) detector. All analyses were performed on an ACQUITY UPLC BEH C18 Reversed Phase Column (Waters) with a mobile phase of acetonitrile and 0.2% acetic acid water solution (1:4, v/v) at a flow rate of 0.50 mL/min at 30 °C. The injection volume was 5µL. Absorbance at 314 nm was detected to measure the concentration of PFD. All results were processed with Empower 3 Chromatography Data Software.

The UHPLC method was validated in terms of linearity, limit of quantification (LOQ), limit of detection (LOD), repeatability and system suitability using above chromatographic condition according to ICH guidelines. The system suitability test was performed. Linearity test solutions were prepared by diluting the standards stock solution. All concentrations were chromatographed, and calibration curves were constructed by plotting average peak area versus concentrations for PFD. LOD and LOQ of PFD were estimated by injecting a series of PFD with known concentration. A signal-to-noise ratio of 3:1 was considered acceptable for estimating the detection limit, and a signal-to-noise ratio of 10:1 was considered acceptable for estimating the quantification limit. Intra-assay precision of the proposed methodology was evaluated by assaying six replicate injections of freshly prepared PFD solution in the same equipment at different concentrations of 100 µg/mL (high concentration), 6.25 µg/ mL (medium concentration) and 0.78

μg/ mL (low concentration). The results of precision were expressed as percentage relative standard deviation (%RSD) of the concentration determined from the calibration curve, and the accuracy was evaluated by the percentage relative error (%Error) at the same concentration levels. The stability of PFD was evaluated at 0h, 2h, 4h, 6h, 10h and 24h in room temperature at different concentrations (100 μg/mL, 50 μg /mL, 10 μg/mL and 1 μg /mL). Each concentration at each time point was chromatographed once. The stability was expressed by calculating the percentage relative error (% Error) to expected concentrations.

3.1.2 Drug loading of exosomes using sonication method

Purified exosomes were mixed with PFD (TCI, America) with the volume ratio of 1:1. The procedure involved sonicating a mixture of the drug and exosomes under the following conditions: an amplitude range of 5% to 25%, for a total of 1 to 4 cycles. Each cycle included 10 seconds of sonication followed by a 60-second cooling period. After sonication, the mixture was incubated at 4 °C overnight to recover the exosomal membrane. Several formulations were prepared as follows:

Table 3.2 Sonication parameters for exosomes formulation optimization.

No.	Sonication Amplitude	Sonication cycles
F1	25%	3
F2	15%	3
F3	5%	4
F4	5%	3
F5	5%	2
F6	5%	1

The size distribution and particles concentration of PFD-loaded exosomes were measured using NTA. Particle recovery was calculated by the following equation:

$$Particle\ recovery(\%) = \frac{Exosomes\ particle\ number\ before\ treatment}{Exosome\ particle\ number\ after\ treatment} x100\%$$

Then, excess free drug was removed by two methods: 1) Exosomes spin column MW 3000 (Invitrogen™) and 2) MagCapture Exosome Isolation Kit PS (Wako, Japan). For removing excess drug with exosomes spin column, the spin column was hydrated and prepared according to manufacturer's instruction. After sonication, 100 µL sample mixture was directly to the center of each gel bed at the top of the columns. The Spin Column was centrifuged at 750g for 2 min at room temperature to collect drug-loaded exosomes that elute within a 1 mL volume, and 5 fractions was collected. The fraction contain drug-loaded exosomes was extracted with acetonitrile and then filtered through a 0.22 µm syringe filter (Millipore, USA) and subjected to UHPLC for PFD quantification and NTA for particles analysis. For removing excess drug with MagCapture Exosome Isolation Kit PS. Briefly, sample mixture was added to the magnetic beads and the mixture was incubated for 3 h on a rotating mixer at 4°C. Subsequently, the beads were washed three times by placing the tubes on a magnetic stand and removing the supernatant. The waste buffers containing free drug was also collected and then filtered through a 0.22 µm syringe filter (Millipore, USA) and subjected to UHPLC for PFD quantification and NTA for particles measurement. PFD-loaded exosomes were eluted by adding 50 µl elution buffer twice. The elute buffer contain drug-loaded exosomes was mixed with acetonitrile (1:1 of volume) and then filtered through a 0.22 µm syringe filter (Millipore, USA) and subjected to UHPLC for PFD quantification. Drug encapsulation efficiency (EE%) was calculated by:

$$EE\%= \frac{Mass\ of\ drug\ initially\ used - \ drug\ in\ waste\ buffer\ and\ wash\ buffer}{Mass\ of\ drug\ initially\ used} x100\%$$

Drug loading efficiency (LE%) was calculated by:

$$LE\% = \frac{Mass\ of\ drug\ encapsulated}{Mass\ of\ drug\ loaded\ exosomes} x100\%$$

3.4 Results

3.1.3 Development and Validation of UHPLC Method for Quantification of Pirfenidone (PFD)

With the mobile phase that contain acetonitrile and 0.2% acetic acid water solution (1:4), all peaks including PFD and unknown component appeared within 3 min and distinctly separated. The peak for PFD displayed at retention time around 1.789 min. However, an unknown substance appeared at retention time of 0.2min. To identify this substance, all buffers which involves in the purification of drug-loaded exosomes process was diluted and inject into UHPLC system and analysed under the same chromatographic condition. The overlay results indicated that the unknown peak (Retention time =0.2 minutes) present in the waste, wash, and lysate buffers coincided with a substance peak in the elution buffer. The elution buffer primarily contains EDTA. Therefore, EDTA, which is consistently present in the drug-loaded sample, does not interfere with the quantification of PFD. A linear relationship was observed between the ratio of the peak area signal of PFD and the corresponding PFD concentration, ranging from 0 to 100 μg/mL, as indicated by the results in Figure 3.2. The correlation coefficient (r^2) exceeded 0.99, demonstrating strong linearity. In terms of precision of quantification, the intra-assay precision (n = 6) at high (100 μg/mL), medium (6.25 μg/mL), and low (0.78 μg/mL). PFD concentrations showed %RSD values of less than 1%, indicating high repeatability of this method for PFD quantification at these levels. The accuracy (%Error) of the method at high and medium concentrations ranged from 1% to -4% of the nominal value of the analyte, which is considered acceptable. However, accuracy at a low concentration (0.78 μg/L) was higher, around -10%. The limit of detection (LOD) and the limit of quantification (LOQ) for PFD were found to be 0.02 μg/mL and 0.07 μg/mL, respectively. Relative error values at 100 μg/mL, 50 μg/mL, 10 μg/mL within 24h were all within -3% to 2%,

indicating PFD compound is stable and show no appreciable degradation within 24h under room temperature at these concentrations. However, at lower concentrations (1 µg/mL), the relative error increased significantly. Overall, the proposed UHPLC method is effective for quantifying PFD, demonstrating excellent system suitability, precision, accuracy, and linearity.

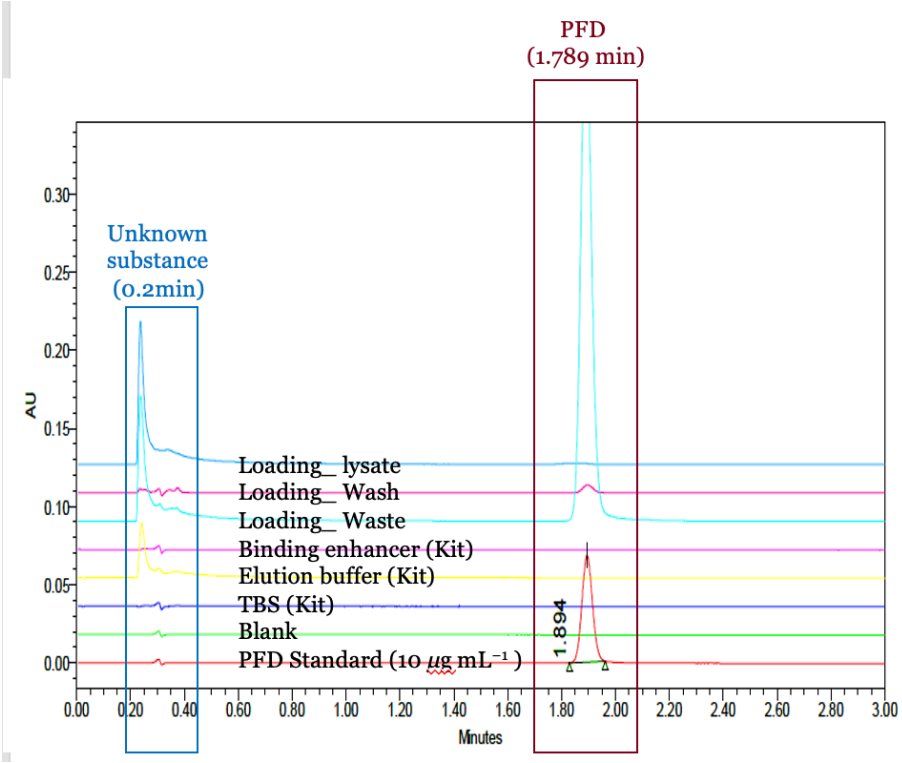


Figure 3.2 System suitability of UHPLC method for PFD quantification.

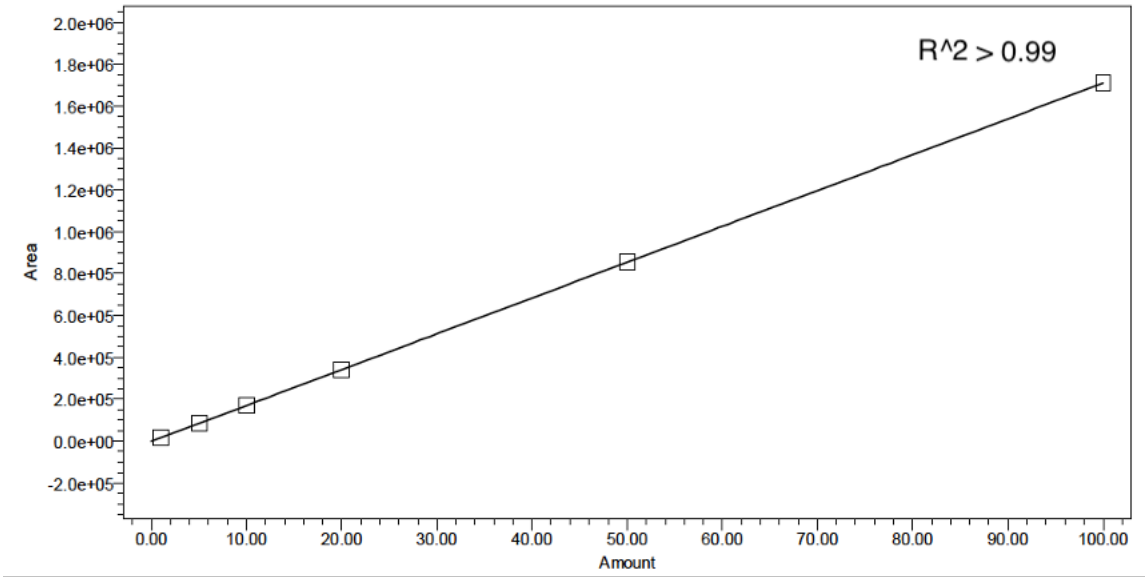


Figure 3.3 Linearity of UHPLC method for PFD quantification.

Table 3.3 Intra-assay precision and accuracy of PFD quantification method

	Mean concentration (µg/mL ±SD)	**%RSD**	**%Error**
High concentration (100 µg/mL)	99.97 ± 0.78	0.78%	-0.03%
Medium concentration (6.25 µg/mL)	6.46 ± 0.02	0.32%	3.32%
Low concentration (0.78 µg/mL)	0.70 ± 0.00	0.62%	-9.63%

Table 3.4 LOQ and LOD of PFD quantification method

Concentration of PFD (µg/mL)	Signal to Noise
0.1	14.5
0.09	13.98
0.08	11.26
0.07	10.48
0.06	9.511
0.05	8.283
0.04	6.250
0.03	4.035
0.02	3.519
0.01	1.732

Table 3.5 Short-term stability of PFD

Concentration of PFD (µg/mL)	%Error					
	0h	2h	4h	6h	10h	24h
100	-0.31%	-0.65%	-0.75%	-0.49%	-0.43%	-0.36%
50	1.32%	0.40%	0.64%	1.27%	1.03%	0.60%
10	-1.98%	-2.35%	-2.36%	-2.12%	-2.22%	1.94%
1	-7.56%	-11.19%	-11.13%	-6.48%	-10.05%	-7.40%

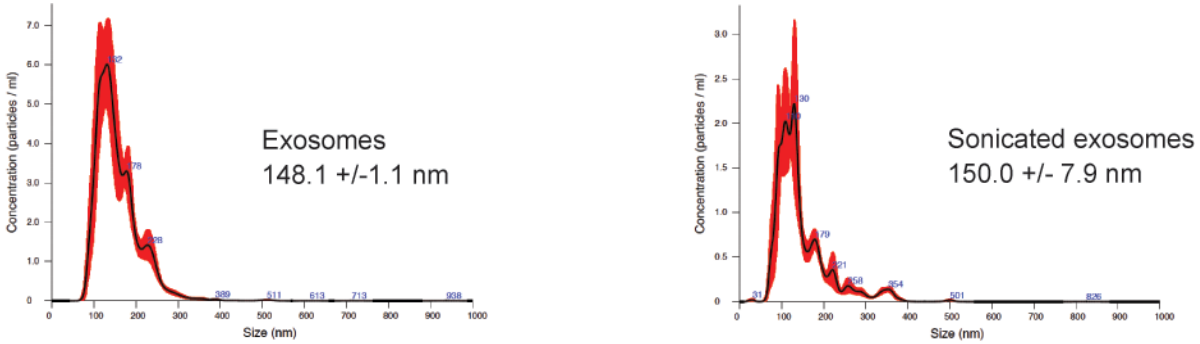
Table 3.6 Summary of UHPLC method for quantification of PFD

UHPLC Parameter	Value
Retention time	1.789 min
Intra-day precision (n=6)	%RSD < ± 1%
Accuracy	%Error < ± 5%
LOD	0.02 µg/mL
LOQ	0.07 µg/mL
Range of linearity	0- 100 µg/mL, R^2>0.99
Short-term stability	Good

3.1.4 Sonication-Based encapsulation of PFD and subsequent purification of PFD-loaded exosomes

Sonication is commonly used to facilitate the incorporation of drugs into exosomes due to its ability to disrupt cell membranes and assist with the loading process. In our study, exosomes were first mixed with of PFD, and an intense sonication condition (25% amplitude, 3 cycles) was initially used to load PFD into the exosomes. NTA showed a negligible increase in the size of particles post-sonication. A significant loss in the exosome particle population following sonication was observed. However, the total number of exosomes decreased to 34% of the original number (Figure 3.4). This reduction indicates that 66% of the exosomes were either disrupted or degraded because of the sonication process. This substantial decrease highlights the impact of sonication on exosome integrity and suggests that the process is disruptive.

A.



B.

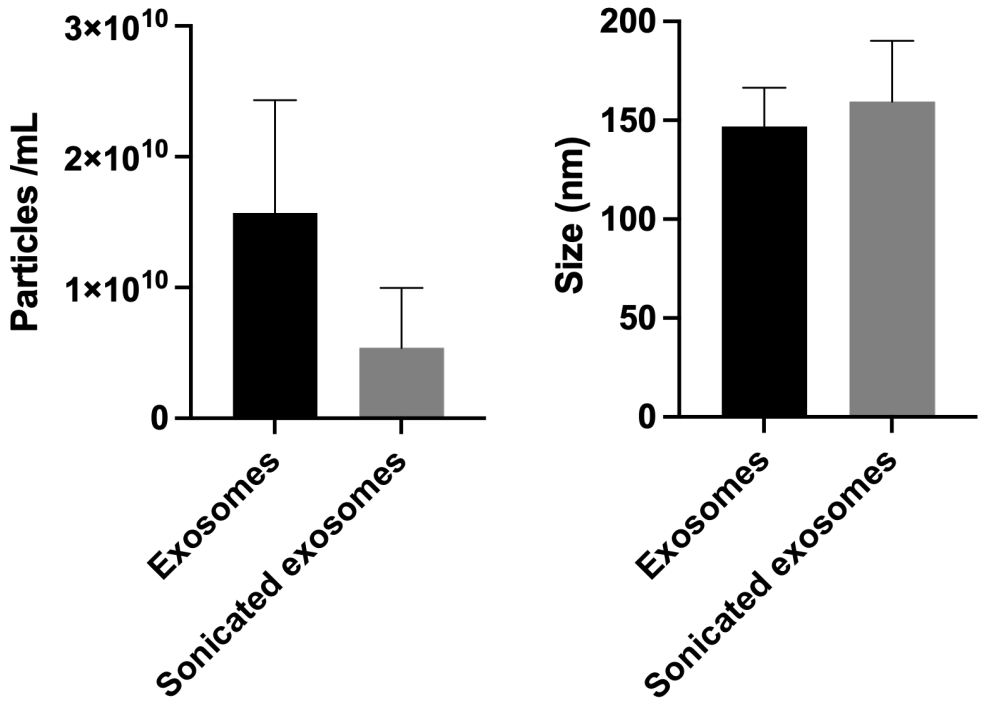


Figure 3.4 Characterization of exosomes and sonicated exosomes. (A) Size distribution of exosomes. (B) Particle concentration of exosomes and sonicated exosomes. Values represent the mean ±SD, n=3.

3.1.5 Comparative analysis of exosome recovery and drug removal methods

To purify PFD-loaded exosomes, Exosome Spin Columns (MW3000) was initially employed to quickly remove low molecular weight components such as buffer elements, salts, nucleotides, and short oligonucleotides from exosome preparations. In this instance, this method was employed to remove unincorporated drug (PFD) from PFD-loaded exosome preparations. Under NTA analysis, the particle sizes distribution of fractions 1 to 5 were similar those of the exosomes, measuring 152.4 nm, 139.1 nm, 149.9 nm, 1754 and 163.4nm, respectively, indicating the presence of exosomes in these fractions. The initial concentration of exosomes was 10^{10} particle/mL. After sonication and purification using Exosome Spin Columns, the concentration analysis revealed that Fraction 1 had the highest exosome particle concentration, measuring 10^{9} particle/mL. This was slightly higher compared to Fractions 2 through 5, each of which had a concentration of 10^{8} particles/mL. Therefore, the particle yield of PFD-loaded exosomes was substantially low, with only 12.04% of the original exosome population retained in Fraction 1, and even lower yield in Fractions 2 through 5 (3.04%, 1.38%, 1.86%, and 3.17%, respectively). PFD-loaded exosomes were possibly trapped in Exosome Spin Column, induce a loss of exosomes particles during purification. Overall, the result indicate that Exosome Spin Column showed low efficiency (21.49% of initial exosomes) for drug removal and resulted in reduced yield and sample dilution.

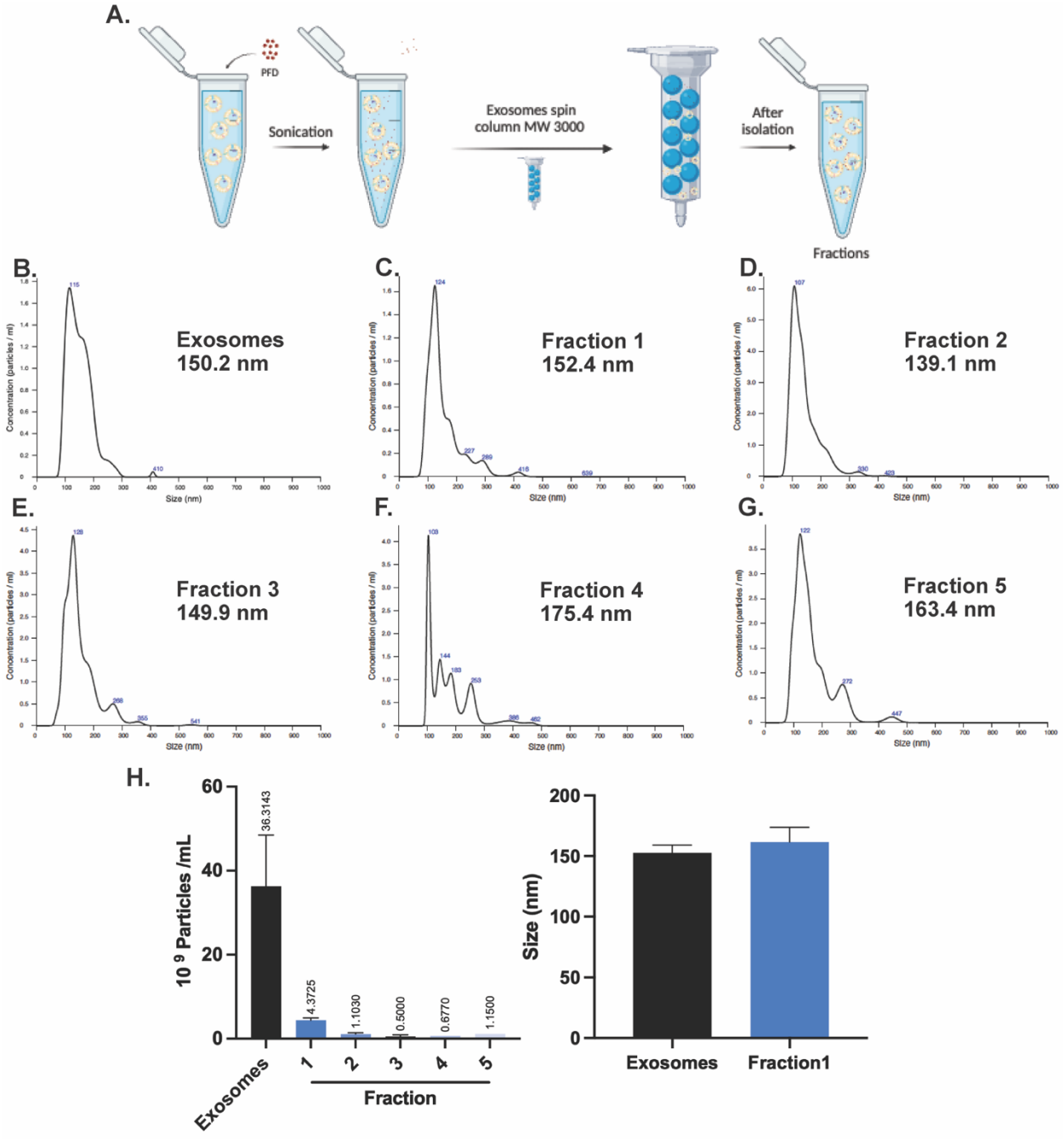


Figure 3.5 PFD-loaded exosomes purified with exosomes spin column. (A). Illustration of Exosome Spin Column purification method of PFD-loaded exosomes. Created with biorender.com (B-G). NTA analysis of exosomes and all fractions. (H) Characterization of exosomes purified with Exosome Spin Column. Values represent the mean ±SD, n=4.

To enhance the yield of PFD-loaded exosomes, an alternative purification method called MagCapture Exosome Isolation Kit was utilized. This approach employs magnetic beads to separate free drug from PFD-loaded exosomes, as only PFD-loaded exosomes bind to the beads. PFD-loaded exosomes were expected to elute from the beads, followed by washing the beads for three times. During these washes, 3 fraction that contain any free drug were also collected separately for analysis. NTA analysis showed only the elute showed a particle population with a relatively homogenous distribution, though with an increased size of around 180 nm. In contrast, the waste fractions 1 to 3 contained particles that were either significantly smaller or larger and exhibited a highly variable size distribution. The initial concentration of exosomes was 10^{10} particle/mL. After sonication and purification using Magcap, the concentration analysis revealed that the elute had high exosome particle concentration (10^9 particle/mL). NTA analysis indicated that the PFD-loaded exosomes were predominantly present in the elute. The particle yield in the elute was approximately 27.19% of the original exosome population as shown in Figure 3.6 F. This suggests that Magcapture Exosome Isolation improved the yield of the PFD- exosomes compared to the Exosome Spin Column method (20.14%). Additionally, unlike the Exosome Spin Column, Exosome Isolation did not cause sample dilution.

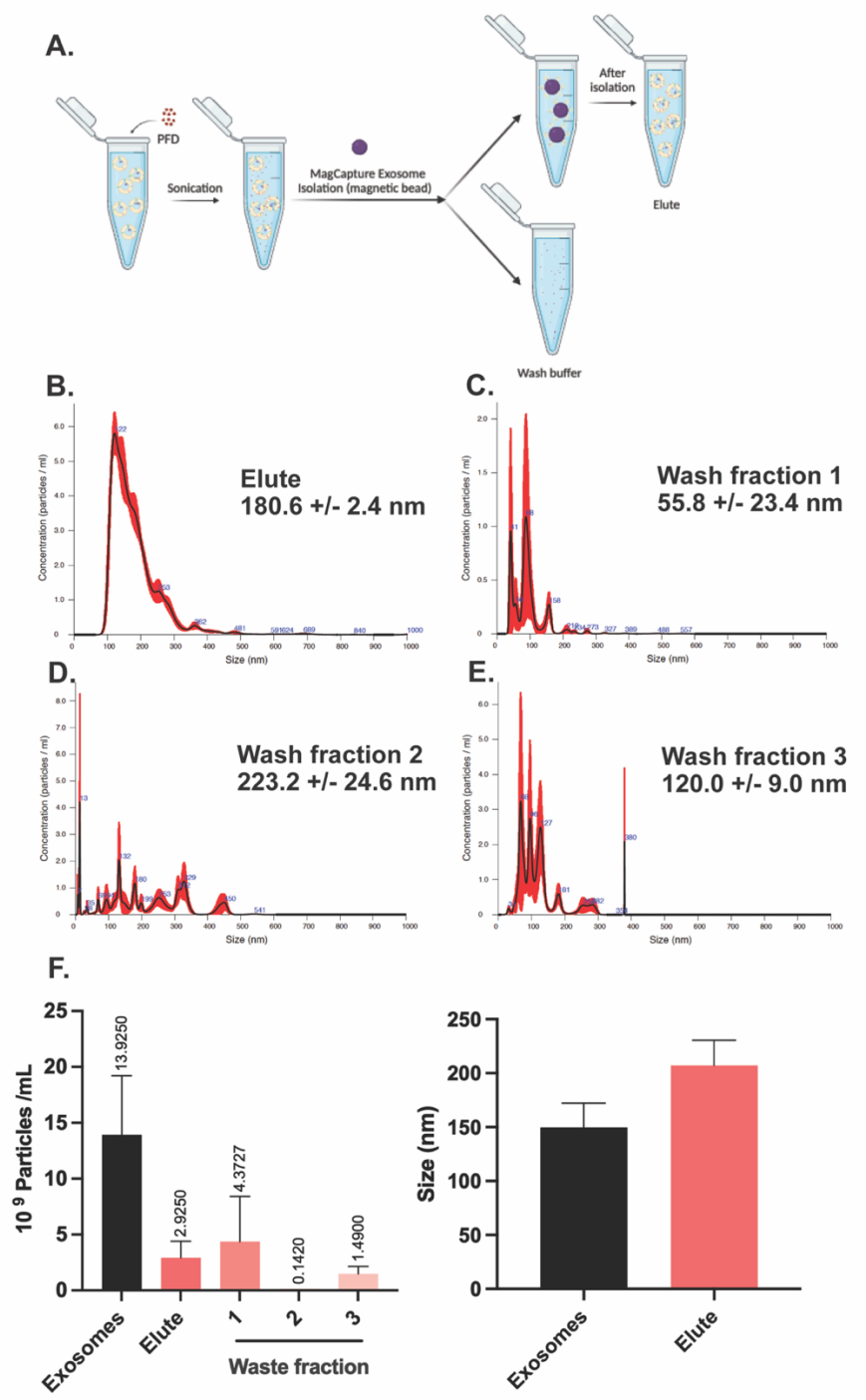


Figure 3.6 PFD-loaded exosomes purified with Magcapture Exosome Isolation method. (A). Illustration of Magcapture Exosome Isolation method of PFD-loaded exosomes. Created with biorender.com (B-E). NTA analysis of exosomes elute and all wash fractions. (F) Characterization of exosomes purified with Magcapture Exosome Isolation method. Values represent the mean ±SD, n=4.

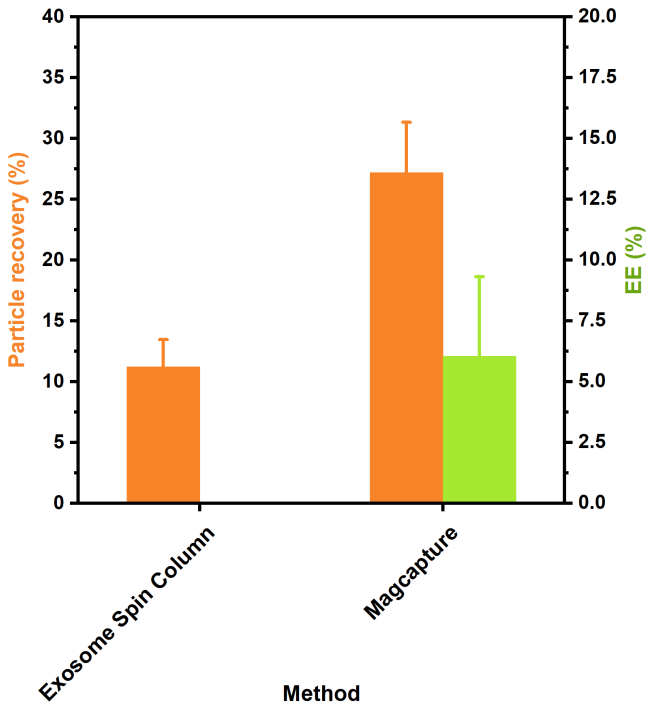


Figure 3.7 Comparison of particle recovery rates and EE% of PFD-loaded exosomes between the Magcapture Exosome Isolation method and the Exosomes Spin Column method. Values represent the mean ±SD, n=4.

Figure 3.7 shows that the Magcapture Exosome Isolation method achieved a particle recovery rate of 27.2% ± 4.2%, higher than the 21.49% obtained with the Exosomes Spin Column method. Additionally, the Magcapture method demonstrated an encapsulation efficiency of 5.50% ± 3.09%, while the Spin Column method showed no detectable encapsulation. This low yield of particle numbers from the Spin Column method explains the lack of measurable drug encapsulation in the exosomes, as the reduced quantity was insufficient to carry a significant amount of drug. These findings suggest that the Magcapture Exosome Isolation method is more

effective for both recovering exosome particles and separating free drug from PFD-loaded exosomes.

3.1.6 Optimization of sonication method for encapsulating PFD into exosomes

Although the drug was detectable after sonication and Magcapture Exosome Isolation of PFD, the overall EE was low. This possibly resulted from high-power sonication, which caused irreversible deformation of the exosomes. The sonication parameters were further optimized through hit and trial method by evaluating particle size, particle recovery (% of the original number of exosomes), EE% and LE% of drug loaded exosomes.

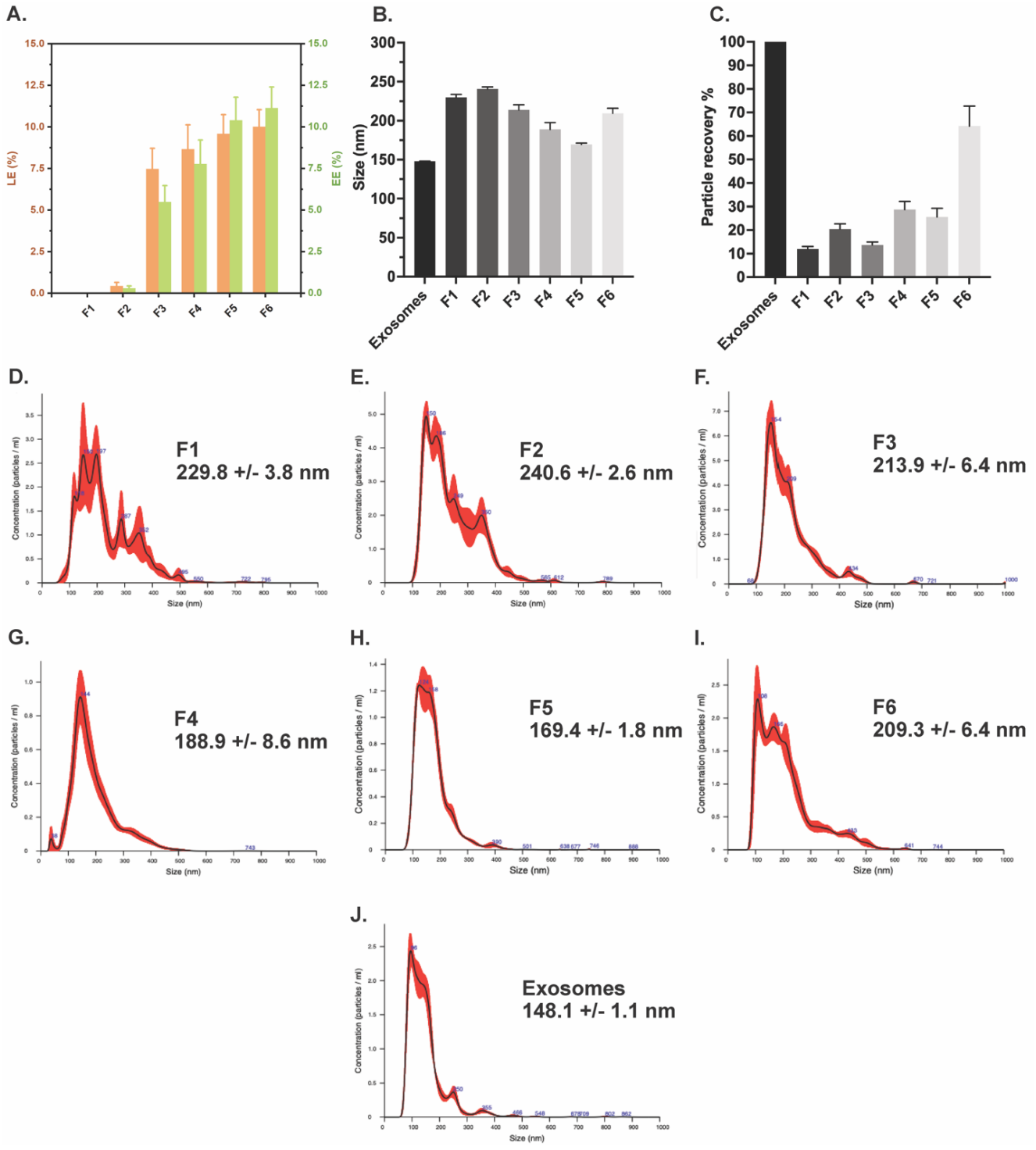


Figure 3.8 Effects of sonication parameters on exosome formulation. (A) EE% and LE% of PFD in exosomes. (B) Average size of PFD- exosome formulations. (C) Particle recovery percentage of exosomes following drug encapsulation. (D-J) Size distribution of all formulations and exosomes. Values represent the mean ±SD, n=3.

Sonication amplitude was used as a variable from 5 % to 25 % (F1, F2 and F4) with constant sonication time and cycles. Low sonication amplitude was effective for encapsulating PFD, achieving EE of 7.780±1.432% and LE of 8.670±1.460% in formulation F4. In contrast, formulations F1 and F2 showed minimal encapsulation, with F2 recording 0.300% EE and 0.441% LE, while F1 had no detectable encapsulation. These results suggest that medium to high sonication amplitudes are linked to reduced drug encapsulation. Regarding particle recovery, F1 exhibited the lowest recovery at 11.973%, compared to F4 at 28.736% and F2 at 20.461%. This indicates considerable exosome loss with increased sonication amplitude. As sonication amplitude increased, the size of the PFD-exosome particles also increased, with measurements of 229.8±3.8nm for F1, 240.6 ±2.6 nm for F2, and 188.9±8.6 nm for F4. However, this increase in amplitude also led to greater heterogeneity in the PFD-exosome size distribution.

Evaluating the impact of sonication cycles at low amplitude revealed that fewer cycles enhance drug encapsulation. Formulation F6, which underwent only 1 cycle, achieved the highest EE of 11.136% ± 1.267% and LE of 10.012% ± 1.026%. This exceeded that of F5, which had 2 cycles (10.406% ± 1.382% EE and 9.586% ± 1.152% LE), F4 with 3 cycles (7.780% ± 1.432% EE and 8.670% ± 1.460% LE), and F3 with 4 cycles (5.495% ± 0.987% EE and 7.477% ± 1.244% LE). Additionally, F6 demonstrated the highest particle recovery, retaining 64.213% of the initial exosome particles, which was significantly greater than F5 (25.543%), F4 (28.74%) and F3 (13.694%). After drug encapsulation, there was a noticeable increase in exosome size across formulations F3 to F6. Specifically, F3 (213.9 ± 6.4 nm) and F6 (209.3 ± 6.4 nm) were larger compared to the sizes observed in F5 (169.4 ± 1.8 nm), F4 (188.9 ± 8.6 nm). Overall, formulation F6 was identified as the optimal formulation, balancing relatively high EE with high particle recovery.

3.5 Discussion

The feasibility of exosomes as drug delivery carrier is often retrained by upstream low exosome production and downstream poor drug encapsulation. Improving both drug encapsulation in exosomes and stability of drug-loaded exosomes has been much challenged to enable the better drug delivery to the specific targeted cells. This chapter aims to address this issue by investigating a workflow for actively encapsulating PFD into exosomes and optimize factors (including drug removal method and sonication parameter) that impact drug encapsulation.

The efficiency of drug encapsulation into exosomes is significantly influenced by the compound's hydrophilicity or hydrophobicity, as well as the loading techniques. Hydrophobic compounds typically show higher EE than hydrophilic compounds[152,169]. Because of the lipidic nature of the exosomal membrane, hydrophobic compounds interact more effectively with the hydrophobic tails of exosome[163]. However, drugs such as curcumin[172,173], PTX[154,160,167] and berberine[171], which are hydrophobic, often show low encapsulation into exosomes when using passive drug-loading methods. PFD is a very hydrophobic compound (log P = 2.14), so in order to enhance drug encapsulation, temporary permeabilization of the exosome membrane is necessary. This can be achieved through sonication, which creates pores in the lipid bilayer of exosomes and facilitates the encapsulation of small molecule drugs that have limited membrane diffusion[178]. However, sonication can disrupt exosomal membrane and negatively impact exosome structure, affecting their shape, size distribution, membrane integrity, and cellular uptake[178,179] . Our findings confirmed that under intense sonication condition (25% amplitude, 3 cycles), a slight increase in exosomes particle size but significantly reduced the exosome population by 66%. This reduction, consistent with previous studies[180], is likely due to fragmentation or degradation from the intense sonic waves. Sonication damages the membrane integrity of exosomes, resulting in a lower yield

of intact exosomes and significantly reducing the number available for drug delivery in this study. Therefore, sonication protocols must be carefully optimized to reduce exosome rupture and maintain a sufficient number of exosomes to carry drug.

After using sonication to encapsulate PFD into exosomes, removing unloaded drugs after the loading process using various purification techniques is essential. This chapter compares drug removal methods based on the particle size, particle recovery and EE% of drug-loaded exosomes. Exosome Spin Column rapidly purified PFD-loaded exosomes while preserving exosomes size. However, the results also indicated a considerably low yield of PFD-loaded exosomes, recovering maximal 20.14% of the original exosome particles. The low yield is likely due to many particles were retained in the column, leading to a loss of PFD-loaded exosomes during the purification process. Furthermore, this method caused sample dilution by separating PFD-loaded exosomes into different fractions (5 fraction with 1ml in each fraction), which further reduced their yield. The significant loss of PFD-loaded exosomes particle explains the undetectable drug encapsulation efficiency. In comparison, the MagCapture Exosome Isolation method significantly improves the yield of PFD-loaded exosomes, recovering approximately 27.2% ± 4.2% of the original exosome population. Additionally, the Magcapture method showed some EE at 5.0% ± 2.3%, whereas the Spin Column method exhibited no detectable encapsulation efficiency. Unlike the Exosome Spin Column, MagCapture Exosome Isolation does not cause sample dilution. EE% was detectable but still consider low. These results indicate that the Magcapture Exosome Isolation method is more effective in both recovering exosomes particles and separating free drug from drug-loaded exosomes.

To maximize drug encapsulation, it is crucial to carefully optimize the sonication parameters, which involves adjusting the amplitude and number of cycles to minimize potential

damage to the exosomes. The particle size, particle recovery (%), drug EE (%) and LE (%) of PFD-loaded exosomes was firstly optimized using a hit-and-trail approach. Sonication amplitude was used as a variable from 5 % to 25 % with constant sonication cycles (F1, F2 and F4). The results showed that increasing the sonication amplitude led to a larger average particle size for PFD-loaded exosomes, but also significantly altered the size of exosomes and induced a more heterogenous distribution. Our data indicated that minimal sonication amplitude is optimal for PFD encapsulation, achieving a particle recovery rate of 28.740%, an EE of 7.780%, and a LE of 8.670% for formulation F4. In contrast, the highest sonication amplitudes appeared to cause greater damage to exosomes, leading to reduced particle number to 11.970% and a non-detectable EE and LE. Further, the optimization of sonication cycles at low amplitude (Formulations F3 to F6) indicates that reducing the number of sonication cycles significantly double drug EE from 5.50 % to 11.14%. This improvement is likely due to fewer sonication cycles causing less disruption to the exosome structure and increase drug encapsulation, which was supported by the observed increase in particle recovery from F3 to F6. Another assumption is the exosomal membrane gets more disorientated when increasing sonication, which may limit the availability of the surface required for binding hydrophobic drug[169]. Although increasing the number of sonication cycles did not create a highly variable size distribution, there was a noticeable increase in exosome size across formulations F3 to F6 after drug encapsulation. This increase in exosome size is consistent with previous studies, which also reported a significant rise in particle size after encapsulating drugs including paclitaxel in glioblastoma-derived and macrophages-derived exosomes[154]. Among all formulations, F6, produced with the lowest sonication amplitude and fewest cycles, was optimal, achieving the highest EE of 11.136% ± 1.267%, LE of 10.012% ± 1.026%, and the best particle recovery rate of 64.213% ± 8.490%. In subsequent chapters, F6 will be referred to as the PFD-

exosomes. In conclusion, the findings emphasize the importance of using mild sonication to improve both drug encapsulation and particle recovery in exosome formulations.

3.6 Conclusion

In conclusion, this chapter systematically optimized the formulation for encapsulating PFD into exosomes, focusing on evaluating drug removal methods and sonication parameters to improve drug encapsulation efficiency, loading efficiency, and overall exosome yield. Our comparison of purification techniques highlights that the MagCapture Exosome Isolation method is significantly superior to the Exosome Spin Column method in recovering drug-loaded exosomes. Our findings indicated that the application of sonication must be carefully controlled to prevent damage to exosomal integrity. Specifically, optimizing sonication conditions—by using lower amplitudes and fewer cycles—led to notable improvements in both drug encapsulation and exosome recovery. Formulations F6 showed the optimal encapsulation with an EE of 11.14% ± 1.27%, a LE of 10.01% ± 1.03%, and the highest particle recovery rate of 64.21% ± 8.49%. These insights provide valuable strategies for enhancing exosome-based drug delivery systems, ultimately facilitating more effective therapeutic applications.

Chapter 4 *In Vitro* and *In Vivo* Assessment of Human Dermal Fibroblast-Derived Exosomes and Pirfenidone- exosomes for Scarless Tissue Repair in Wound Healing

4.1 Overview

Dermal fibroblasts are essential for wound healing because they regulate collagen metabolism and the remodeling of the extracellular matrix (ECM). Strategies that focus on optimizing these fibroblasts' functions, particularly their ability to synthesize and degrade collagen, aim to improve healing outcomes and minimize scar formation. In pursuit of effective anti-scarring strategies, pirfenidone (PFD), an FDA (Food and Drug Administration)-approved anti-fibrotic agent, emerges as a promising candidate due to its ability to regulate collagen dynamics. Although PFD has shown efficacy in reducing hypertrophic scars, its instability poses challenges for cellular delivery. To address this, we have proposed loading PFD into exosomes derived from dermal fibroblasts, hypothesizing that these natural carriers can enhance intracellular delivery and therapeutic efficacy. The study revealed that exosomes from human dermal fibroblasts enhance fibroblast migration and proliferation through an autocrine mechanism, suggesting their potential as a cell-free therapy for wound healing. Notably, this research is the first to show that exosomes can serve as effective drug carriers for PFD, improving its anti-fibrotic properties *in vitro* and *in vivo*. *In vivo* experiments demonstrated that PFD-exosomes accelerate healing and organized the ECM in repaired tissues by reducing excessive collagen buildup. Specifically, they reduced the expression of Pro-Collagen I alpha 1 and TIMP-1 while increasing MMP-1 production in dermal fibroblasts. By regulating fibroblast activity and collagen metabolism, PFD-exosomes effectively minimized excessive ECM deposition, presenting a promising strategy for enhancing wound healing and reducing fibrotic scarring.

Keywords: Exosomes, Wound Healing, Fibroblast Migration and Proliferation, Collagen Metabolism

4.2 Introduction

Dermal fibroblasts represent the main organizers in wound repair by modulating the synthesis and degradation of proteins in ECM[23]. They are primarily responsible for producing collagen—the predominant structural protein in the ECM that provides mechanical support and integrity to both healthy skin and scar tissues[181]. More than 20 subtypes of collagen have been identified, with collagen type I composing about 70–90% of the total collagen in human skin. When a wound heals, it typically forms a normotrophic scar, which appears flat and slightly raised but remains within the boundaries of the original wound. Normotrophic scars exhibit increased collagen synthesis compared to normal skin, with collagen fibers packed more closely and less loosely[181]. Hypertrophic and keloidal scars show even predominantly increases in collagen synthesis, leading to abnormally thicker collagen bundles[182]. These scars appear raised above the skin's surface and often present with a reddish or darker color compared to the surrounding skin. Overall, the presence of all scar types reflects abnormal collagen composition and organization, leading to an unideal wound-healing outcome[24]. Therefore, strategies that regulate dermal fibroblast activity and specifically target collagen synthesis are essential for reducing scar formation during healing.

Fibroblasts also control collagen degradation through their secretion of enzymes known as matrix metalloproteinases (MMPs), which break down most structural components of ECM[183]. Specifically, MMP-1 and MMP-8 preferentially cleave collagen type I. Given the significant impact of MMP activity on healing, their function is stringently regulated at multiple levels including gene expression, protein secretion, extracellular activation upon their release, and finally through the inhibition by tissue inhibitors of metalloproteinases (TIMPs)[184]. TIMPs, natural inhibitors of MMPs produced by fibroblasts, bind specifically to MMPs, sterically blocking their

active site in a one-to-one stoichiometry. Together, MMPs and TIMPs balance the dynamic process of collagen degradation, impacting ECM remodeling and overall healing outcome. Although MMPs are essential for regular repair, the imbalance between MMPs and TIMPs during the wound healing process leads to complications, such as keloid scar formation[185]. Interestingly, mammalian fetuses exhibit scarless tissue repair due to a unique expression profile with higher MMP levels and lower TIMP levels, which supports effective wound healing with minimal scarring. Given the significant impact of the balance between MMPs and TIMPs on healing outcomes, targeting fibroblasts based on their production of these proteins could be an effective strategy for managing collagen degradation. Therefore, approaches that regulate fibroblast activity and focus specifically on collagen degradation through MMPs and TIMPs are essential for reducing scar formation and promoting scarless healing.

In response to the need for effective scarless wound healing, developing an anti-scarring treatment that modulates dermal fibroblast activity appears to be a practical strategy. Pirfenidone (PFD), an FDA-approved compound with broad anti-fibrotic properties, has demonstrated a potential solution in this regard. PFD primarily targets fibroblast cells and prevents scarring *in vitro* and *in vivo* by regulating collagen production and fibril assembly[186]. In normal human dermal fibroblasts, PFD inhibits the fibrogenic signals of TGF-β1 by disrupting intracellular p38-mediated MAPK activation, regulating the transcription of profibrotic genes, and blocking myofibroblast differentiation[1]. For instance, a topical gel containing 8% PFD applied over six months has resulted in significant regression of hypertrophic scars in pediatric patients[188]. Moreover, PFD-loaded spray dressings have been associated with effective scar prophylaxis, likely due to their regulation of collagen synthesis and degradation involving key cytokines like MMP-1[189]. However, PFD is very hydrophobic (log P = 2.14) and has a low molecular weight (185 g/mol). These properties allow

PFD to interact with multiple molecular targets and cell types. For example, PFD inhibits cellular proliferation and migration in both normal and keloid-derived keratinocytes[190]. To further enhance the effectiveness of PFD and targeting fibroblasts, it has been encapsulated in cerium oxide nanocapsules to protect it against reactive oxygen species (ROS) and achieve efficient intracellular delivery. This process reduces ROS and TGF-β levels while improving collagen fiber arrangement and proportion[191]. However, in this study PFD's small molecular weight and instability in the presence of intracellular ROS pose challenges for effective cellular delivery. An alternative approach is to load PFD into dermal fibroblasts- derived exosomes. We hypothesize that these natural carriers can facilitate intracellular delivery to dermal fibroblasts, potentially enhancing PFD's therapeutic effectiveness in modulating fibroblast activity *in vitro* and ultimately promoting scarless wound healing *in vivo*.

In the previous chapters, we successfully isolated high-purity exosomes and encapsulated the anti-fibrotic compound PFD into exosomes. This chapter further investigates the effects of exosomes and PFD-exosomes on dermal fibroblasts functions, including their proliferation, migration, and the modulation of collagen synthesis and degradation *in vitro*. Subsequently, the effects of exosomes and PFD-exosomes was evaluated *in vivo* using a full-thickness wound model to evaluate their efficacy in promoting wound healing and scarless tissue repair.

4.3 Materials and methods

4.3.1 *In vitro* cellular uptake of fluorescent-labeled exosomes by dermal fibroblasts

Exosomes were stained with different fluorescent dyes including 10 μM DiI and 8 μM PKH26 dye (PKH26 Red Fluorescent Cell Linker Kit, Sigma, PKH26GL) to identify the optimal dye for exosomes labelling. Briefly, 100 μL of exosome samples with 10^9 particles/mL concentration were labeled with 100 μL dye solution. The mixture was incubated for 20 minutes while rotating at room temperature. Excess dye was removed by Exosome Spin Columns (Invitrogen™, Thermo Fisher Scientific) according to the manufacturer's instruction. Dye solutions was also loaded on Exosome Spin Columns, and the elutes from the column served as a negative control group. Dermal fibroblasts directly stained with dye also served as a positive control. Dermal fibroblasts were seeded in a 96-well plate at a density of 3000 cells/well and incubated at 37°C for 24 h. After rinsing the cells three times with PBS, each well was treated with a mixture of 100 μL labeled exosomes and 100 μL of complete EMEM for up to 24 hours. The cells were then labeled with 300 nM 4′,6-diamino-2-phenylindole (DAPI, Invitrogen™, Thermo Fisher Scientific) for 10 minutes. Cellular uptake was imaged by fluorescence microscope (EVOS® FL Auto Imaging System, Thermo Fisher Scientific).

4.3.2 *In vitro* MTS assay

Here, *in vitro* MTS assay is a colorimetric method used to assess cell viability and proliferation based on the metabolic conversion of MTS into a formazan product by viable cells. Briefly, dermal fibroblasts were seeded in a 96-well microplate in complete EMEM at a density of 4000 cells/well (100 μL per well) and incubated at 37°C in 5% CO_2 overnight to achieve 80%-90% confluency. After 24h, the cell culture medium was removed and treated with 200 μL positive,

negative, and treatment groups. The treatment group were different dose of PFD, exosomes, and PFD- exosomes diluted in EMEM (Wisent, 320-030-CL) to achieve 200 µL total volume. Cells cultured in EMEM alone were used as a negative control. Cells treated with 1% (v/v) Triton X-100 were used as a positive control. After exposure to the control and treatment group, cells are incubated at 37°C, 5% CO_2 for 12h and 24h. Cell viability of exosomes and PFD-exosomes to dermal fibroblast cells were then determined using the MTS assay (CellTiter 96 AQueous one solution cell proliferation assay, Promega) following the manufacturer's instruction with minor modification. Briefly, 20 µL CellTiter 96 AQueous one solution was diluted in 200 µL in phenol red -free EMEM (Wisent, 320-030-CL) in each well. Microplates were incubated at 37°C for 2h in a humidified, 5% CO_2 atmosphere, and the absorbance at 490nm was then measured using a 96-well microplate reader (Varioskan LUX, Thermo Fisher Scientific). The amount of 490nm absorbance is directly proportional to the number of living cells in the culture. Relative cell viability was calculated by the following equation:

$$\%\ Relative\ cell\ viability = \frac{Abs\ 490nm\ in\ treatment\ group - Abs\ 490\ nm\ in\ blank}{Abs\ 490nm\ in\ negative - Abs\ 490nm\ in\ blank} x\ 100\%$$

4.3.3 *In vitro* scratch assay

The effect of exosomes and PFD-exosomes on fibroblast migration was tested by *in vitro* scratch assay on human dermal fibroblasts, as previously described[192]. Dermal fibroblasts were seeded in a 24-well plate in complete EMEM at a density of 50,000 cells/well and incubated at 37°C to achieve 90% confluence before treatment. Cells were serum-starved for 12h before creating scratches on cell monolayer. An artificial scratch gap was created on the cell monolayer by a sterile 10µL pipet tip, and cell debris was removed by washing with PBS twice. Cell culture medium was removed and treated with 1000µL positive, negative, and treatment groups. Cells

cultured in serum-starved medium were served as a negative control, and cells cultured in a serum-rich medium served as positive controls. 100μL exosomes and PFD- exosomes were added to 1900μL serum-starved medium to achieve a final concentration of $5x10^8$ particles/ml. After 24h, cells were labeled with 8 μM PKH26 dye and incubated for 45 min. The adherent cells were washed with PBS twice after the removal of excess PKH26 dye. The image of cell migration was captured to evaluate the closure rate. Fluorescent images of the *in vitro* wounds were taken at 0, 12, and 24 h with a fluorescent microscope (EVOS FL Auto Imaging System, Thermo Fisher Scientific). The extent of cell migration was determined by measuring the area of scratch gap closure by ImageJ software. The percentage of migration was calculated by the following equation:

$$\% \, Migration = \frac{Initial \, scratch \, gap \, area - scratch \, gap \, area}{Initial \, scratch \, gap \, area} \, x \, 100\%$$

4.3.4 *In vitro* COL1A1 gene expression of dermal fibroblasts

In order to study how exosomes and PFD-exosomes modulate multiple ECM-related gene expression, Dermal fibroblasts were seeded in 12 well plates at a density of 20,000 cells/ well and grown at 37°C for 48h in complete EMEM. Cells were exposed to exosomes, PFD-exosomes for 48h. Total RNA of treated cells was isolated with E.Z.N.A.® Total RNA Kit I (Omega Biotek) post-treatment according to the manufacturer's instruction. RNA amount and purity of samples was measured using NanoDrop 1000 (ThermoFisher). 0.4 μg total RNA was used as a template to convert to cDNA. The expression of target genes COL1A1 (collagen type I alpha 1, Hs00164004_m1 was analyzed by quantitative real-time PCR with TaqMan® RNA-to-C_T™ 1-Step Kit and Assays-on Demand Gene Expression probes (Applied Biosystems) following the manufacturer's instruction with minor optimization. qRT-PCR reactions were performed on 96 well plates with 20 μL volumes for each reaction. All samples were analyzed in triplicate in an

individual study. Thermal cycling conditions are displayed in Table 4.1. Products were detected with the Applied Biosystems™ StepOnePlus™ Real-Time PCR System. Expression of each target gene in all control and treatment groups was normalized to housekeeping genes GAPDH (glyceraldehyde 3-phosphate dehydrogenase, Applied Biosystems, Hs02786624_g1). Quantitative PCR data were expressed as "fold changes" relative to control levels.

Table 4.1 Optimal PCR reaction formulation for gene expression analysis

Component (Life Technologies Gene Expression Assays)	Volume for Each Reaction (µL)
TaqMan ®RT-PCR Mix (2x)	10
TaqMan ®Gene Expression Assay (20x)	1
TaqMan ®RT Enzyme Mix (40x)	0.5
RNA template (0.4 µg) diluted in RNase-free H2O	8.5
Total Volume	20

Table 4.2 Optimal PCR reaction program

Step	Temperature	Time	Cycles
Reverse transcription	48°C	15 minutes	1
Enzyme activation	95°C	10 minutes	1
Denature	95°C	15 seconds	40
Anneal/extend	60°C	1 minute	

4.3.5 *In vitro* protein expression of dermal fibroblasts treated with exosomes and PFD-exosomes

Dermal fibroblasts were seeded in 12 well plates at a density of 20,000 cells/ well and grown for 48h in complete EMEM. Cells were treated with exosomes, PFD-exosomes, for 12h.

Supernatants from cell cultures were collected and analyzed for TIMP-1, MMP-1, and Pro-Collagen I alpha 1 concentration using sandwich-type ELISA assays (R&D Systems) following the manufacturer's instructions with minor optimization. Briefly, 96-well microplates were pre-coated with 100µL per well of the optimal concentration of diluted capture antibodies and incubated overnight at 4 °C. The plate was washed three times with wash buffer and then blocked by 300 µL Reagent Diluent for 1h at room temperature. The plate was washed three times again with wash buffer before loading 100 µL standards and samples. Samples were then incubated at room temperature for 2h. After that, the plate was washed three times again with wash buffer and was incubated with 100 µL per well of the diluted detection antibodies at room temperature for 2h. 100 µL per well of the Streptavidin- HRP (diluted to 1:40) was added to each well and incubated at room temperature for 20 minutes, avoiding direct light. After washing the plate again with wash buffer, 100 µL of substrate solution was added to each well and incubated for 20 minutes to develop the color. 50 µL Stop Solution was added to stop the reaction. The absorbance was immediately determined by a microplate reader (Varioskan LUX, Thermo Fisher Scientific) set to 450 nm and corrected by 570 nm.

Table 4.3 Optimal ELISA antibodies and antigens concentration

	Pro-Collagen I alpha 1	**MMP-1**	**TIMP-1**
Capture antibody	4 µg /ml	800 ng/ml	2 µg /ml
Detection antibody	100 ng/ml	125 ng/ml	50 ng/ml
Range of detected antigen	31.3 pg/ml to 2000 pg/ml	62.5 pg/ml to 4000 pg/ml	31.3 pg/ml to 2000 pg/ml

4.3.6 *In vivo* wound healing model

The animal protocol for *in vivo* study was approved by the Animal Care Committee at University of Waterloo. 5 to 8 week-old SKH-1 hairless male mice were purchased from Charles River Laboratories (QC, Canada). Upon their arrival, all mice were kept in standard conditions with free access to food and water. Donut-like splint rings are prepared by cutting from a 0.5-mm-thick silicone sheet. (Inner diameter 6 mm, outer diameter 15 mm, thickness 0.5 mm). On the day of surgery, mice were anesthetized with 2% isoflurane. The dorsal skin of the back from the midline was pulled with fingers. It was punched through the folded skin (both layers) with a 5mm diameter sterile single biopsy punch to create two symmetrical full-thickness excisional wounds beside the midline that extend through the subcutaneous tissue. A 3M Vetbond tissue adhesive was spread on one side of the donut-like splint rings and the rings was carefully placed around the wound with the glue side facing down so that the wound was centered within the ring. All treatments, suspended in PBS, were administered topically by pipetting the solution into the center of the ring.

The sample size for this animal study was determined using G*Power software, focusing on t-tests within the "Means: Difference between two independent means (two groups)" test family. Employing an "A priori: Compute required sample size-given α, power, and effect size" type of power analysis, the parameters chosen included an error probability (α) of 0.05 and a power of 0.95 with one tail. An equal sample size in both groups (n1=n2) was assumed. The effect size, derived from previous studies, was assumed to be 2, indicating a substantial difference. Specifically, a 20% difference in the percentage of wound closure was considered relevant, with a standard deviation estimate of 10%[193,194]. Consequently, the estimated sample size for each group was determined to be 7 mice per group.

In the low dosage group, animals were randomized into three groups and received treatments as follows:

Group 1: Exosomes = 4 mice. Where 2 wounds were made on the back of each mouse, one wound was treated with exosomes and one wound was served as the control (PBS treatment) (n=4). 100 μg exosomes in 15μL PBS was daily administrated on Day3, Day 5 and Day7 to make a total dose of 300 μg exosomes treatment to the wound.

Group 2: PFD-exosomes = 4 mice. Where 2 wounds were made on the back of each mouse, one wound was treated with PFD-exosomes and one wound was served as the control (PBS treatment) (n=4). 100 μg PFD- exosomes in 15 μL PBS was daily administrated on Day3, Day 5 and Day7 to make a total dose of 300 μg PFD-exosomes treatment to the wound.

Group 3: PFD = 4 mice. Where 2 wounds were made on the back of each mouse, one wound was be treated with PFD and one wound was served as the control (PBS treatment) (n=4). 10 μg PFD in 15 μL PBS was daily administrated on Day3, Day 5 and Day7 to make a total dose of 30 μg PFD treatment to the wound.

In the high dosage group, animals were randomized into three groups and received treatments as follows:

Group 1: Exosomes = 3 mice. Where 2 wounds were made on the back of each mouse, one wound was treated with exosomes and one wound was served as the control (PBS treatment) (n=3). 200 μg exosomes in 15μL PBS was daily administrated from Day3 to Day8 to make a total dose of 1200 μg exosomes treatment to the wound.

Group 2: PFD-exosomes = 3 mice. Where 2 wounds were made on the back of each mouse, one wound was treated with PFD-exosomes and one wound was served as the control (PBS

treatment) (n=3). 200 µg PFD- exosomes in 15 µL PBS was daily administrated from Day3 to Day8 to make a total dose of 1200 µg PFD-exosomes treatment to the wound.

Group 3: PFD = 3 mice. Where 2 wounds were made on the back of each mouse, one wound was be treated with PFD and one wound was served as the control (PBS treatment) (n=3). 20 µg PFD in 15 µL PBS was daily administrated from Day3 to Day8 to make a total dose of 120 µg PFD treatment to the wound.

A flexible first aid tape was applied to cover the rings and seal the treatment liquid. All wounds were then covered with bandages and 3M™ Tegaderm™ Transparent Dressings before mice being individually housed. Wound size and appearance were photographed and measured every other day. Wound healing rate were expressed as a percentage of the respective initial wound. Mice were all sacrificed on day 13 and wound tissue was collected through biopsy punch for further histological analysis.

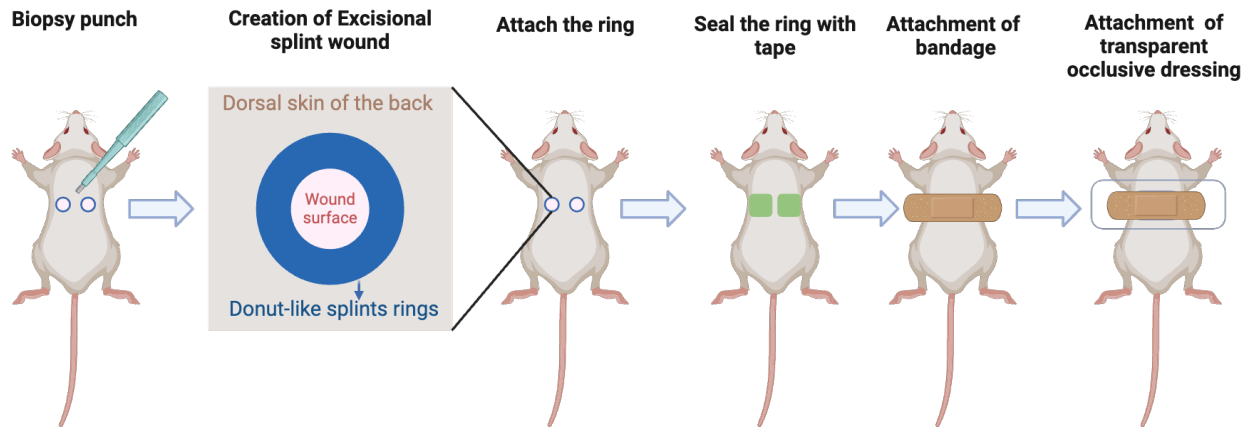


Figure 4.1 *In vivo* wound healing model using SKH-1 mice. Surgical technique for creating a full-thickness excisional splint wound in mice. Created with biorender.com.

4.3.7 Histological analysis

4.3.7.1 Collagen (Sirius Red/Fast Green) assay

On day 13, the animals were euthanized, and their wounds along with the surrounding tissue were carefully harvested by 8mm diameter sterile single biopsy punch. These tissues were then divided into two halves for further experiments. The specimens were fixed in 4% paraformaldehyde (in PBS, 0.01 M, pH 7.4) for 24 hours. After fixation, the samples were transferred to a 30% sucrose solution (in PBS, 0.01 M, pH 7.4) and stored at 4°C for 48 hours. The skin tissues were embedded in Tissue-Plus™ O.C.T. Compound (Fisher Scientific, Canada) at -20°C. The frozen tissue blocks were then sectioned using a cryostat into slices approximately 10 μm thick. These sections were allowed to air-dry at room temperature before being placed in a 37°C environment for 30 minutes. Once dried, the slides were gently washed with PBS at room temperature. Next, the tissue sections were immersed in Kahle fixative, a solution of distilled water, ethanol, formaldehyde, and acetic acid, and incubated at room temperature for 10 minutes. The sections were then gently washed again with PBS. A 20 μL dye solution was applied to each tissue section for 5 minutes at room temperature. Following staining, the dye was thoroughly rinsed off with distilled water, and the tissue sections were examined under a microscope (Zeiss, Imager A1 with Axiocam 305 color camera). ImageJ software (Fiji) was used to analyze collagen fiber density and collagen expression through color deconvolution of stained tissues.

4.3.8 Statistical analysis

All data are presented as means ± standard deviation (SD) and were analyzed using GraphPad Prism software (version 10.2.0). T-tests were used to compare means between two different groups, while one-way analysis of variance (ANOVA) was used to determine the

significance level between three or more groups. A two-way ANOVA was used to determine the significance level between two independent variables. P value $\leqslant$ 0.05 was considered to be statistically significant. *, **, and *** stood for $P < 0.05$, $P < 0.001$, and $P < 0.0001$ respectively.

4.4 Results

4.4.1 Cellular uptake of exosomes *in vitro* by their parent cells

Due to exosomes' lipid bi-layer structure, lipophilic membrane dyes including DiI and PKH26 are commonly used for labeling exosomes due to their membrane-permeable nature and stable fluorescence. They exhibit strong fluorescence in the red spectrum, making them easily detectable and compatible with various fluorescence-based detection methods, such as fluorescence microscopy. Here, exosomes were labeled with both DiI and PKH26, and excess dye was removed using Exosome Spin Columns (Invitrogen™, Thermo Fisher Scientific). Interestingly, only exosomes labeled with PKH26 were detectable under fluorescence microscopy, suggesting a superior labeling efficiency or fluorescence intensity compared to DiI labeling. Furthermore, the cellular uptake of exosomes was visible after PKH26 labeling, indicating successful delivery and internalization by recipient cells.

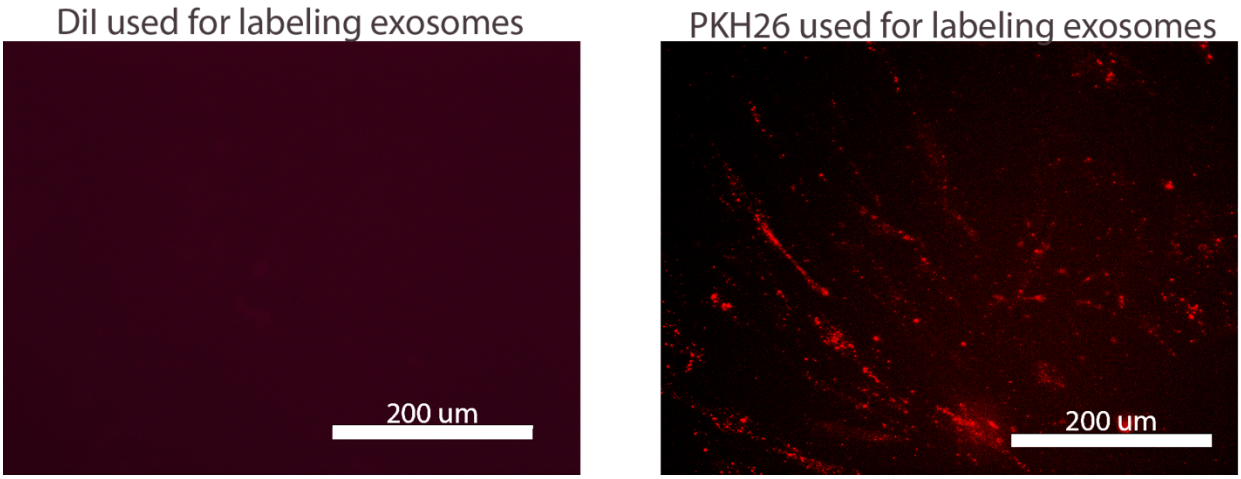
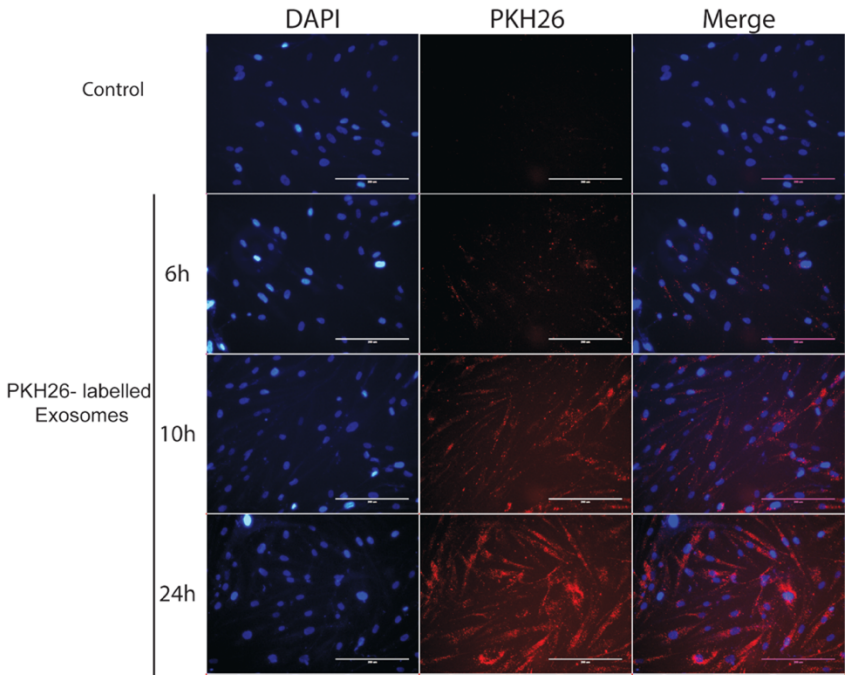


Figure 4.2 Selection of fluorescent dyes used for labeling exosomes *in vitro*.

After confirming the successful labeling of purified exosomes with the lipophilic dye PKH26, we proceeded to incubate them with dermal fibroblasts. However, drawbacks of PKH26 tracers include: 1) they tend to form micelles or aggregates; 2) they may label other lipid-based components in the extracellular space; 3) they impact the metabolism of treat cells *in vitro*. It has been reported that PKH26 dye molecule itself tends to form micelles or aggregates and overlap the size range of exosomes. Therefore, to exclude the possibility that the fibroblasts were stained by PKH26 micelles or aggregates rather than labeled exosomes, 4 μM PKH26 solution was also loaded on Exosome Spin Columns, and the elutes from the column were served as a negative control group in our study. The result showed that there is no obvious uptake that was visualized on the image for PKH26 control group. This indicates that the number of potential PKH26 aggregates or micelles can be ignored. Our observations revealed efficient transfer of PKH26-labeled exosomes into the dermal fibroblasts. The predominant localization of these exosomes in the cytoplasm and perinuclear region suggests their successful internalization by fibroblasts. The cytoplasmic and perinuclear distribution of exosomes indicates their potential ability to deliver cargo such as proteins, lipids, and nucleic acids into cellular compartments where they can exert functional effects. Shown as Figure 4.3 A and Figure 4.4 A, no uptake was observed in the negative control condition. When increasing doses of exosomes (from 12.5 to 100 μg) treated to dermal fibroblasts, and our results indicate a dose-dependent increase in red fluorescence as shown in Figure 4.4 B. Fluorescence images also demonstrated a time-dependent accumulation of PKH26-labeled exosomes by dermal fibroblast cells, with further observation showing continued accumulation of exosomes over 24h as shown in Figure 4.4 A.

A.



B.

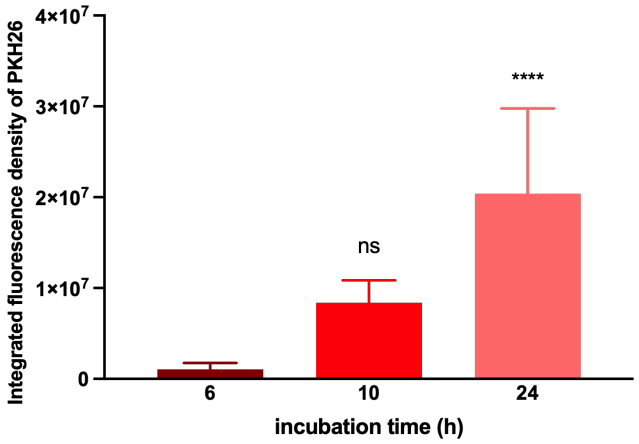
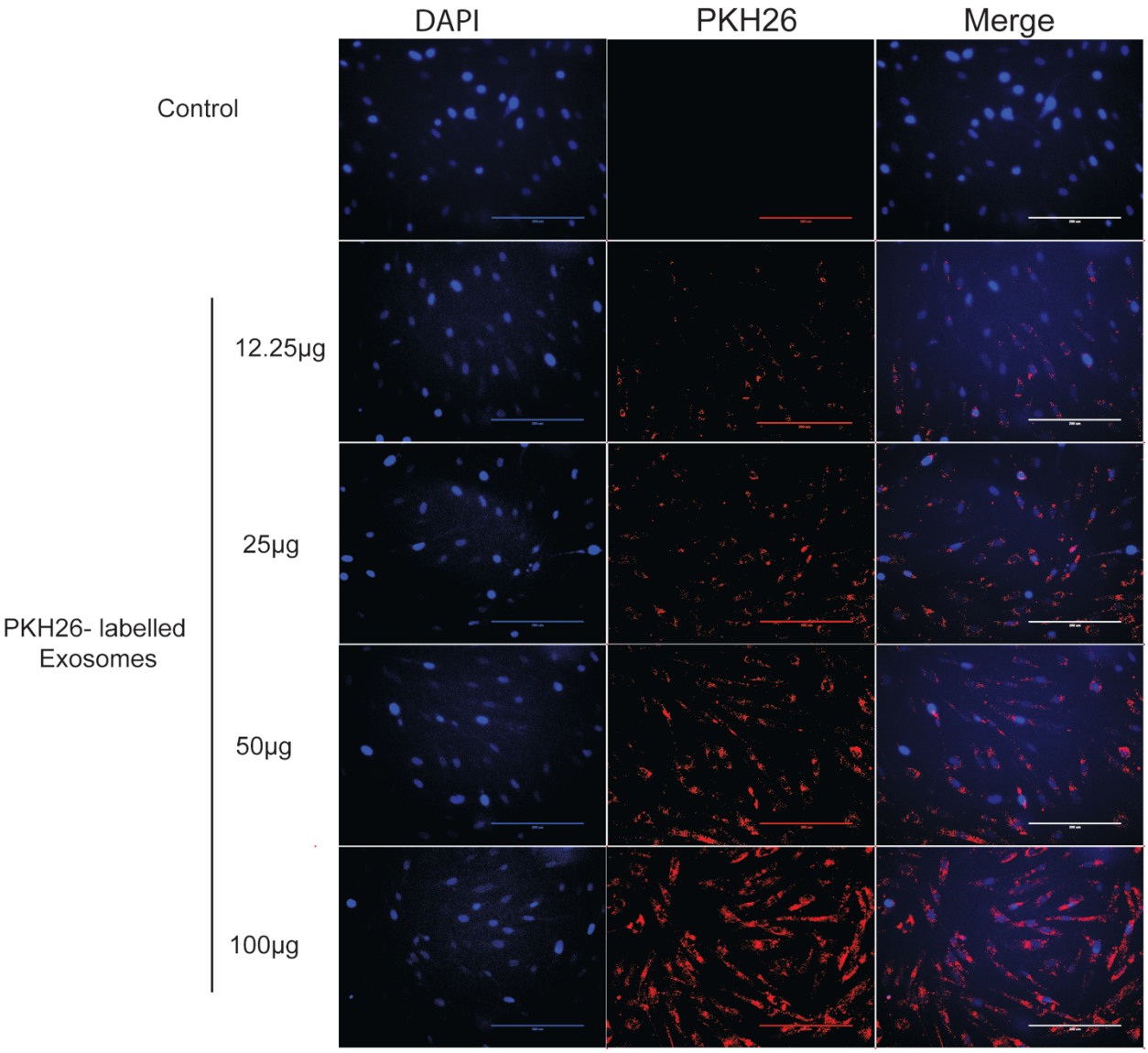


Figure 4.3 *In vitro* time-dependent cellular uptake of exosomes by dermal fibroblasts. (A) The nuclei of dermal fibroblasts were stained with DAPI, while exosomes were stained with PKH26. Cellular uptake of exosomes was visualized at 6, 10, and 24 hours using the EVOS® FL Auto Imaging System (scale bar = 200 nm). (B) Semi-quantitative analysis of exosome uptake is shown in the bar graph, depicting the integrated density of PKH26. All images were analyzed using ImageJ. Data are presented as mean ± SD (n = 6), representing the average from six representative images. Statistical analyses were performed by a one-way ANOVA with Tukey's multiple comparison test.

A.


DAPI
PKH26
Merge
Control
PKH26- labelled Exosomes
12.25µg
25µg
50µg
100µg

B.

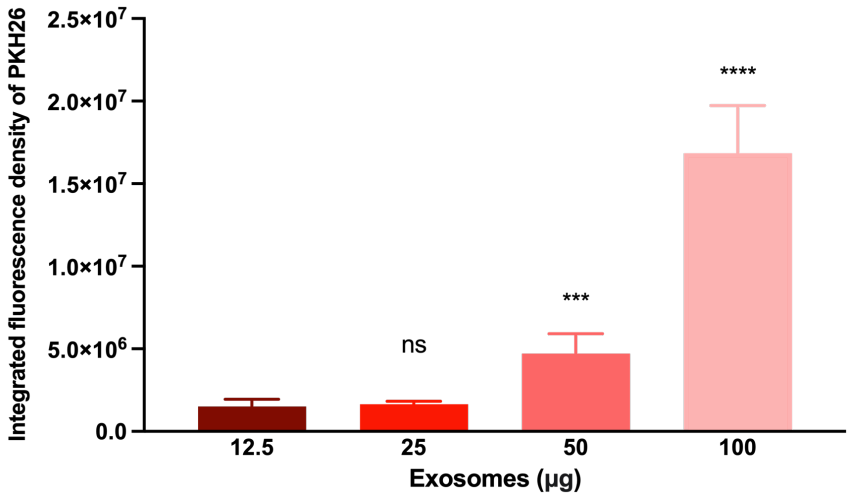


Figure 4.4 *In vitro* dose-dependent cellular uptake of exosomes by dermal fibroblast at 24 hours. (A) Dermal fibroblast nuclei were stained with DAPI, while exosomes were stained with PKH26. The uptake of exosomes was visualized at 6, 10, and 24 hours using the EVOS® FL Auto Imaging System (scale bar = 200 nm). (B) Semi-quantitative analysis of exosome uptake is represented in the bar graph, showing the integrated density of PKH26. All images were analyzed using ImageJ. Data are presented as mean ± SD (n = 6), representing the average from six representative images. Statistical analyses were performed by a one-way ANOVA with Tukey's multiple comparison test.

4.4.2 Exosomes and PFD- exosomes promote dermal fibroblast proliferation *in vitro*

The impact of different concentrations of PFD, exosomes, and PFD-exosomes on dermal fibroblasts viability was evaluated in dermal fibroblasts with MTS assay. To determine if PFD had any effect on dermal fibroblasts' cell viability, different concentrations of PFD at the microgram level (considering the PFD loading capacity in exosomes) were first treated to dermal fibroblasts. As shown in Figure 4.5A, PFD (from 5 μg/ml to 100 μg /ml) did not have a significant impact on relative cell viability; significant inhibition or promotion of cell growth at all doses was not observed. In our further evaluation, both exosomes and PFD- exosomes at all concentrations (10-100 μg/ml) did not display significant cytotoxicity after being treated with dermal fibroblasts after 12h, shown as Figure 4.5 B and C. Interestingly, both exosomes and PFD-exosomes showed enhanced cell viability after 24 hours (above 100% as compared to negative control), indicating substantial fibroblast proliferation. A dose-dependent response was observed with exosome treatment. Specifically, it appeared that only the higher concentration of exosomes (above 25 μg/ml) could significantly enhance the viability in dermal fibroblasts. Similarly, the presence of PFD-exosomes also promoted the proliferation of dermal fibroblasts in a dose-dependent manner as compared to negative control.

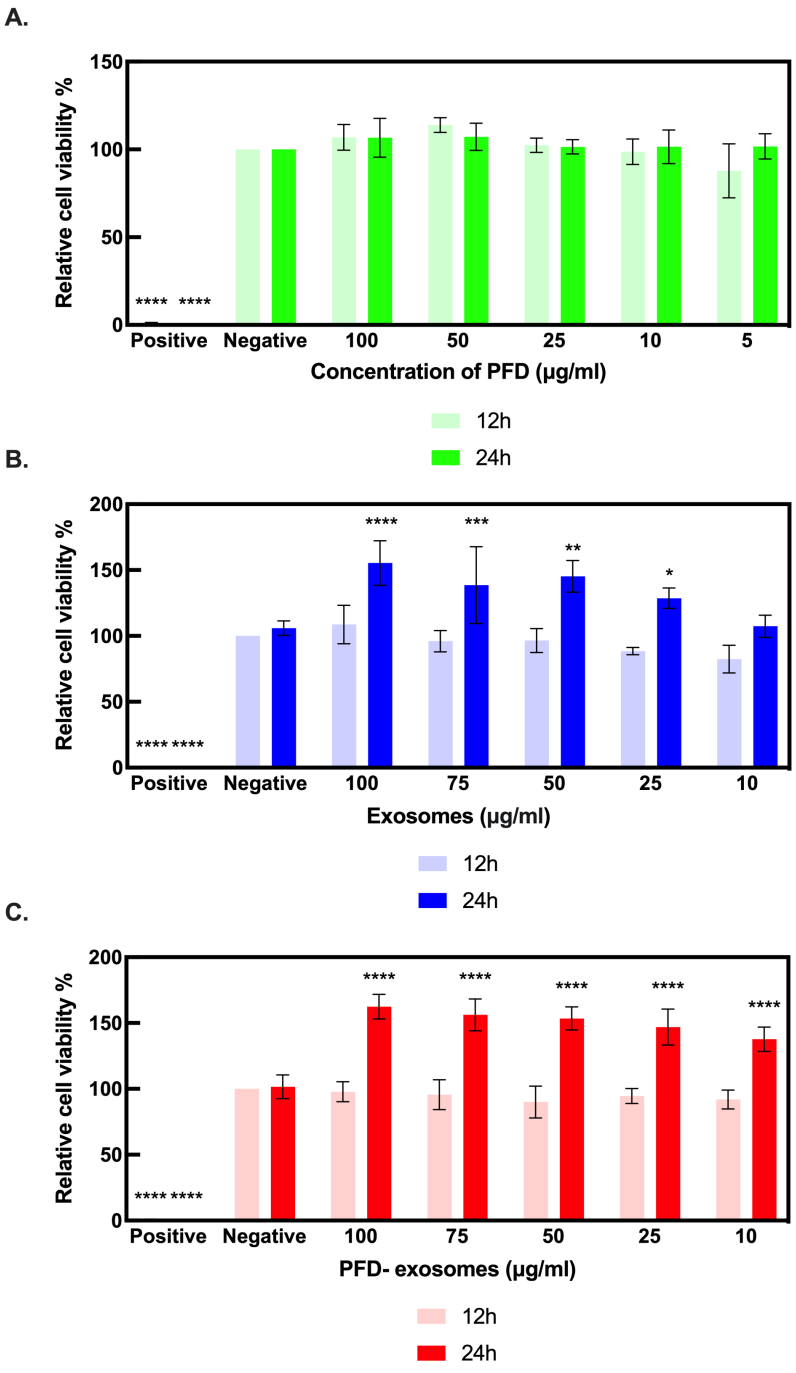
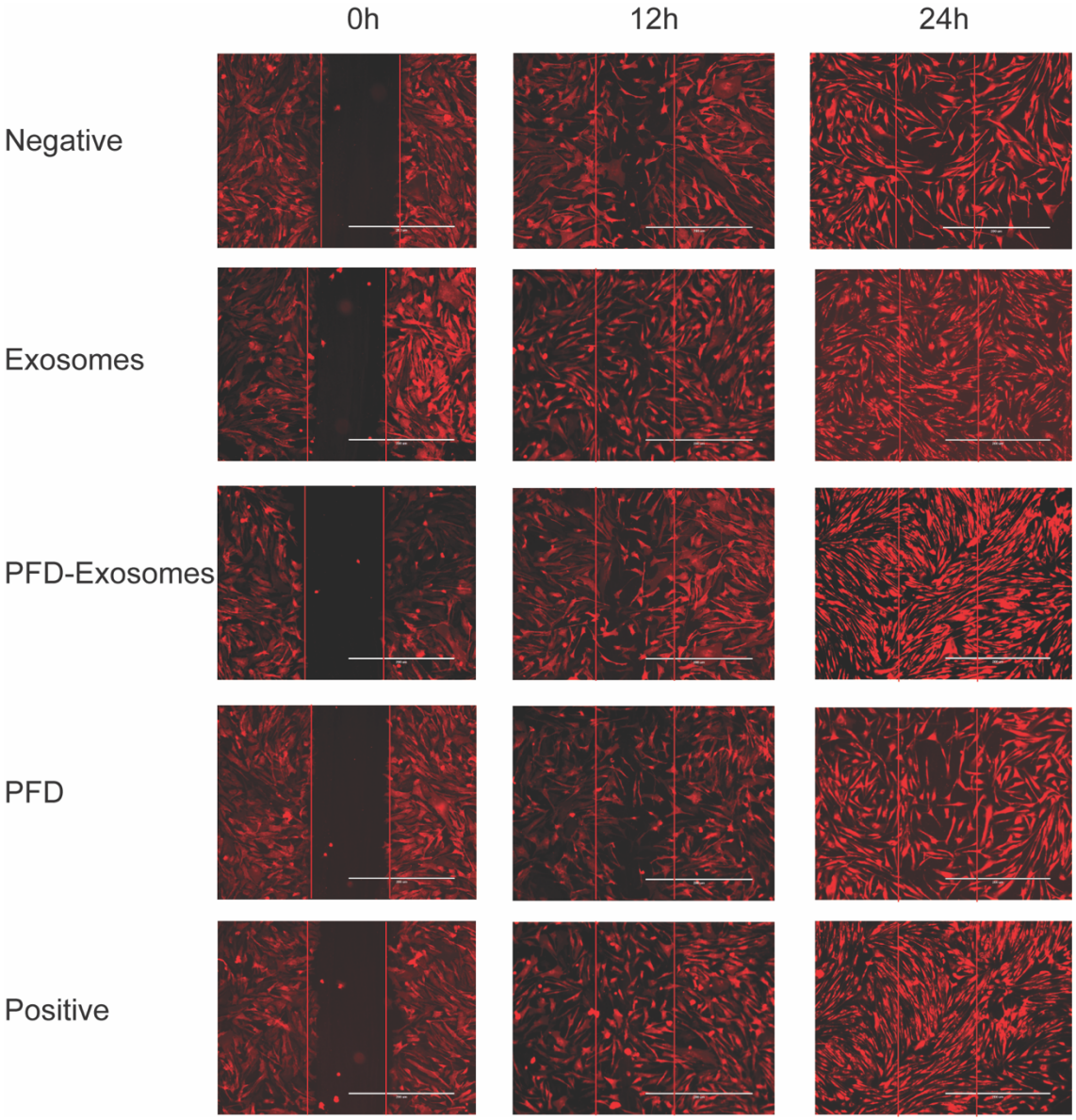


Figure 4.5 ***In vitro*** **cytotoxicity of (A) PFD, (B) Exosomes, and (C) PFD-exosomes.** The negative control consisted of untreated cells in serum-starved EMEM, while the positive control included cells treated with Triton™ X-100 (1% v/v) in EMEM. Values are presented as mean ± SD (n = 6). Statistical analyses were performed by a two-way ANOVA with Šídák's multiple comparisons test.

4.4.3 Exosomes and PFD- exosomes promote dermal fibroblast migration *in vitro*

In vitro scratch assay, also known as wound healing assay is a tool to evaluate cell migration in response to treatments on 2D surfaces over time *in vitro*[195]. Here, we studied exosomes and PFD- exosomes in their ability to induce dermal fibroblast migration with this method. To visualize cell migration, dermal fibroblasts were stained with PKH26 fluorescent dye, presenting the cell membrane with red fluorescence observed under the microscope. Fibroblasts exhibited multidirectional movement rather than migrating strictly linearly, making it challenging to measure cell migration by measuring the scratch width. Therefore, we quantify migration by calculating the percentage closure of the cell scratch area over time, providing a more accurate measurement of cell movement. Cell gap closure of dermal fibroblast cells expressed as a percentage of the initial wound. By 12h post-wounding, both exosomes and PFD-loaded exosomes induced faster migration of dermal fibroblasts compared to the negative control at 12 hours post-wounding. However, PFD-exosomes showed relatively slower migration (67.36 ± 7.06 %) than exosomes alone (83.08 ± 8.89 %). In contrast, PFD alone showed a significant delay in cell migration (41.25± 3.04 %) compared to all other groups. After 24h, the closure percentages for exosomes (91.21 ± 1.79 %) and PFD- exosomes (92.42 ± 1.94 %) were comparable to the positive control (91.16 ± 4.48 %), suggesting a significant efficacy in promoting dermal fibroblasts migration. Again, PFD alone exhibited a delayed migration (67.13± 7.42 % of closure).

A.



B.

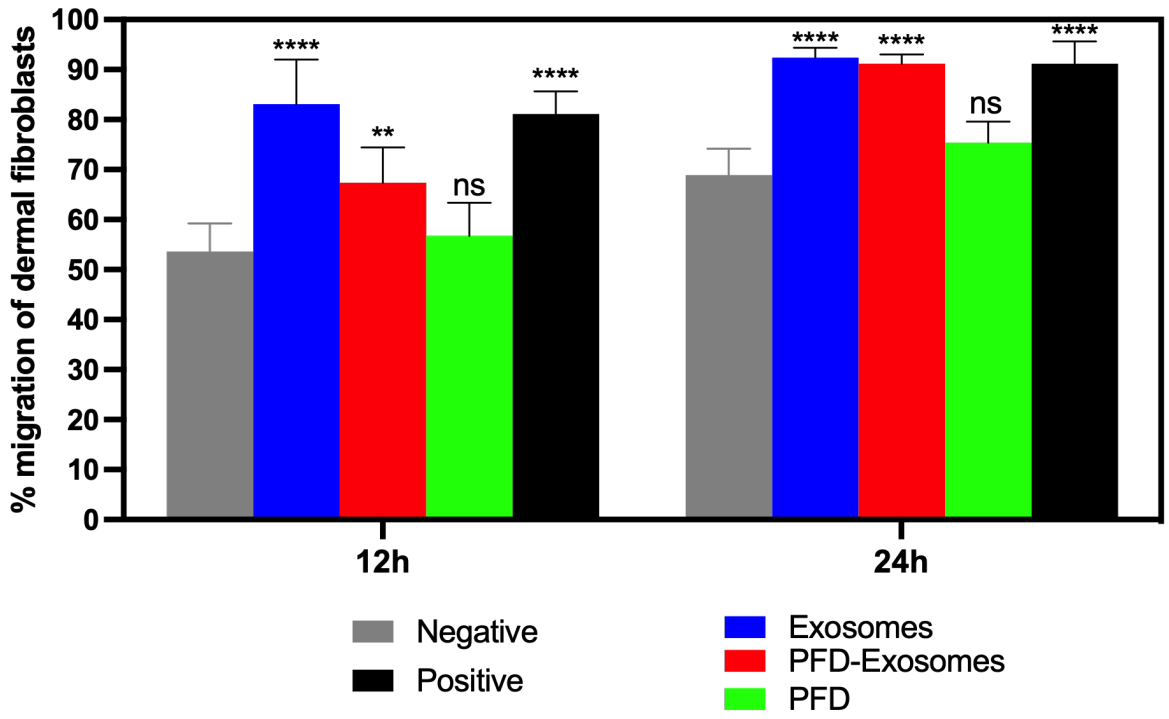


Figure 4.6 *In vitro* scratch wound healing analysis of exosomes and PFD-exosomes.

(A) Migration of cells was tracked using the fluorescent marker PKH26. (B) Bar graph illustrating the percentage of dermal fibroblast cell migration at 12h and 24h post-treatment. Negative control represents untreated cells in serum-starved medium, while positive control consists of cells in serum-rich medium with growth factors. Data are presented as mean ± SD; n = 4. Statistical analyses were performed by a two-way ANOVA with Šídák's multiple comparisons test.

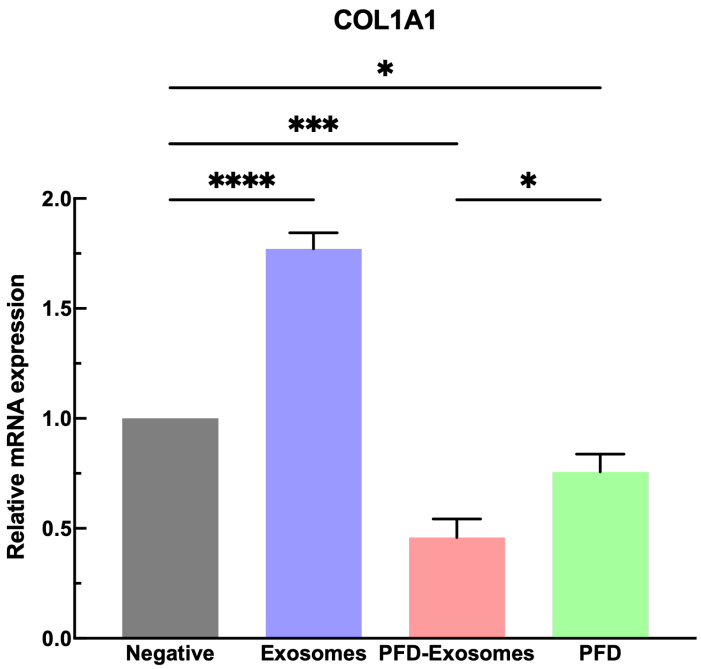
4.4.4 PFD-exosomes induce down regulation of COL1A1 mRNA expression and Pro-Collagen I Alpha 1 synthesis in dermal fibroblasts *in vitro*

To investigate the potential impact of exosomes and PFD-exosomes on collagen synthesis in dermal fibroblasts, we first assessed the expression of Pro-Collagen I alpha 1, a precursor molecule for collagen type I synthesis encoded by the COL1A1 gene. Using qRT-PCR, we found a significant 1.7-fold increase in intracellular COL1A1 mRNA levels following exosome treatment

in vitro. In contrast, cells treated solely with PFD showed slightly reduction in COL1A1 expression (75%). Furthermore, PFD-exosomes actively suppressed COL1A1 expression, reducing mRNA levels by 47% in fibroblasts. Subsequently, we measured the expression of Pro-Collagen I alpha 1 (an early indicator of collagen type I synthesis) at the protein level using an ELISA assay.

Not completely consistent with the finding in mRNA level, the result indicated that exosomes alone did not significantly alter the expression of ~~extracellular~~ Pro-Collagen I alpha 1 in culture media. However, when PFD was incorporated into exosomes, there was a substantial 58% decrease in Pro-Collagen I alpha 1 level compared to control conditions. This reduction was significantly greater than that observed with PFD treatment alone, which decreased Pro-Collagen I alpha 1 level by 73%. These results suggest the effective inhibitions of PFD-exosomes on both intracellular COL1A1 mRNA expression and extracellular Pro-Collagen I alpha 1 protein synthesis by dermal fibroblasts, highlighting their potential role in reducing collagen production invitro.

A.



B.

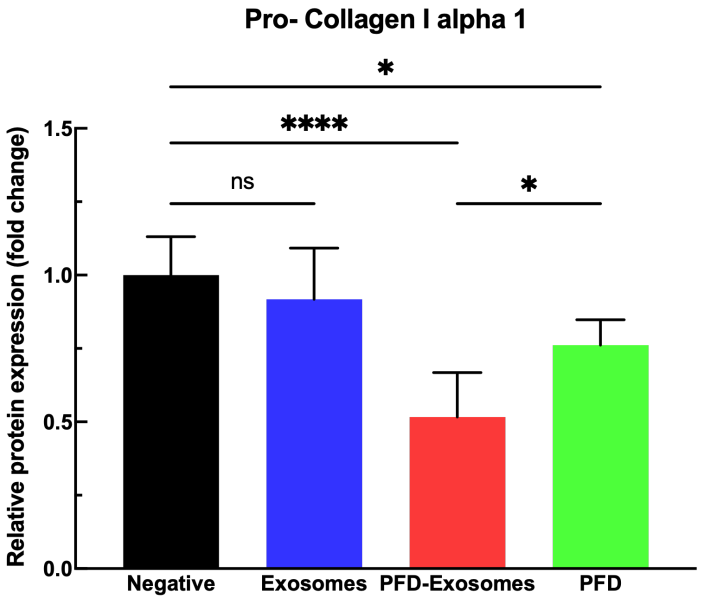
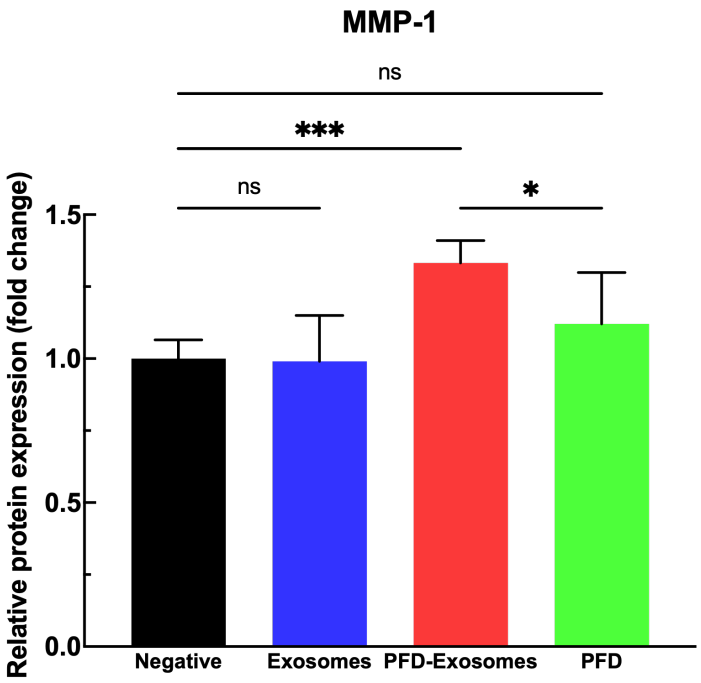


Figure 4.7 Exosomes and PFD- exosomes affected the expression of genes associated with ECM remodelling by dermal fibroblasts *in vitro*. (A) The expression of COL1A1 mRNA in fibroblasts (B) The expression of Pro-Collagen I alpha 1 protein in culture media. Values represent mean ± SD; n = 3. Statistical analyses were performed by a one-way ANOVA with Tukey's multiple comparison test.

4.4.5 PFD-exosomes induce MMP-1 upregulation and TIMP-1 downregulation *in vitro*

Given the essential balance of MMP-1/TIMP-1 in collagen breakdown, the impact of exosomes and PFD-exosomes on their expression modulated by dermal fibroblasts was also investigated. The result showed that exosomes again did not alter the protein level of both MMP-1 and TIMP-1 *in vitro*. Treatment with PFD-exosomes to fibroblasts led to a notable 1.4-fold increase in MMP-1 expression produced, demonstrating a stronger effect compared to treatment with PFD alone, which resulted in a 1.2-fold increase. A notable downregulation in TIMP-1 (inhibitor of MMP-1) expression was observed following PFD-exosomes treatment, with levels decreasing to 45% as depicted in the Figure 4.8 B. In contrast, treatment with PFD alone reduced TIMP-1 expression by approximately 55%. Taken together, these findings suggest that encapsulating PFD into exosomes effectively reduces the protein expression of TIMP-1 *in vitro* while increasing MMP-1 production simultaneously. This modulation indicates the potential role of PFD-exosomes in optimizing fibroblast function in collagen degradation, which may lead to less scar formation outcome.

A.



B.

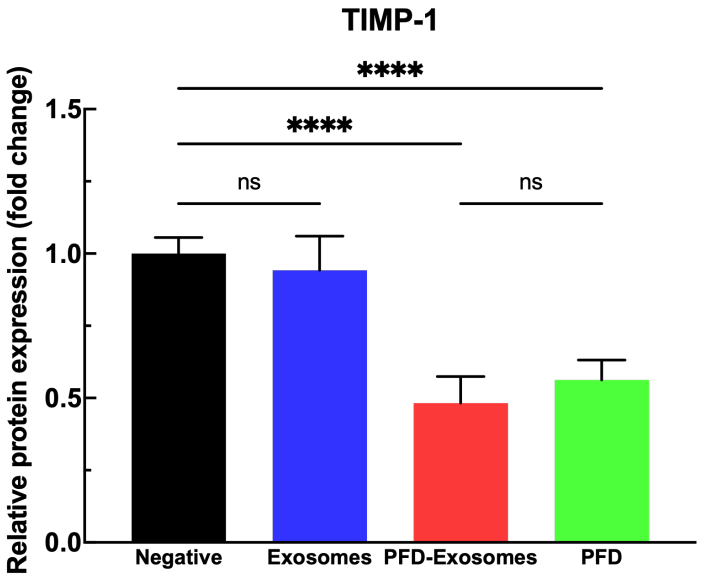


Figure 4.8 Exosomes and PFD- exosomes affected the expression of proteins associated with collagen degradation by dermal fibroblasts *in vitro*. (A) The expression of MMP-1 (B) The expression of TIMP-1. Values represent mean ± SD; n = 3. Statistical analyses were performed by a one-way ANOVA with Tukey's multiple comparison test.

4.4.6 Exosomes and PFD- exosomes accelerated cutaneous wound healing in SKH-1 Mice *in vivo*

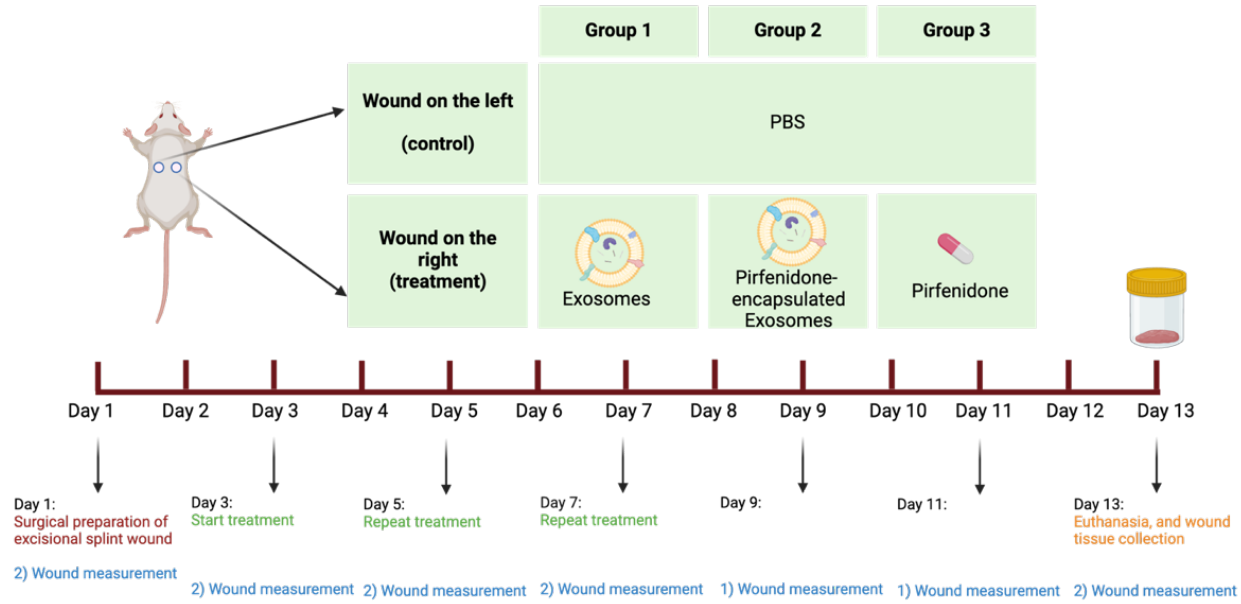
Since fibroblasts-derived exosomes showed a positive effect in dermal fibroblast proliferation and migration *in vitro*, their efficacy was further investigated in a pilot full-thickness excisional wound healing study in healthy SKH-1mice. Two full-thickness skin injury in mice which involves the loss of subcutaneous tissue, sensory nerve endings and some neuroimmune functions was established on the back of mice.

For the initial dosage, mice were randomly divided into three groups, with each mouse receiving two treatments. One treatment involved exosomes (300 μg), PFD-exosomes (300 μg, containing 30 μg of PFD), or PFD only (30 μg), while the other side was treated with PBS as a control. Treatments were repeatedly given on Days 3, 5, and 7 to evaluate their impact on wound healing over 13 days. Representative images of the wound for each group are shown in Figure 4.9. Over time, all groups exhibited a progressive reduction in wound without any signs of persistent inflammation (significantly red and swollen) or wound infection, indicating normal healing processes. Scab formation indicates the beginning of the proliferation stage, during which the wound surface smooths out and new epidermal and dermal tissues start to develop. Over a 13-day period, we measured the median healing times for wounds to become red, smooth, and scabbed under different treatments, resulting in the following order: exosomes (7 days) = PFD-exosomes (8 days) < PBS (8 days) < PFD (9 days).

Exosome treatment alone significantly reduced wound size from Day 5 to Day 9 compared to the PBS control post-treatment. In contrast, PFD-exosomes showed a significant effect only on Day 5, with no lasting impact observed by Days 7 and 9. By Day 13, topical treatment with exosomes and PFD-exosomes led to smaller wound sizes, measuring 1.630 mm^2 and 2.167 mm^2,

respectively. These were significantly smaller than the wound sizes observed in the PBS control group (3.311 mm^2) and the PFD group (3.437 mm^2). Analysis of wound closure rates revealed that exosome treatment alone significantly achieved higher healing rates than all other groups, particularly between Day 5 and Day 13. This indicates that exosomes are the most effective for promoting wound closure. In contrast, the PFD treatment resulted in larger wound sizes and slower healing rates throughout the 13 days postoperatively compared to both the exosome and PFD-exosomes treatments. Although PFD-exosomes was not as effective as exosomes alone, it promoted wound healing at all time points from Day 5 to Day 13, showing faster wound reduction than both the PBS and PFD groups. This suggests that encapsulating PFD in exosomes may help mitigate the inhibitory effects of PFD, facilitating wound closure that is otherwise hindered when using PFD alone.

A.



B.

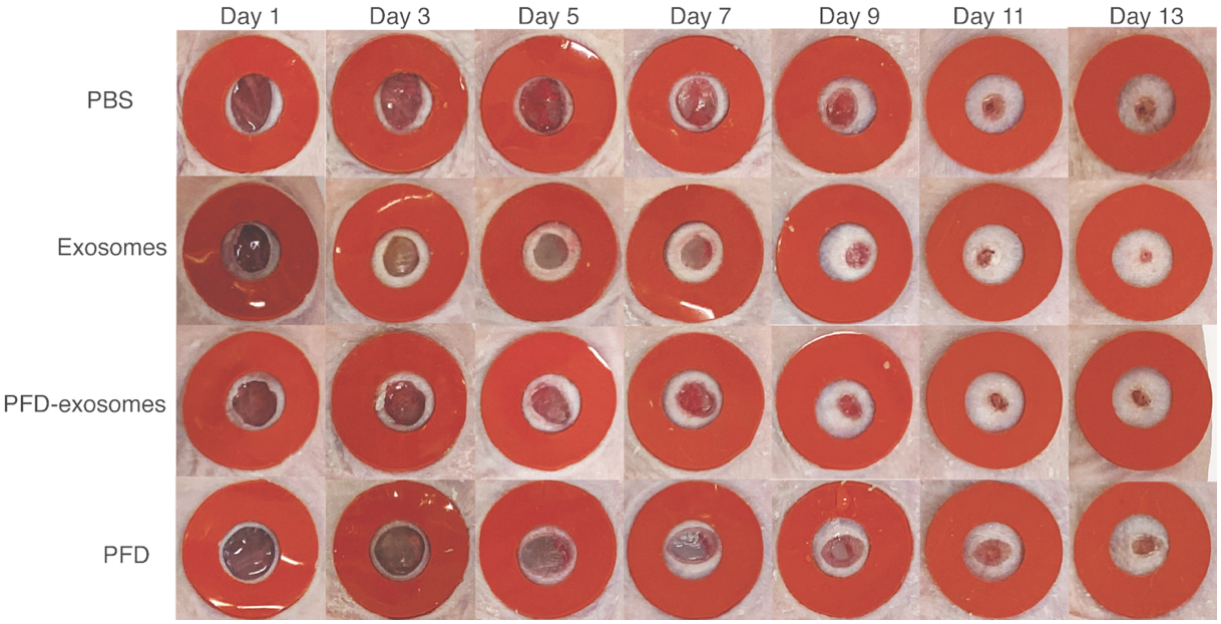


Figure 4.9 Low-dosage exosome and PFD-exosome treatments for wound healing in SKH-1 mice. (A) Dosage regimen and timeline for the *in vivo* study, created with BioRender.com. (B) Representative images of wound healing at various time points following treatment with 300 µg exosomes, 300 µg PFD-exosomes, and 30 µg PFD. PBS was used as a positive control.

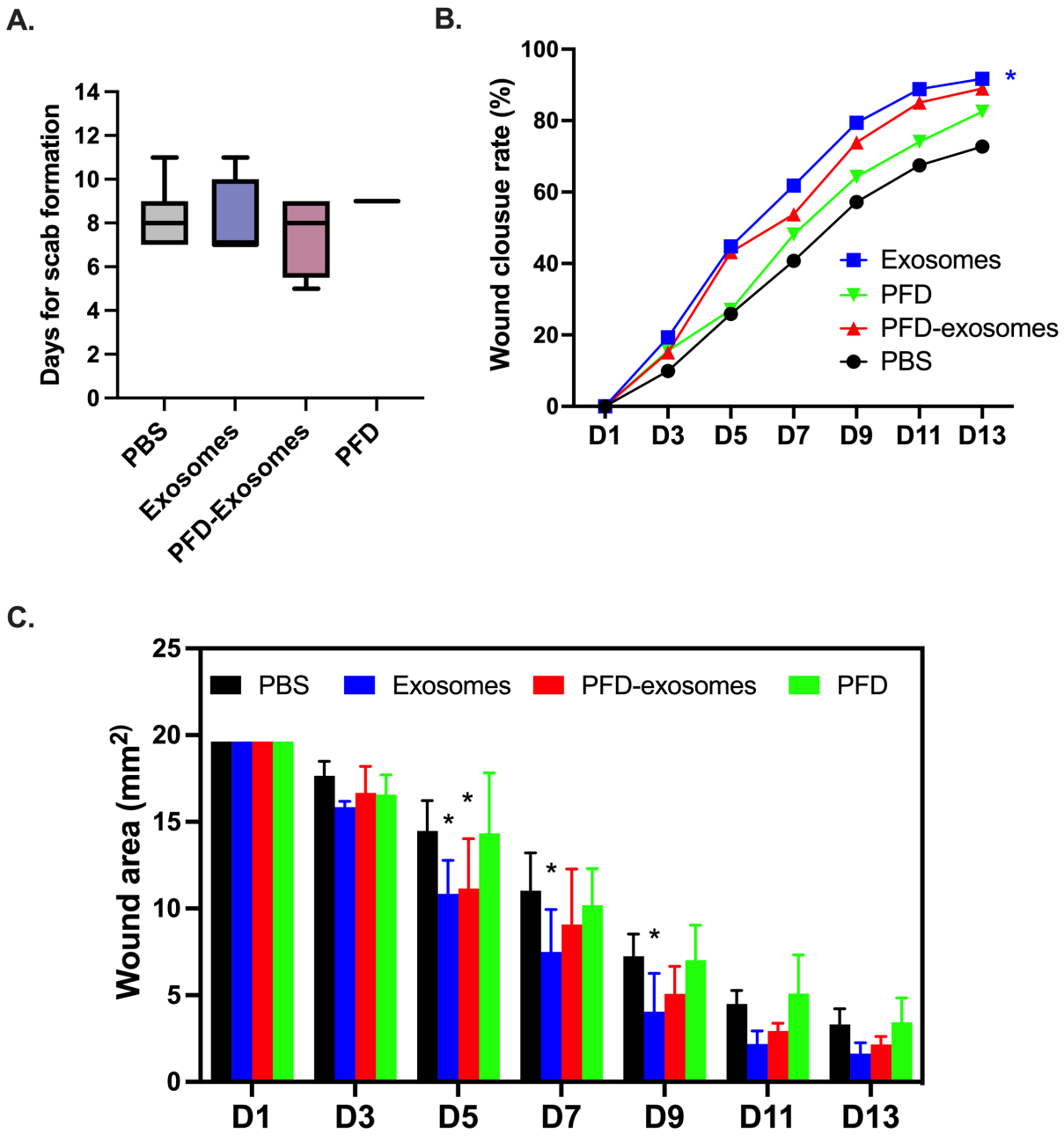
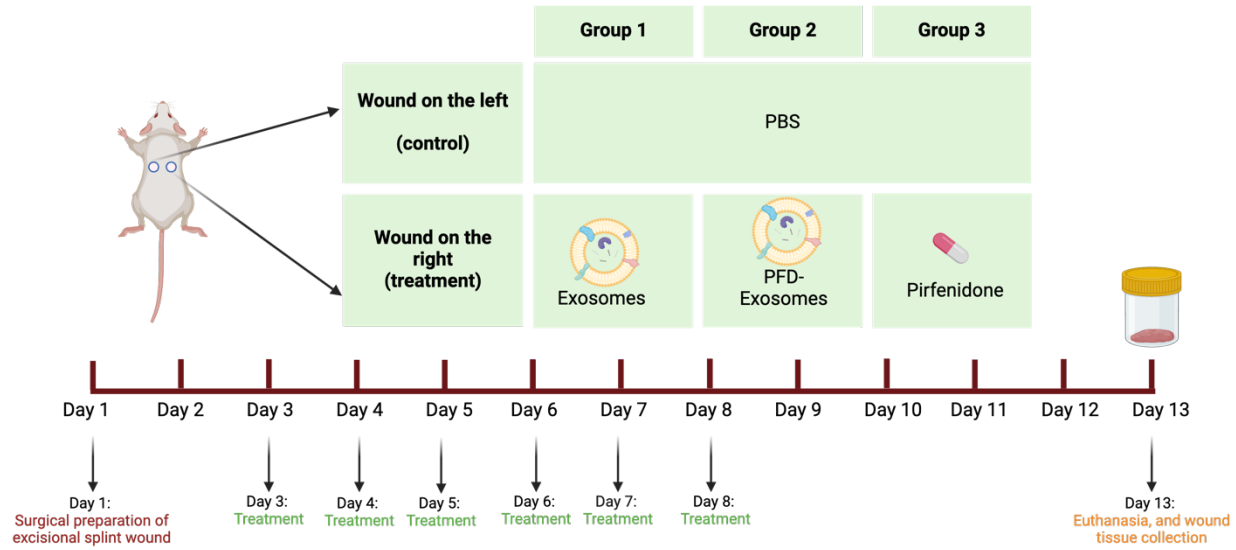


Figure 4.10 Quantitative analysis of wound closure in low-dosage exosome and PFD-exosome Treatments *in vivo*. (A) Median healing times for scab formation. (B)Wound size at each time point normalized with respect to day 1. (n = 4 per treatment group). (C) Wound closure rates (%) for all groups for up to 13 days. (n = 4 per treatment group). Statistical analyses were performed by a two-way ANOVA with Dunnett's multiple comparisons test.

As shown in Figure 4.11, with a higher dose of exosomes (1200 µg) and PFD-exosomes (1200 µg), both exosome and PFD-exosomes significantly reduced wound size from Day 5 and Day 7 compared to the PBS control post-treatment. By Day 13, exosomes demonstrated an improvement in wound healing, reducing the wound size to 2.604 mm². PFD-exosomes showed the most significant healing effect, with the smallest wound size (~2.119 mm²) at end point. In contrast, PFD alone had little impact, resulting in a wound size of 3.477 mm², which was similar to that observed with PBS treatment (~3.416 mm²). Analysis of wound closure rates revealed that exosome and PFD-exosomes treatment both significantly achieved higher healing rates than all other control groups between Day 5 and Day 13.

A.



B.

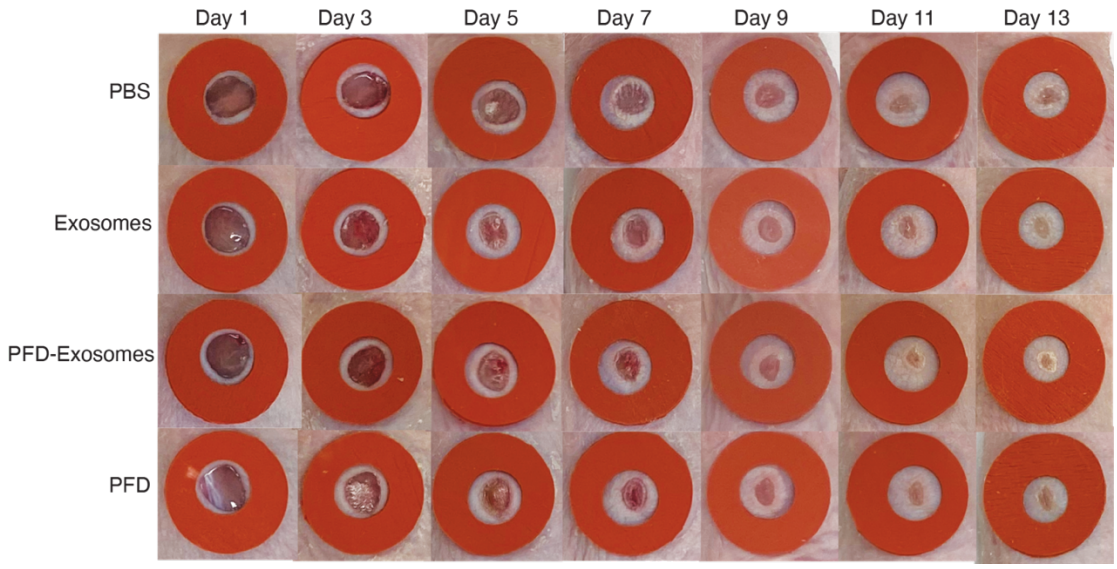


Figure 4.11 High-dosage exosome and PFD-exosome treatments for wound healing in SKH-1 mice. (A) Dosage regimen and timeline for the *in vivo* study, created with BioRender.com. (B) Representative images of wound healing at various time points following treatment with 1200 µg exosomes, 1200 µg PFD-exosomes, and 120 µg PFD. PBS was used as a positive control.

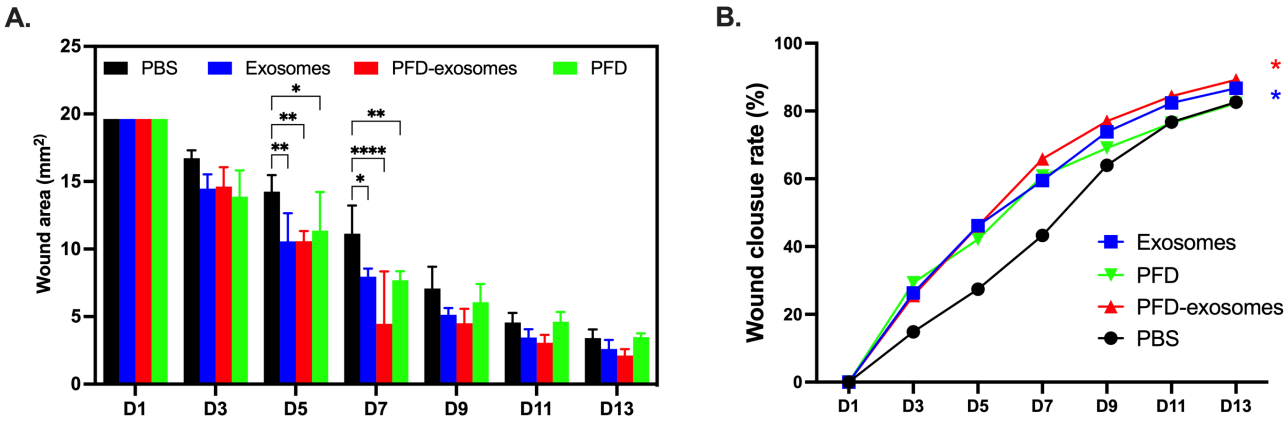


Figure 4.12 Quantitative analysis of wound closure in high-dosage exosome and PFD-exosome Treatments *in vivo*. (A) Wound size at each time point normalized with respect to day 1. (n = 3 per treatment group). (B) Wound closure rates (%) for all groups for up to 13 days. (n = 3 per treatment group). Statistical analyses were performed by a two-way ANOVA with Dunnett's multiple comparisons test.

4.4.7 PFD-exosomes reduced collagen expression and improved dermal organization in SKH-1 Mice *in vivo*

Histological analysis was conducted to evaluate the effect of exosomes (300 μg) and PFD-exosomes (300 μg) on the formation of new dermal and epidermal structures, as well as overall tissue regeneration. Frozen skin sections from the wound area were stained using Sirius Red/Fast Green to assess the collagen (red) and non-collagen fibers (green) in the healed tissues. From general observations in Figure 4.13, all groups showed reconstruction of epithelial and dermal layers. All stained sections provided a clear contrast between collagen and non-collagen elements, revealing the epidermis over a continuous, undulating basement membrane and collagen bundles in the dermis arranged in multiple directions. On day 13, the PBS group showed a noticeably thickened and uneven new epidermis, along with a thick and extensive layer of new granulation tissue in the dermis. Both collagen and non-collagen components were densely produced and arranged. The newly formed epidermis was thinner and flatter after exosomes treatment, with a dermal layer rich in both collagen and non-collagen fibers. In contrast, the PFD-only group showed a thicker, more evenly regenerated epidermis. As expected, the dermis in this group contained a higher proportion of non-collagen components compared to collagen. Notably, in the PFD-exosome group, the epidermis was thinner and more uneven than in the PBS control group. The dermis in this group appeared more loosely organized, with less collagen cross-linking than in the other groups. The collagen in the PFD-exosome group was arranged in a reticular pattern, similar to the structure of unwounded skin after 13 days. This collagen organization is consistent with scarless skin repair, where collagen initially accumulates and then partially reduces and rearranges into tissue.

A quantitative analysis was performed to assess the impact of different treatments on collagen tissue density and collagen expression as shown in Figure 4.13. The PFD-exosome group showed a significant reduction in tissue density (73.48%) compared to the PBS control (99.89%), while PFD alone had a more modest effect, reducing tissue density to 90.85%. Regarding collagen expression, the exosome-treated group displayed levels nearly identical to the PBS control, indicating that exosomes alone have little impact on collagen expression. In contrast, PFD alone resulted in a decrease in collagen expression (72.05%), although it remained slightly higher than the PFD-exosome group. This suggests that PFD's effect on collagen expression is less pronounced when delivered without exosomes. Notably, the PFD-exosome group showed a significant reduction in collagen (66.62%) compared to the PBS control (95.36%), indicating that PFD-exosomes has a negative effect on collagen expression.

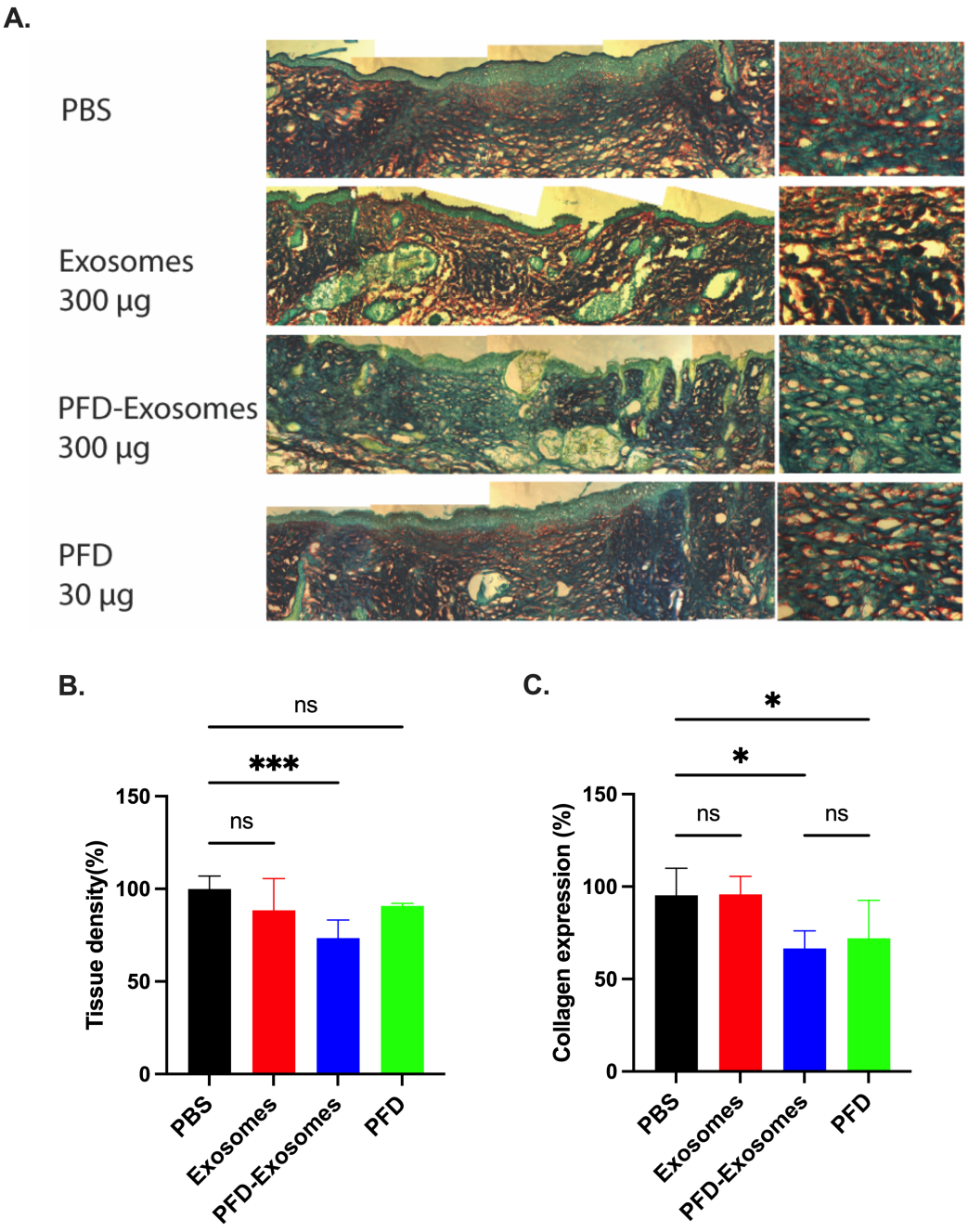


Figure 4.13 Histological analysis of wound skin sections collected on day 13 (Low dosage group). Collagen and non-collagen fiber distribution in tissues was evaluated using Sirius Red/Fast Green staining. Sirius Red stains total collagen fibers in red, while non-collagen proteins appear green. (A) Quantitative analysis of tissue density. (B) Collagen expression. Values represent mean ± SD; n = 4. Statistical analyses were performed by a one-way ANOVA with Tukey's multiple comparison test.

When the dosage was increased (as shown in Figure 4.14), exosomes (1200 μg) alone led to a moderate reduction in tissue density (~12.2%). PFD (120 μg) alone caused a more significant decrease of 30.96%. However, PFD-exosomes (1200 μg) had the strongest effect, reducing tissue density by 34.03% compared to the control. A higher dose of PFD-exosomes (1200 μg) also significantly reduced collagen expression in SKH-1 mice *in vivo*. Treatment with PFD alone resulted in a 44.3% reduction in collagen expression, compared to the PBS control. PFD-exosomes demonstrated the most potent effect, reducing collagen expression by 82.11%, with an expression level of just 17.89%. The delivery of PFD through exosomes produced the greatest reduction in collagen expression, indicating a synergistic effect.

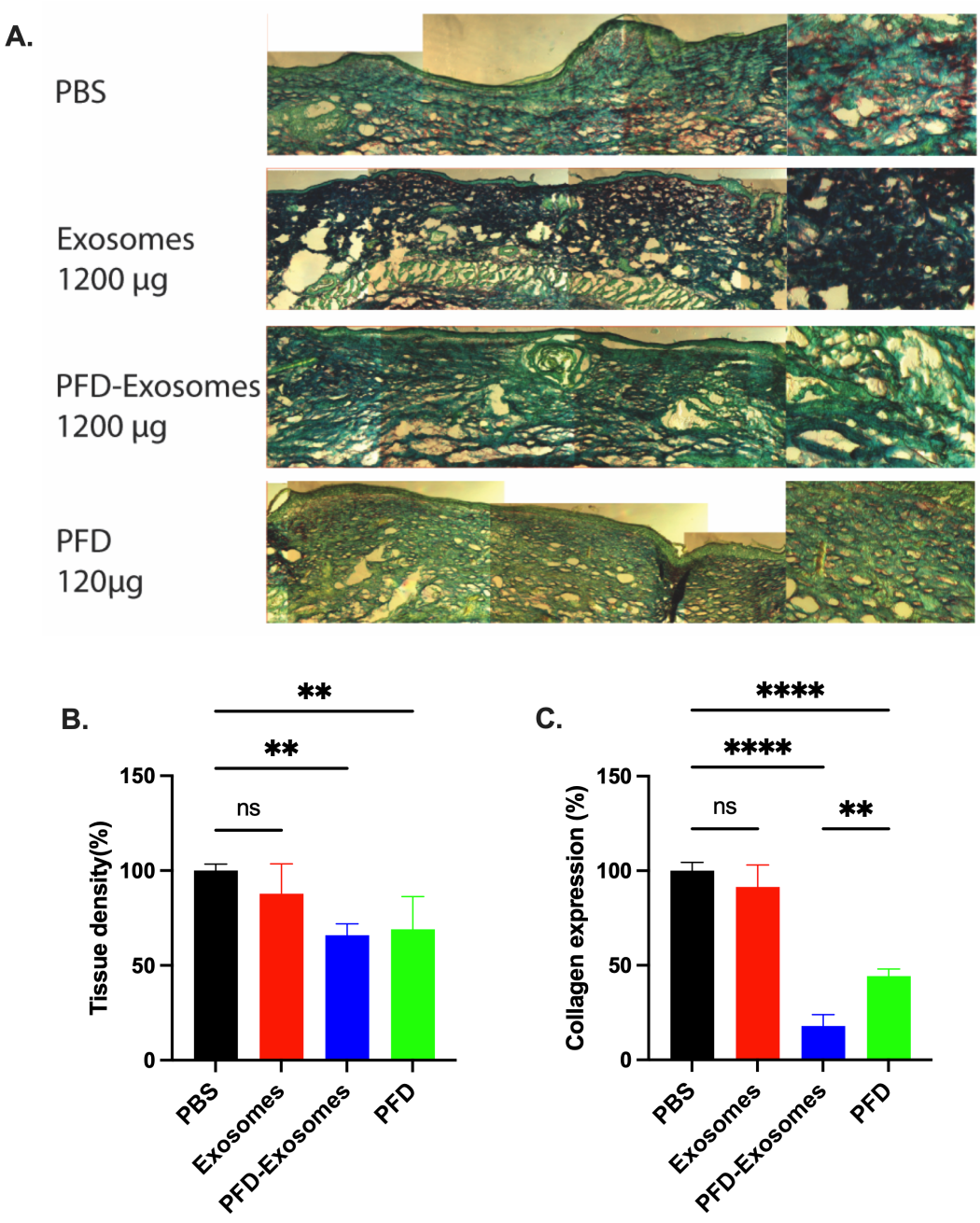


Figure 4.14 Histological analysis of wound skin sections collected on day 13 (High dosage group). Collagen and non-collagen fiber distribution in tissues was evaluated using Sirius Red/Fast Green staining. Sirius Red stains total collagen fibers in red, while non-collagen proteins appear green. (A) Quantitative analysis of tissue density. (B) Collagen expression. Values represent mean ± SD; n = 3. Statistical analyses were performed by a one-way ANOVA with Tukey's multiple comparison test.

4.5 Discussion

Dermal fibroblasts are key cellular targets for scarless wound healing, as they significantly contribute to the repair process through their abilities to proliferate, migrate, and remodel the ECM. This chapter aim to comprehensive understand the *in vitro* effects of exosomes derived from dermal fibroblasts and PFD-exosomes on fibroblast functions, specifically their impact on proliferation, migration, and gene expression associated with ECM remodeling. Furthermore, we conducted an *in vivo* pilot study to explore the effects of exosomes and PFD-exosomes on wound closure and the scarless tissue repair.

We first demonstrated the robustness of PKH26 as a fluorescent label for tracking exosomes and its utility in studying exosome uptake dynamics *in vitro*. A dose-dependent and time-dependent cellular uptake was then observed for exosomes derived from dermal fibroblasts *in vitro*. Our result coincides with previous studies[196,197], indicating a successful uptake of exosomes by the same source of cells. The number of exosomes administered influences the extent of cellular uptake, with higher doses leading to increased internalization. The duration of exposure to exosomes also affects their uptake efficiency, indicating a dynamic process of interaction between the cells and exosomes over time. Overall, the cellular uptake highlights the capability of exosomes to integrate into their originating cells, demonstrating their potential as autocrine factors and effective carriers for delivering drugs to specific cells. This finding can be explained by the necessity for exosomes derived from donor cells to be incorporated back into the donor cells through an autocrine mechanism, which is essential for maintaining cellular equilibrium[24]. Currently, we can hypothesize that exosomes are taken up by cells primarily through fusion with or binding to the plasma membrane. A previous study also demonstrated that exosomes can be internalized by neighboring fibroblasts, and this process can be blocked by anti-annexin

antibodies[198]. This suggests that annexin proteins are likely involved in the cellular uptake of exosomes.

The proliferation and migration capabilities of dermal fibroblasts have laid a good foundation for wound closure. Our studies have shown that exosomes and PFD-exosomes are both noncytotoxic to dermal fibroblasts *in vitro* after 12h treatment. After 24h, both exosomes and PFD-exosomes stimulate proliferation in a dose-dependent manner. Herein, we hypotheses exosomes derived from dermal fibroblasts alone could induce their parent cells' proliferation as an autocrine factor. Studies have consistently shown that exosomes possess the capability to enhance proliferation in their originating cells under both physiological and pathological circumstances. For example, exosomes originating specifically from hepatocytes have shown the unique ability to induce proliferation of hepatocytes *in vitro* and promote liver regeneration *in vivo*. In contrast to exosomes derived from other liver-derived cells such as Kupffer cells and liver sinusoidal endothelial cells, which do not induce hepatocyte proliferation, the study suggests that hepatocyte-derived exosomes deliver sphingosine kinase 2 (SK2) and therefore promote hepatocyte proliferation[1]. Another example is exosomes derived from non-small cell lung cancer (NSCLC), which promote cell proliferation and attenuated apoptosis in NSCLC by delivering alpha-smooth muscle actin (ASMA), thereby influencing the behavior of their parent cells and supporting the progression of NSCLC[200]. These studies provide evidence of the proliferative effect of exosomes on their originating cells in an autocrine manner, suggesting that this effect is largely due to the delivery of exosomal proteins. We hypothesize dermal fibroblast-derived exosomes also contain exosomal cargos that stimulate fibroblasts proliferation. Dermal fibroblast's exosomal cytokines include growth-regulated protein alpha (GRO-α), the cytokine interleukin-6 (IL-6), interleukin-8 (IL-8) and the monocyte chemoattractant protein-1 (MCP-1)[198] was found related to fibroblast

proliferation. In a previous study, exosomes derived from dermal fibroblasts' 3D cell culture were found to restore fibroblast proliferation that was initially suppressed by anti-IL-6 antibodies. Similarly, in monolayered-cultured fibroblasts, treatment with anti-IL-6 antibodies inhibited scratch closure, while exosomes enhanced the migration rate of these cells[198]. These results indicate that exosomal IL-6, acting as a multifunctional cytokine, partially promotes both migration and proliferation of dermal fibroblasts.

Exosomal microRNAs, in addition to exosomal proteins, also contribute to promote fibroblast proliferation and migration *in vitro*. For example, young fibroblasts-derived exosomes promoted fibroblasts migration by delivering miR-125b[194]. Furthermore, 2D-cultured fibroblasts release exosomes containing miR-27b[90]. Notably, abundant miR-27b was also detected in the MSC-derived EVs, while EV-transferred miR-27b improved cutaneous wound healing in mice and improved proliferation and migration of dermal fibroblasts *in vitro*[201]. In our study, we found both fibroblast- derived exosome and PFD-exosome treatments enhanced fibroblast migration and led to full cell gap closure within 24 hours, indicating their advantages in enhancing dermis closure *in vitro*. However, the migration observed in fibroblasts at 24h (in Figure 4.6) is partially influenced by their proliferation as described in the result. Considering the overall effects of PFD-exosomes on promoting fibroblasts proliferation and migration, initial *in vitro* assays suggest they are safe and beneficial for promoting complete wound healing.

Excessive scar formation poses a significant challenge in skin regeneration, often resulting from an overproduction of collagen, inadequate degradation of the ECM, and poor cellular coordination. Collagen biosynthesis initiates with the production of procollagen alpha chains, which are synthesized in the endoplasmic reticulum (ER) of dermal fibroblasts. Within the ER, these alpha chains assemble into procollagen triple helices before being transported to the Golgi

apparatus for secretion into the extracellular space, where they spontaneously form collagen fibrils[202]. In this study, we assessed collagen type I expression both intracellularly (COL1A1 mRNA) and extracellularly (Pro-Collagen I alpha 1 protein). Our results confirmed previous findings indicating that PFD reduces collagen biosynthesis on both transcriptional level and translation level.[187,203]. In the drug-free exosome group, a discrepancy was observed between mRNA and protein levels. Treatment with exosomes alone resulted in increased COL1A1 mRNA levels, but there was no corresponding increase in Pro-Collagen I alpha 1 protein. This difference may be attributed to the presence of exosomal microRNAs, which may bind to specifically to COL1A1 mRNA and inhibit its translation into protein. One such microRNA, miR-196a, has been found in exosomes, including those from fibroblasts[90], and it bind with collagen mRNA. Downregulated miR-196a leads to a high expression of type I collagen in normal dermal fibroblasts[204]. The results demonstrated that exosomes significantly enhanced the delivery of PFD to dermal fibroblasts, effectively reducing collagen production at both the mRNA and protein levels *in vitro*.

Since wound healing also requires the coordinated action of MMPs/TIMPs and the distinctive pattern of their expression has been implicated in scarless healing in mammalian fetuses, in this study we have also these characteristics are exhibited in dermal fibroblasts after treatment of exosomes and PFD-exosomes *in vitro*. We found that exosomes alone again do not have a significant impact on the expression of MMP-1 and TIMP-1 proteins. After PFD alone and PFD-exosomes treatment on dermal fibroblasts, substantial differences in up-regulation of MMP-1 and downregulation of TIMP-1 were found. PFD-exosomes showed greater potency on up-regulating MMP-1 than PFD alone, indicating the enhanced effectiveness of delivering PFD via exosomes. However, this supercity was not as significant as for reducing TIMP-1. The reduction in TIMP-1

expression may enhance the impact of elevated MMP-1 levels induced by PFD-exosomes, leading to increased collagen degradation turnover. Overall, the *in vitro* findings indicate that PFD-exosomes affect dermal fibroblast activity in two key ways: 1) by reducing collagen production at both the mRNA and protein levels, leading to decreased synthesis of the ECM and 2） by promoting collagen degradation and remodeling by increasing the expression of MMP-1 while decreasing TIMP-1 levels, which further enhances ECM degradation.

Given the complexity of skin repair as a regenerative process, we further evaluated the effects of exosomes and PFD-exosomes topical treatment *in vivo* using a full-thickness wound model on SKH-1 mice. To assess wound healing accurately, we employed a silicone ring splint attached around the wound to slow down natural contraction and prevent involuntary movement during the healing process. Over a 13-day period, we observed exosomes and PFD-exosomes both accelerated wound reduction and consistently achieving higher healing rates than controls (PBS and PFD). This suggests that fibroblast-derived exosomes are key factors to promote wound closure, partially due to their ability to enhance fibroblast proliferation and migration in an autocrine manner, as observed *in vitro*. Previous studies have also suggested that theses exosomes actively promoted endothelial cells proliferation and angiogenesis[99,193], as wells re-epithelialization by directly enhancing keratinocyte proliferation or indirectly increasing wound contraction[99]. These factors were not examined in the current study; however, they collectively contribute to accelerated wound closure. Furthermore, histological observations revealed that PFD-exosomes evidently reduced both the collagen tissue density and collagen expression *in vivo* compared to other groups, demonstrating greater effectiveness than PFD alone. This may be due to PFD-exosomes significantly suppressing collagen production in dermal fibroblasts at both the mRNA and protein levels, which in turn reduces collagen biosynthesis and fiber formation.

Consequently, the newly formed ECM exhibited a loose structure, with collagen arranged in a reticular matrix similar to that of unwounded skin. In the later stages of healing, ECM reconstruction is crucial, as optimal wound healing relies on the remodeling of collagen into a well-organized network to restore normal tissue structure[205]. This loose and orderly arrangement of collagen in newly formed ECM suggests that PFD-exosomes improved collagen disposition and lead to a scarless healing pattern.

4.6 Conclusion

In this chapter, we illustrated how exosomes derived from human dermal fibroblasts can be taken up by fibroblasts *in vitro*, enhancing their migration and proliferation in an autocrine manner. Exosomes have the potential to serve as a standalone, cell-free therapy to accelerate wound healing. This study is the first to demonstrate that exosomes, as drug carriers, can enhance the effectiveness of PFD, offering a promising approach for anti-fibrotic therapy. In our *in vivo* models, PFD-exosomes not only improved the healing process but also organize the ECM in repaired dermal tissue by reducing excessive collagen deposition. PFD-exosomes effectively decreased the expression of Pro-Collagen I alpha 1 and TIMP-1, while simultaneously increasing MMP-1 production in dermal fibroblasts *in vitro*. By specifically modulating fibroblast activity and regulating collagen metabolism, PFD-exosomes minimized ECM deposition during tissue repair. This innovative platform holds significant potential for enhancing wound healing outcomes and reducing fibrotic scarring.

Chapter 5 Conclusion and Future Direction

5.1 Result conclusion and significance of study

In the first chapter, we developed a method for isolating high-purity exosomes from *in vitro* cultured human dermal fibroblasts, with a detailed workflow for their harvesting, isolation, and characterization. Our findings indicated that the affinity method produces exosomes of higher purity and better dispersion. Characterization through various biophysical techniques, such as TEM and AFM, as well as comprehensive molecular assays like antibody arrays and ELISA, confirmed the successful isolation of high-purity exosomes from conditioned media.

The following chapter explored the use of exosomes as drug delivery platform, specifically focusing on the encapsulation and formulation optimization of the antifibrotic compound PFD. We optimized an active drug encapsulation method using sonication and evaluated various parameters, including drug removal techniques, to improve drug encapsulation and overall exosome yield. Our analysis showed that the MagCapture method significantly outperforms the Exosome Spin Column method for recovering drug-loaded exosomes. We also found that carefully controlling sonication conditions—specifically by using lower amplitudes and fewer cycles—enhances both drug encapsulation efficiency and exosome recovery. After formulation optimization, formulation F6 yielded the best encapsulation, achieving a drug encapsulation efficiency of 11.136% ± 1.267%, a loading efficiency of 10.012% ± 1.026%, and a particle recovery rate of 64.213% ± 8.490%.

In the fourth chapter, we explored the potential of exosomes as therapeutics for and drug delivery carriers under the content of wound healing. Our findings indicated that exosomes derived from human dermal fibroblasts can be effectively taken up by fibroblasts *in vitro*, promoting their migration and proliferation through an autocrine mechanism. *In vivo* results further suggested that exosomes alone could serve as an effective cell-free therapy to accelerate wound healing. Further, this study is ground-breaking in demonstrating that exosomes can enhance the effectiveness of

PFD as a drug carrier, paving the way for new antifibrotic therapies. In our *in vivo* models, PFD-exosomes not only improved healing but also organized the ECM in repaired dermal tissue by reducing excessive collagen deposition. PFD-exosomes were also found to simultaneously decrease Pro-Collagen I alpha 1 and TIMP-1 expression while increasing MMP-1 production in dermal fibroblasts *in vitro*. By specifically modulating fibroblast activity and regulating collagen metabolism, PFD-exosomes mitigated excessive ECM deposition during tissue repair (as illustrate in Figure 5.1).

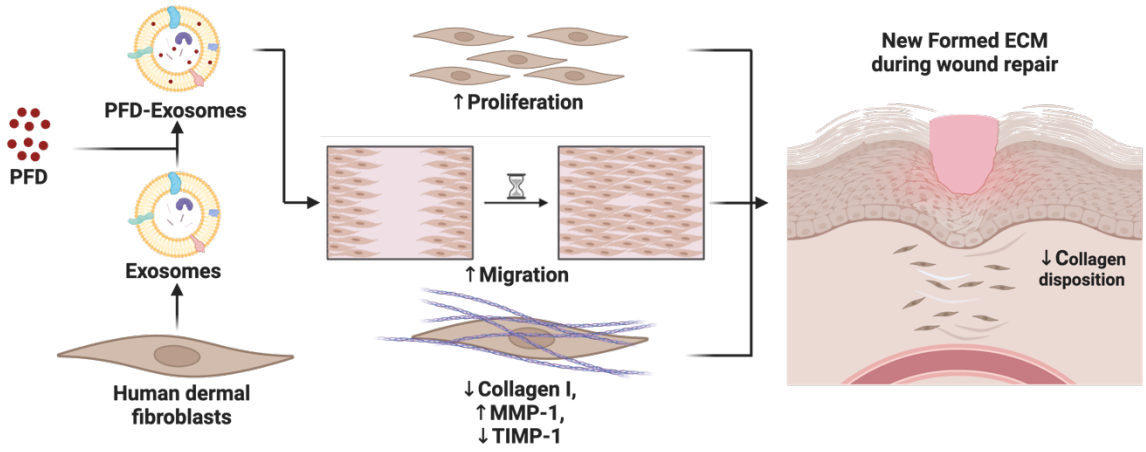


Figure 5.1 Graphical result conclusion. A proposed mechanism of PFD-exosomes by which accelerating closure while simultaneously minimizing scar formation. Created with biorender.com.

The significance of this study lies in its comprehensive exploration of high-purity exosome isolation and the optimization of exosome-based drug delivery systems, which serve as a foundation for their clinical applications. Importantly, the research demonstrates the therapeutic potential of exosomes, showing that they can serve as an effective cell-free therapy to accelerate wound healing. Additionally, PFD-exosomes represents an innovative strategy in pre-scarring interventions, promising improved wound healing outcomes and minimizing scarring. Overall, this

study paves the way for innovative applications of exosomes in clinical therapies for wound healing.

5.2 Limitations and future directions

Our study has certain limitations that should be acknowledged. While we successfully isolated exosomes with relatively high purity, the production yield remains insufficient for clinical translation. Currently, a static flask system was employed, which is less labor-intensive than bioreactors; however, bioreactors can produce over 100 times more exosomes. Scaling up production with bioreactors is promising, as they allow precise control over CO_2, O_2, and pH levels. Factors such as cell seeding density, passage number, and medium selection significantly affect exosome cargo. Optimizing these parameters is crucial for standardized exosomes mass production. Higher cell seeding densities may reduce the number of exosomes produced per cell and increase contamination risks from culture medium proteins[206]. Additionally, prolonged cell culture and multiple passages can lead to variability in exosome production[207]. Modulating cultivation conditions can enhance exosome release and production[208]. For example, acidic pH and increased glucose levels have been linked to higher exosome yields[209]. Conversely, glucose starvation can alter protein composition and increase release. Future research should focus on optimizing these factors while adhering to Good Manufacturing Practices (GMP) to improve the quality and scalability of exosome production for clinical use.

Finding an efficient way of isolating exosomes is always necessary. In this study, conventional isolation techniques (PEG precipitation and affinity methods) were evaluated for their feasibility of obtaining exosomes. Nevertheless, challenges such as high sample consumption, high costs, long processing times, and low recovery of exosomes, make these methods unsuitable for clinical applications. Microfluidic-based methods are future tools in new exosome separation

technology, and they are promising alternatives to gold-standard conventional methods. Exploiting exosomes' size, surface charge, or specific markers, microfluidics can achieve rapid separation, and higher separation yield of exosomes with lower sample volume. Also, microfluidics could integrate multiple steps of exosome isolation and characterization into a single device or lab-on-a chip platform, reducing manual handling and improving reproducibility[210].

Exploring new technologies is essential for enhancing drug encapsulation in exosomes. One promising method in this area is Exo-Fect™ (System Biosciences), a chemical transfection technology that has demonstrated significantly higher RNA loading into milk exosomes compared to traditional electroporation techniques[211]. Advancements in molecular design and engineering are also being explored to improve drug loading. For instance, Yim et al. developed a novel protein loading technique using optically reversible protein-protein interactions (EXPLORs) for intracellular drug delivery[212]. In this method, a protein is linked to the photoreceptor cryptochrome 2 (CRY2), which interacts with the CIB1 protein anchored to exosomes via CD9. This allows precise manipulation of drug loading using blue light. Exosomes from light-treated HEK293T cells demonstrated a significant increase in loaded mCherryCRY2 protein, achieving a loading capacity estimated to be 40 times greater than traditional extrusion methods. Moreover, lab-on-a-chip systems utilizing microfluidic technologies have proven effective in improving drug encapsulation[213]. For example, Exo-Load microfluidic device enhances loading efficiency for drugs like DOX and PTX into exosomes derived from glioma cells[213]. This mechanical technique leverages controlled deformation of exosomes to increase membrane permeability, facilitating the introduction of different molecular weight cargos while preserving exosomal integrity. The efficiency of loading varies with flow rate due to differences in shear forces created by the defined dimensions of the nanochannels.

Understanding the cellular mechanisms of exosomes is crucial for their role in communication between cells and their therapeutic applications. In this study, our knowledge about how exosomes are taken up by cells is limited, with the primary methods believed to be fusion with or binding to the plasma membrane. Future studies should investigate whether receptor-dependent pathways are involved in this uptake, potentially using inhibitors for pathways like clathrin-mediated endocytosis, caveolae-mediated endocytosis, micropinocytosis, and phagocytosis. Notable markers for these pathways include low-density lipoprotein and transferrin for clathrin, and cholera toxin subunit B for caveolae, etc.[214] Research in this area will enhance our understanding of exosome uptake and the basics of exosomes therapeutic functions.

In this study, we aimed to isolate less heterogeneous exosomes from cell media. However, each single cell line produces various subpopulations of exosomes, characterized by distinct morphologies, charges, and profiles of surface proteins and microRNAs[215]. These variations lead to different biophysical properties and biological effects. We can only hypothesize that proteins (such as IL-6) and miRNAs (including miR-27b[90] and miR-125b[194]) derived from fibroblasts play crucial roles in regulating fibroblast behavior and promoting tissue regeneration. However, there is a need for a comprehensive analysis of microRNA and protein profiles in exosomes derived from individual strain. Future research should focus on characterizing individual vesicles and conducting detailed molecular profiling, including proteomics and genomics, to facilitate the precise application of exosomes populations. While this study demonstrates that exosomes stimulate fibroblast behavior—specifically proliferation and migration—it does not investigate any signaling pathways related to wound healing that could further illuminate the biological function of fibroblast-derived exosomes. Understanding these cellular mechanisms may guide the

development of targeted therapeutic strategies, maximizing the potential of exosomes in wound healing.

Our pilot animal study has limitations. Firstly, exosomes and PFD-exosomes are administered repeatedly as a liquid dosage form topically. However, incorporating exosomes into wound dressings or sponges may offer a more effective approach for sustained release. This method allows for easier application and consistent release of exosomes to an open wound. Second, the *in vivo* study is limited to a 13-day observation period and does not explore multiple timing and dosage options for administration, both of which are essential for future clinical applications. This duration may not be adequate to evaluate the long-term effects of PFD-exosome treatment on wound healing and collagen remodeling. Additionally, this platform is intended for pre-scarring interventions; however, established scars may also potentially be reversible with PFD. Investigating delayed administration could provide more insights into its prognostic role of this platform. Third, our experiments focused solely on the impact of exosomes on dermal fibroblasts. However, other critical mechanisms, such as endothelial cell proliferation and angiogenesis, were mentioned but not investigated, limiting our understanding of how exosomes contribute to overall healing. Further studies are needed to evaluate the effects of our platform on more dermal cell types involved in wound healing. Finally, while histological observations indicated differences in collagen density and cross-linking, the specific methods used for skin histology, such as hematoxylin and eosin (HE) staining or immunofluorescence, were not provided. Without comprehensive histological analysis, the conclusion that PFD-exosomes result in scarless healing may be overly simplistic. The study also lacks comparative data on scarring outcomes, including functional assessments of healed tissue or long-term follow-up, which are essential for validating claims of "scarless" healing.

References

1. Sheridan RL, Hinson MI, Liang MH, et al. Long-term Outcome of Children Surviving Massive Burns. *JAMA*. 2000;283(1):69-73. doi:10.1001/jama.283.1.69

2. Hunt O, Burden D, Hepper P, Stevenson M, Johnston C. Self-reports of psychosocial functioning among children and young adults with cleft lip and palate. *Cleft Palate Craniofac J*. 2006;43(5):598-605. doi:10.1597/05-080

3. Brown BC, McKenna SP, Siddhi K, McGrouther DA, Bayat A. The hidden cost of skin scars: quality of life after skin scarring. *Journal of Plastic, Reconstructive & Aesthetic Surgery*. 2008;61(9):1049-1058. doi:10.1016/j.bjps.2008.03.020

4. Block L, Gosain A, King TW. Emerging Therapies for Scar Prevention. *Advances in Wound Care*. 2015;4(10):607-614. doi:10.1089/wound.2015.0646

5. Scar Treatment Market To Generate $52.8 Bn Revenue by 2030. P&S Intelligence. Accessed October 28, 2024. https://www.psmarketresearch.com/press-release/global-scar-treatment-market

6. Mohamed SA, Hargest R. Surgical anatomy of the skin. *Surgery (Oxford)*. 2022;40(1):1-7. doi:10.1016/j.mpsur.2021.11.021

7. Pasparakis M, Haase I, Nestle FO. Mechanisms regulating skin immunity and inflammation. *Nat Rev Immunol*. 2014;14(5):289-301. doi:10.1038/nri3646

8. Wong R, Geyer S, Weninger W, Guimberteau JC, Wong JK. The dynamic anatomy and patterning of skin. *Experimental Dermatology*. 2016;25(2):92-98. doi:10.1111/exd.12832

9. Atit R, Thulabandu V, Chen D. Dermal fibroblast in cutaneous development and healing. *Wiley Interdiscip Rev Dev Biol*. 2018;7(2):10.1002/wdev.307. doi:10.1002/wdev.307

10. Graham HK, Eckersley A, Ozols M, Mellody KT, Sherratt MJ. Human Skin: Composition, Structure and Visualisation Methods. In: Limbert G, ed. *Skin Biophysics: From Experimental Characterisation to Advanced Modelling*. Springer International Publishing; 2019:1-18. doi:10.1007/978-3-030-13279-8_1

11. Pratsinis H, Mavrogonatou E, Kletsas D. Scarless wound healing: From development to senescence. *Advanced Drug Delivery Reviews*. 2019;146:325-343. doi:10.1016/j.addr.2018.04.011

12. Falanga V, Isseroff RR, Soulika AM, et al. Chronic wounds. *Nat Rev Dis Primers*. 2022;8(1):1-21. doi:10.1038/s41572-022-00377-3

13. Basu S, Shukla V. Complications of Wound Healing. In: Mani R, Romanelli M, Shukla V, eds. *Measurements in Wound Healing: Science and Practice*. Springer; 2013:109-144. doi:10.1007/978-1-4471-2987-5_7

14. Guo B, Dong R, Liang Y, Li M. Haemostatic materials for wound healing applications. *Nat Rev Chem*. 2021;5(11):773-791. doi:10.1038/s41570-021-00323-z

15. Golebiewska EM, Poole AW. Platelet secretion: From haemostasis to wound healing and beyond. *Blood Reviews*. 2015;29(3):153. doi:10.1016/j.blre.2014.10.003

16. Wilgus TA, Roy S, McDaniel JC. Neutrophils and Wound Repair: Positive Actions and Negative Reactions. *Advances in Wound Care*. 2013;2(7):379. doi:10.1089/wound.2012.0383

17. Krzyszczyk P, Schloss R, Palmer A, Berthiaume F. The Role of Macrophages in Acute and Chronic Wound Healing and Interventions to Promote Pro-wound Healing Phenotypes. *Frontiers in Physiology*. 2018;9:419. doi:10.3389/fphys.2018.00419

18. Mahmoud NN, Hamad K, Al Shibitini A, et al. Investigating Inflammatory Markers in Wound Healing: Understanding Implications and Identifying Artifacts. *ACS Pharmacol Transl Sci*. 2024;7(1):18-27. doi:10.1021/acsptsci.3c00336

19. Widgerow AD. Current Concepts in Scar Evolution and Control. *Aesth Plast Surg*. 2011;35(4):628-635. doi:10.1007/s00266-010-9635-2

20. Pastar I, Stojadinovic O, Yin NC, et al. Epithelialization in Wound Healing: A Comprehensive Review. *Advances in Wound Care*. 2014;3(7):445. doi:10.1089/wound.2013.0473

21. Varkey M, Ding J, Tredget EE. Superficial Dermal Fibroblasts Enhance Basement Membrane and Epidermal Barrier Formation in Tissue-Engineered Skin: Implications for Treatment of Skin Basement Membrane Disorders. *Tissue Engineering Part A*. 2013;20(3-4):540. doi:10.1089/ten.tea.2013.0160

22. Asahara T, Murohara T, Sullivan A, et al. Isolation of putative progenitor endothelial cells for angiogenesis. *Science*. 1997;275(5302):964-967. doi:10.1126/science.275.5302.964

23. Tomasek JJ, Gabbiani G, Hinz B, Chaponnier C, Brown RA. Myofibroblasts and mechano-regulation of connective tissue remodelling. *Nat Rev Mol Cell Biol*. 2002;3(5):349-363. doi:10.1038/nrm809

24. Canady J, Karrer S, Fleck M, Bosserhoff AK. Fibrosing connective tissue disorders of the skin: molecular similarities and distinctions. *J Dermatol Sci*. 2013;70(3):151-158. doi:10.1016/j.jdermsci.2013.03.005

25. Desmoulière A, Redard M, Darby I, Gabbiani G. Apoptosis mediates the decrease in cellularity during the transition between granulation tissue and scar. *Am J Pathol*. 1995;146(1):56-66.

26. Caley MP, Martins VLC, O'Toole EA. Metalloproteinases and Wound Healing. *Adv Wound Care (New Rochelle)*. 2015;4(4):225-234. doi:10.1089/wound.2014.0581

27. Zhou S, Xie M, Su J, Cai B, Li J, Zhang K. New insights into balancing wound healing and scarless skin repair. *J Tissue Eng*. 2023;14:20417314231185848. doi:10.1177/20417314231185848

28. Schilling JA. Wound Healing. *Surgical Clinics of North America*. 1976;56(4):859-874. doi:10.1016/S0039-6109(16)40983-7

29. Hayden T. Scarred by disease. *Nature Medicine*. 2011;17(1):18-20. doi:10.1038/nm0111-18

30. Signorini M, Clementoni MT. Clinical Evaluation of a New Self-Drying Silicone Gel in the Treatment of Scars: A Preliminary Report. *Aesth Plast Surg*. 2007;31(2):183-187. doi:10.1007/s00266-005-0122-0

31. Elsaie ML. Update on management of keloid and hypertrophic scars: A systemic review. *Journal of Cosmetic Dermatology*. 2021;20(9):2729-2738. doi:10.1111/jocd.14310

32. Bleasdale B, Finnegan S, Murray K, Kelly S, Percival SL. The Use of Silicone Adhesives for Scar Reduction. *Advances in Wound Care*. 2015;4(7):422-430. doi:10.1089/wound.2015.0625

33. Sadeghinia A, Sadeghinia S. Comparison of the Efficacy of Intralesional Triamcinolone Acetonide and 5-Fluorouracil Tattooing for the Treatment of Keloids. *Dermatologic Surgery*. 2012;38(1):104. doi:10.1111/j.1524-4725.2011.02137.x

34. Coentro JQ, Pugliese E, Hanley G, Raghunath M, Zeugolis DI. Current and upcoming therapies to modulate skin scarring and fibrosis. *Advanced Drug Delivery Reviews*. 2019;146:37-59. doi:10.1016/j.addr.2018.08.009

35. Pugliese E, Coentro JQ, Zeugolis DI. Advancements and Challenges in Multidomain Multicargo Delivery Vehicles. *Advanced Materials*. 2018;30(13):1704324. doi:10.1002/adma.201704324

36. Coentro JQ, di Nubila A, May U, et al. Dual drug delivery collagen vehicles for modulation of skin fibrosis in vitro. *Biomed Mater*. 2022;17(2):025017. doi:10.1088/1748-605X/ac5673

37. Pan BT, Johnstone RM. Fate of the transferrin receptor during maturation of sheep reticulocytes in vitro: Selective externalization of the receptor. *Cell*. 1983;33(3):967-978. doi:10.1016/0092-8674(83)90040-5

38. Harding C, Stahl P. Transferrin recycling in reticulocytes: pH and iron are important determinants of ligand binding and processing. *Biochemical and Biophysical Research Communications*. 1983;113(2):650-658. doi:10.1016/0006-291X(83)91776-X

39. Zhu S, Li S, Yi M, Li N, Wu K. Roles of Microvesicles in Tumor Progression and Clinical Applications. *International Journal of Nanomedicine*. 2021;16:7071-7090. doi:10.2147/IJN.S325448

40. Kalluri R, LeBleu VS. The biology, function, and biomedical applications of exosomes. *Science*. 2020;367(6478):eaau6977. doi:10.1126/science.aau6977

41. Jahangiri B, Saei AK, Obi PO, et al. Exosomes, autophagy and ER stress pathways in human diseases: Cross-regulation and therapeutic approaches. *Biochimica et Biophysica Acta (BBA) - Molecular Basis of Disease*. 2022;1868(10):166484. doi:10.1016/j.bbadis.2022.166484

42. Yuan YG, Wang JL, Zhang YX, Li L, Reza AMMT, Gurunathan S. Biogenesis, Composition and Potential Therapeutic Applications of Mesenchymal Stem Cells Derived Exosomes in Various Diseases. *International Journal of Nanomedicine*. 2023;18:3177-3210. doi:10.2147/IJN.S407029

43. Donoso-Quezada J, Ayala-Mar S, González-Valdez J. The role of lipids in exosome biology and intercellular communication: Function, analytics and applications. *Traffic*. 2021;22(7):204-220. doi:10.1111/tra.12803

44. Gurunathan S, Kang MH, Kim JH. A Comprehensive Review on Factors Influences Biogenesis, Functions, Therapeutic and Clinical Implications of Exosomes. *Int J Nanomedicine*. 2021;16:1281-1312. doi:10.2147/IJN.S291956

45. Wei Y, Wang D, Jin F, et al. Pyruvate kinase type M2 promotes tumour cell exosome release via phosphorylating synaptosome-associated protein 23. *Nat Commun*. 2017;8(1):14041. doi:10.1038/ncomms14041

46. Haraszti RA, Miller R, Dubuke ML, et al. Serum Deprivation of Mesenchymal Stem Cells Improves Exosome Activity and Alters Lipid and Protein Composition. *iScience*. 2019;16:230-241. doi:10.1016/j.isci.2019.05.029

47. Li J, Zhang Y, Dong PY, Yang GM, Gurunathan S. A comprehensive review on the composition, biogenesis, purification, and multifunctional role of exosome as delivery vehicles for cancer therapy. *Biomedicine & Pharmacotherapy*. 2023;165:115087. doi:10.1016/j.biopha.2023.115087

48. Lee YJ, Shin KJ, Chae YC. Regulation of cargo selection in exosome biogenesis and its biomedical applications in cancer. *Exp Mol Med*. 2024;56(4):877-889. doi:10.1038/s12276-024-01209-y

49. Valapala M, Vishwanatha JK. Lipid Raft Endocytosis and Exosomal Transport Facilitate Extracellular Trafficking of Annexin A2 *. *Journal of Biological Chemistry*. 2011;286(35):30911-30925. doi:10.1074/jbc.M111.271155

50. O'Grady T, Njock MS, Lion M, et al. Sorting and packaging of RNA into extracellular vesicles shape intracellular transcript levels. *BMC Biology*. 2022;20(1):72. doi:10.1186/s12915-022-01277-4

51. Prasai A, Jay JW, Jupiter D, Wolf SE, El Ayadi A. Role of Exosomes in Dermal Wound Healing: A Systematic Review. *Journal of Investigative Dermatology*. 2022;142(3, Part A):662-678.e8. doi:10.1016/j.jid.2021.07.167

52. Phillips D, Noble D. Bubbling beyond the barrier: exosomal RNA as a vehicle for soma–germline communication. *The Journal of Physiology*. 2024;602(11):2547-2563. doi:10.1113/JP284420

53. Andreu Z, Yáñez-Mó M. Tetraspanins in Extracellular Vesicle Formation and Function. *Frontiers in Immunology*. 2014;5. Accessed October 26, 2022. https://www.frontiersin.org/articles/10.3389/fimmu.2014.00442

54. The emerging roles of exosomes in the modulation of immune responses in cancer | Genome Medicine | Full Text. Accessed October 28, 2024. https://genomemedicine.biomedcentral.com/articles/10.1186/s13073-018-0535-4

55. Kawamoto E, Masui-Ito A, Eguchi A, et al. Integrin and PD-1 Ligand Expression on Circulating Extracellular Vesicles in Systemic Inflammatory Response Syndrome and Sepsis. *Shock*. 2019;52(1):13. doi:10.1097/SHK.0000000000001228

56. Kawakami K, Fujita Y, Kato T, et al. Integrin β4 and vinculin contained in exosomes are potential markers for progression of prostate cancer associated with taxane-resistance. *Int J Oncol*. 2015;47(1):384-390. doi:10.3892/ijo.2015.3011

57. Rieu S, Géminard C, Rabesandratana H, Sainte-Marie J, Vidal M. Exosomes released during reticulocyte maturation bind to fibronectin via integrin α4β1. *European Journal of Biochemistry*. 2000;267(2):583-590. doi:10.1046/j.1432-1327.2000.01036.x

58. Hoshino A, Costa-Silva B, Shen TL, et al. Tumour exosome integrins determine organotropic metastasis. *Nature*. 2015;527(7578):329-335. doi:10.1038/nature15756

59. Mu W, Xu Y, Gu P, et al. Exosomal CD44 Cooperates with Integrin α6β4 to Support Organotropic Metastasis via Regulating Tumor Cell Motility and Target Host Cell Activation. *Engineering*. 2021;7(10):1413-1423. doi:10.1016/j.eng.2020.08.013

60. Krishn SR, Singh A, Bowler N, et al. Prostate cancer sheds the αvβ3 integrin in vivo through exosomes. *Matrix Biology*. 2019;77:41-57. doi:10.1016/j.matbio.2018.08.004

61. Singh A, Fedele C, Lu H, Nevalainen MT, Keen JH, Languino LR. Exosome-mediated Transfer of αvβ3 Integrin from Tumorigenic to Non-Tumorigenic Cells Promotes a Migratory Phenotype. *Mol Cancer Res*. 2016;14(11):1136-1146. doi:10.1158/1541-7786.MCR-16-0058

62. Fedele C, Singh A, Zerlanko BJ, Iozzo RV, Languino LR. The αvβ6 Integrin Is Transferred Intercellularly via Exosomes. *J Biol Chem*. 2015;290(8):4545-4551. doi:10.1074/jbc.C114.617662

63. Skokos D, Le Panse S, Villa I, et al. Mast Cell-Dependent B and T Lymphocyte Activation Is Mediated by the Secretion of Immunologically Active Exosomes1. *The Journal of Immunology*. 2001;166(2):868-876. doi:10.4049/jimmunol.166.2.868

64. Van Niel G, Raposo G, Candalh C, et al. Intestinal epithelial cells secrete exosome–like vesicles. *Gastroenterology*. 2001;121(2):337-349. doi:10.1053/gast.2001.26263

65. Sanderson RD, Bandari SK, Vlodavsky I. Proteases and glycosidases on the surface of exosomes: Newly discovered mechanisms for extracellular remodeling. *Matrix Biology*. 2019;75-76:160-169. doi:10.1016/j.matbio.2017.10.007

66. Mosquera-Heredia MI, Morales LC, Vidal OM, et al. Exosomes: Potential Disease Biomarkers and New Therapeutic Targets. *Biomedicines*. 2021;9(8):1061. doi:10.3390/biomedicines9081061

67. Runz S, Keller S, Rupp C, et al. Malignant ascites-derived exosomes of ovarian carcinoma patients contain CD24 and EpCAM. *Gynecologic Oncology*. 2007;107(3):563-571. doi:10.1016/j.ygyno.2007.08.064

68. Niu L, Song X, Wang N, Xue L, Song X, Xie L. Tumor-derived exosomal proteins as diagnostic biomarkers in non-small cell lung cancer. *Cancer Sci*. 2019;110(1):433-442. doi:10.1111/cas.13862

69. Chauhan S, Danielson S, Clements V, Edwards N, Ostrand-Rosenberg S, Fenselau C. Surface Glycoproteins of Exosomes Shed by Myeloid-Derived Suppressor Cells Contribute to Function. *J Proteome Res*. 2017;16(1):238-246. doi:10.1021/acs.jproteome.6b00811

70. de Gassart A, Géminard C, Février B, Raposo G, Vidal M. Lipid raft-associated protein sorting in exosomes. *Blood*. 2003;102(13):4336-4344. doi:10.1182/blood-2003-03-0871

71. Kumar MA, Baba SK, Sadida HQ, et al. Extracellular vesicles as tools and targets in therapy for diseases. *Sig Transduct Target Ther*. 2024;9(1):1-41. doi:10.1038/s41392-024-01735-1

72. Figueroa JM, Skog J, Akers J, et al. Detection of wild-type EGFR amplification and EGFRvIII mutation in CSF-derived extracellular vesicles of glioblastoma patients. *Neuro Oncol*. 2017;19(11):1494-1502. doi:10.1093/neuonc/nox085

73. Nafar F, Williams JB, Mearow KM. Astrocytes Release HspB1 in Response to Amyloid-β Exposure in vitro. *Journal of Alzheimer's Disease*. 2016;49(1):251-263. doi:10.3233/JAD-150317

74. Zhang Y, Liu Y, Liu H, Tang WH. Exosomes: biogenesis, biologic function and clinical potential. *Cell & Bioscience*. 2019;9(1):19. doi:10.1186/s13578-019-0282-2

75. Willms E, Johansson HJ, Mäger I, et al. Cells release subpopulations of exosomes with distinct molecular and biological properties. *Sci Rep*. 2016;6(1):22519. doi:10.1038/srep22519

76. Shelke GV, Yin Y, Jang SC, et al. Endosomal signalling via exosome surface TGFβ-1. *Journal of Extracellular Vesicles*. 2019;8(1):1650458. doi:10.1080/20013078.2019.1650458

77. Treps L, Perret R, Edmond S, Ricard D, Gavard J. Glioblastoma stem-like cells secrete the pro-angiogenic VEGF-A factor in extracellular vesicles. *J Extracell Vesicles*. 2017;6(1):1359479. doi:10.1080/20013078.2017.1359479

78. Zhang H, Deng T, Liu R, et al. Exosome-delivered EGFR regulates liver microenvironment to promote gastric cancer liver metastasis. *Nat Commun*. 2017;8(1):15016. doi:10.1038/ncomms15016

79. Esser J, Gehrmann U, D'Alexandri FL, et al. Exosomes from human macrophages and dendritic cells contain enzymes for leukotriene biosynthesis and promote granulocyte migration. *Journal of Allergy and Clinical Immunology*. 2010;126(5):1032-1040.e4. doi:10.1016/j.jaci.2010.06.039

80. Kahlert C, Melo SA, Protopopov A, et al. Identification of Double-stranded Genomic DNA Spanning All Chromosomes with Mutated KRAS and p53 DNA in the Serum Exosomes of Patients with Pancreatic Cancer *. *Journal of Biological Chemistry*. 2014;289(7):3869-3875. doi:10.1074/jbc.C113.532267

81. Németh A, Orgovan N, Sódar BW, et al. Antibiotic-induced release of small extracellular vesicles (exosomes) with surface-associated DNA. *Sci Rep*. 2017;7:8202. doi:10.1038/s41598-017-08392-1

82. Valadi H, Ekström K, Bossios A, Sjöstrand M, Lee JJ, Lötvall JO. Exosome-mediated transfer of mRNAs and microRNAs is a novel mechanism of genetic exchange between cells. *Nat Cell Biol*. 2007;9(6):654-659. doi:10.1038/ncb1596

83. Liu X hua, Sun M, Nie F qi, et al. Lnc RNA HOTAIR functions as a competing endogenous RNA to regulate HER2 expression by sponging miR-331-3p in gastric cancer. *Mol Cancer*. 2014;13:92. doi:10.1186/1476-4598-13-92

84. Zhao R, Zhang Y, Zhang X, et al. Exosomal long noncoding RNA HOTTIP as potential novel diagnostic and prognostic biomarker test for gastric cancer. *Molecular Cancer*. 2018;17(1):68. doi:10.1186/s12943-018-0817-x

85. Pan B, Qin J, Liu X, et al. Identification of Serum Exosomal hsa-circ-0004771 as a Novel Diagnostic Biomarker of Colorectal Cancer. *Front Genet*. 2019;10:1096. doi:10.3389/fgene.2019.01096

86. Li C, Ni YQ, Xu H, et al. Roles and mechanisms of exosomal non-coding RNAs in human health and diseases. *Sig Transduct Target Ther*. 2021;6(1):1-31. doi:10.1038/s41392-021-00779-x

87. Rezaie J, Feghhi M, Etemadi T. A review on exosomes application in clinical trials: perspective, questions, and challenges. *Cell Communication and Signaling*. 2022;20(1):145. doi:10.1186/s12964-022-00959-4

88. Boukouris S, Mathivanan S. Exosomes in bodily fluids are a highly stable resource of disease biomarkers. *Proteomics Clin Appl*. 2015;9(3-4):358-367. doi:10.1002/prca.201400114

89. Han C, Sun X, Liu L, et al. Exosomes and Their Therapeutic Potentials of Stem Cells. *Stem Cells Int*. 2016;2016:7653489. doi:10.1155/2016/7653489

90. Hu S, Li Z, Cores J, et al. Needle-Free Injection of Exosomes Derived from Human Dermal Fibroblast Spheroids Ameliorates Skin Photoaging. *ACS Nano*. 2019;13(10):11273-11282. doi:10.1021/acsnano.9b04384

91. Kotmakçı M, Çetintaş VB. Extracellular Vesicles as Natural Nanosized Delivery Systems for Small-Molecule Drugs and Genetic Material: Steps towards the Future Nanomedicines. *Journal of Pharmacy & Pharmaceutical Sciences*. 2015;18(3):396-413. doi:10.18433/J36W3X

92. Subhan BS, Ki M, Verzella A, Shankar S, Rabbani PS. Behind the Scenes of Extracellular Vesicle Therapy for Skin Injuries and Disorders. *Advances in Wound Care*. 2022;11(11):575-597. doi:10.1089/wound.2021.0066

93. Wang L, Hu L, Zhou X, et al. Exosomes secreted by human adipose mesenchymal stem cells promote scarless cutaneous repair by regulating extracellular matrix remodelling. *Sci Rep*. 2017;7(1):13321. doi:10.1038/s41598-017-12919-x

94. Shabbir A, Cox A, Rodriguez-Menocal L, Salgado M, Badiavas EV. Mesenchymal Stem Cell Exosomes Induce Proliferation and Migration of Normal and Chronic Wound Fibroblasts, and Enhance Angiogenesis In Vitro. *Stem Cells and Development*. 2015;24(14):1635-1647. doi:10.1089/scd.2014.0316

95. Li Y, Zhang J, Shi J, et al. Exosomes derived from human adipose mesenchymal stem cells attenuate hypertrophic scar fibrosis by miR-192-5p/IL-17RA/Smad axis. *Stem Cell Res Ther*. 2021;12(1):221. doi:10.1186/s13287-021-02290-0

96. Liu J, Yan Z, Yang F, et al. Exosomes Derived from Human Umbilical Cord Mesenchymal Stem Cells Accelerate Cutaneous Wound Healing by Enhancing Angiogenesis through Delivering Angiopoietin-2. *Stem Cell Rev and Rep*. 2021;17(2):305-317. doi:10.1007/s12015-020-09992-7

97. Fang S, Xu C, Zhang Y, et al. Umbilical Cord-Derived Mesenchymal Stem Cell-Derived Exosomal MicroRNAs Suppress Myofibroblast Differentiation by Inhibiting the Transforming Growth Factor-β/SMAD2 Pathway During Wound Healing. *Stem Cells Transl Med*. 2016;5(10):1425-1439. doi:10.5966/sctm.2015-0367

98. Zhao B, Li X, Shi X, et al. Exosomal MicroRNAs Derived from Human Amniotic Epithelial Cells Accelerate Wound Healing by Promoting the Proliferation and Migration of Fibroblasts. *Stem Cells International*. 2018;2018(1):5420463. doi:10.1155/2018/5420463

99. Geiger A, Walker A, Nissen E. Human fibrocyte-derived exosomes accelerate wound healing in genetically diabetic mice. *Biochemical and Biophysical Research Communications*. 2015;467(2):303-309. doi:10.1016/j.bbrc.2015.09.166

100. Yang J, Chen Z, Pan D, Li H, Shen J. Umbilical Cord-Derived Mesenchymal Stem Cell-Derived Exosomes Combined Pluronic F127 Hydrogel Promote Chronic Diabetic Wound Healing and Complete Skin Regeneration. *Int J Nanomedicine*. 2020;15:5911-5926. doi:10.2147/IJN.S249129

101. Zhao D, Yu Z, Li Y, Wang Y, Li Q, Han D. GelMA combined with sustained release of HUVECs derived exosomes for promoting cutaneous wound healing and facilitating skin regeneration. *J Mol Hist*. 2020;51(3):251-263. doi:10.1007/s10735-020-09877-6

102. Yang Y, Zhang J, Wu S, et al. Exosome/antimicrobial peptide laden hydrogel wound dressings promote scarless wound healing through miR-21-5p-mediated multiple functions. *Biomaterials*. 2024;308:122558. doi:10.1016/j.biomaterials.2024.122558

103. Joorabloo A, Liu T. Engineering exosome-based biomimetic nanovehicles for wound healing. *Journal of Controlled Release*. 2023;356:463-480. doi:10.1016/j.jconrel.2023.03.013

104. Hu Y, Tao R, Chen L, et al. Exosomes derived from pioglitazone-pretreated MSCs accelerate diabetic wound healing through enhancing angiogenesis. *Journal of Nanobiotechnology*. 2021;19(1):150. doi:10.1186/s12951-021-00894-5

105. Yu M, Liu W, Li J, et al. Exosomes derived from atorvastatin-pretreated MSC accelerate diabetic wound repair by enhancing angiogenesis via AKT/eNOS pathway. *Stem Cell Res Ther*. 2020;11(1):350. doi:10.1186/s13287-020-01824-2

106. Wang J, Chen D, Ho EA. Challenges in the development and establishment of exosome-based drug delivery systems. *J Control Release*. Published online October 12, 2020. doi:10.1016/j.jconrel.2020.10.020

107. Sabnis N, Lacko AG. Drug delivery via lipoprotein-based carriers: answering the challenges in systemic therapeutics. *Therapeutic Delivery*. 2012;3(5):599-608. doi:10.4155/tde.12.41

108. Grigor'eva AE, Dyrkheeva NS, Bryzgunova OE, Tamkovich SN, Chelobanov BP, Ryabchikova EI. Contamination of exosome preparations, isolated from biological fluids. *Biochem Moscow Suppl Ser B*. 2017;11(3):265-271. doi:10.1134/S1990750817030040

109. Cvjetkovic A, Lötvall J, Lässer C. The influence of rotor type and centrifugation time on the yield and purity of extracellular vesicles. *J Extracell Vesicles*. 2014;3. doi:10.3402/jev.v3.23111

110. Lobb RJ, Becker M, Wen S, et al. Optimized exosome isolation protocol for cell culture supernatant and human plasma. *J Extracell Vesicles*. 2015;4(0):27031. doi:10.3402/jev.v4.27031

111. Gupta S, Rawat S, Arora V, et al. An improvised one-step sucrose cushion ultracentrifugation method for exosome isolation from culture supernatants of mesenchymal stem cells. *Stem Cell Research & Therapy*. 2018;9(1):180. doi:10.1186/s13287-018-0923-0

112. Sódar BW, Kittel Á, Pálóczi K, et al. Low-density lipoprotein mimics blood plasma-derived exosomes and microvesicles during isolation and detection. *Scientific Reports*. 2016;6:24316. doi:10.1038/srep24316

113. Yuana Y, Levels J, Grootemaat A, Sturk A, Nieuwland R. Co-isolation of extracellular vesicles and high-density lipoproteins using density gradient ultracentrifugation. *Journal of Extracellular Vesicles*. 2014;3(1):23262. doi:10.3402/jev.v3.23262

114. Onódi Z, Pelyhe C, Terézia Nagy C, et al. Isolation of High-Purity Extracellular Vesicles by the Combination of Iodixanol Density Gradient Ultracentrifugation and Bind-Elute Chromatography From Blood Plasma. *Front Physiol*. 2018;9. doi:10.3389/fphys.2018.01479

115. Baranyai T, Herczeg K, Onódi Z, et al. Isolation of Exosomes from Blood Plasma: Qualitative and Quantitative Comparison of Ultracentrifugation and Size Exclusion Chromatography Methods. *Plos One*. 2015;10(12):e0145686. doi:10.1371/journal.pone.0145686

116. Ana GV, Marta MT, Laura CP, Franquesa M, Beyer K, Borràs FE. Size-Exclusion Chromatography-based isolation minimally alters Extracellular Vesicles' characteristics compared to precipitating agents. *Sci Reports*. 2016;6(1):srep33641. doi:10.1038/srep33641

117. Böing A, Pol E, Grootemaat A, Coumans F, Sturk A, Nieuwland R. Single-step isolation of extracellular vesicles by size-exclusion chromatography. *J Extracell Vesicles*. 2014;3(0). doi:10.3402/jev.v3.23430

118. Hagel L, Östberg M, Andersson T. Apparent pore size distributions of chromatography media. *Journal of Chromatography A*. 1996;743(1):33-42. doi:10.1016/0021-9673(96)00130-6

119. Burgess RR. A brief practical review of size exclusion chromatography: Rules of thumb, limitations, and troubleshooting. *Protein Expression and Purification*. 2018;150:81-85. doi:10.1016/j.pep.2018.05.007

120. Heinemann ML, Ilmer M, Silva LP, et al. Benchtop isolation and characterization of functional exosomes by sequential filtration. *Journal of Chromatography A*. 2014;1371:125-135. doi:10.1016/j.chroma.2014.10.026

121. Busatto S, Vilanilam G, Ticer T, et al. Tangential Flow Filtration for Highly Efficient Concentration of Extracellular Vesicles from Large Volumes of Fluid. *Cells*. 2018;7(12):273. doi:10.3390/cells7120273

122. Ouahabi OE, Salim H, Pero-Gascon R, Benavente F. A simple method for the analysis of extracellular vesicles enriched for exosomes from human serum by capillary electrophoresis with ultraviolet diode array detection. *Journal of Chromatography A*. 2021;1635:461752. doi:10.1016/j.chroma.2020.461752

123. Weng Y, Sui Z, Shan Y, et al. Effective isolation of exosomes with polyethylene glycol from cell culture supernatant for in-depth proteome profiling. *Analyst*. 2016;141(15):4640-4646. doi:10.1039/C6AN00892E

124. Liu W zhao, Ma Z jun, Kang X wen. Current status and outlook of advances in exosome isolation. *Anal Bioanal Chem*. 2022;414(24):7123-7141. doi:10.1007/s00216-022-04253-7

125. Patel GK, Khan MA, Zubair H, et al. Comparative analysis of exosome isolation methods using culture supernatant for optimum yield, purity and downstream applications. *Scientific Reports*. 2019;9(1):5335. doi:10.1038/s41598-019-41800-2

126. Zarovni N, Corrado A, Guazzi P, et al. Integrated isolation and quantitative analysis of exosome shuttled proteins and nucleic acids using immunocapture approaches. *Methods*. 2015;87:46-58. doi:10.1016/j.ymeth.2015.05.028

127. Yavuz CT, Prakash A, Mayo JT, Colvin VL. Magnetic separations: From steel plants to biotechnology. *Chemical Engineering Science*. 2009;64(10):2510-2521. doi:10.1016/j.ces.2008.11.018

128. Livshits MA, Khomyakova E, Evtushenko EG, et al. Isolation of exosomes by differential centrifugation: Theoretical analysis of a commonly used protocol. *Scientific Reports*. 2015;5(1):1-14. doi:10.1038/srep17319

129. Tauro BJ, Greening DW, Mathias RA, et al. Comparison of ultracentrifugation, density gradient separation, and immunoaffinity capture methods for isolating human colon cancer cell line LIM1863-derived exosomes. *Methods*. 2012;56(2):293-304. doi:10.1016/j.ymeth.2012.01.002

130. Welton J, Webber J, Botos LA, Jones M, Clayton A. Ready-made chromatography columns for extracellular vesicle isolation from plasma. *J Extracell Vesicles*. 2015;4(0):27269. doi:10.3402/jev.v4.27269

131. McNamara RP, Caro-Vegas CP, Costantini LM, et al. Large-scale, cross-flow based isolation of highly pure and endocytosis-competent extracellular vesicles. *J Extracell Vesicles*. 2018;7(1). doi:10.1080/20013078.2018.1541396

132. Midekessa G, Godakumara K, Ord J, et al. Zeta Potential of Extracellular Vesicles: Toward Understanding the Attributes that Determine Colloidal Stability. *ACS Omega*. 2020;5(27):16701-16710. doi:10.1021/acsomega.0c01582

133. Szatanek R, Baj-Krzyworzeka M, Zimoch J, Lekka M, Siedlar M, Baran J. The Methods of Choice for Extracellular Vesicles (EVs) Characterization. *Int J Mol Sci*. 2017;18(6):1153. doi:10.3390/ijms18061153

134. Théry C, Witwer KW, Aikawa E, et al. Minimal information for studies of extracellular vesicles 2018 (MISEV2018): a position statement of the International Society for Extracellular Vesicles and update of the MISEV2014 guidelines. *Journal of Extracellular Vesicles*. 2018;7(1):1535750. doi:10.1080/20013078.2018.1535750

135. Webber J, Clayton A. How pure are your vesicles? *Journal of Extracellular Vesicles*. 2013;2(1):19861. doi:10.3402/jev.v2i0.19861

136. Yurtsever A, Yoshida T, Behjat AB, Araki Y, Hanayama R, Fukuma T. Structural and mechanical characteristics of exosomes from osteosarcoma cells explored by 3D-atomic force microscopy. *Nanoscale*. 2021;13(13):6661-6677. doi:10.1039/D0NR09178B

137. Wu JY, Li YJ, Hu XB, Huang S, Xiang DX. Preservation of small extracellular vesicles for functional analysis and therapeutic applications: a comparative evaluation of storage conditions. *Drug Delivery*. 2021;28(1):162. doi:10.1080/10717544.2020.1869866

138. Witwer KW, Buzás EI, Bemis LT, et al. Standardization of sample collection, isolation and analysis methods in extracellular vesicle research. *Journal of Extracellular Vesicles*. 2013;2(1):20360. doi:10.3402/jev.v2i0.20360

139. Yeo RWY, Lai RC, Zhang B, et al. Mesenchymal stem cell: An efficient mass producer of exosomes for drug delivery. *Advanced Drug Delivery Reviews*. 2013;65(3):336-341. doi:10.1016/j.addr.2012.07.001

140. Wong T, McGrath JA, Navsaria H. The role of fibroblasts in tissue engineering and regeneration. *British Journal of Dermatology*. 2007;156(6):1149-1155. doi:10.1111/j.1365-2133.2007.07914.x

141. Lyu TS, Ahn Y, Im YJ, et al. The characterization of exosomes from fibrosarcoma cell and the useful usage of Dynamic Light Scattering (DLS) for their evaluation. *PLOS ONE*. 2021;16(1):e0231994. doi:10.1371/journal.pone.0231994

142. Lai JJ, Chau ZL, Chen S, et al. Exosome Processing and Characterization Approaches for Research and Technology Development. *Adv Sci (Weinh)*. 2022;9(15):2103222. doi:10.1002/advs.202103222

143. Golan ME, Stice SL. Extracellular vesicle lyophilization for enhanced distribution to the point of care. *Extracellular Vesicle*. 2024;3:100041. doi:10.1016/j.vesic.2024.100041

144. Kar R, Dhar R, Mukherjee S, et al. Exosome-Based Smart Drug Delivery Tool for Cancer Theranostics. *ACS Biomater Sci Eng*. 2023;9(2):577-594. doi:10.1021/acsbiomaterials.2c01329

145. Trivedi M, Talekar M, Shah P, Ouyang Q, Amiji M. Modification of tumor cell exosome content by transfection with wt-p53 and microRNA-125b expressing plasmid DNA and its effect on macrophage polarization. *Oncogenesis*. 2016;5(8):e250-e250. doi:10.1038/oncsis.2016.52

146. Ran N, Gao X, Dong X, et al. Effects of exosome-mediated delivery of myostatin propeptide on functional recovery of mdx mice. *Biomaterials*. 2020;236:119826. doi:10.1016/j.biomaterials.2020.119826

147. Pascucci L, Coccè V, Bonomi A, et al. Paclitaxel is incorporated by mesenchymal stromal cells and released in exosomes that inhibit in vitro tumor growth: A new approach for drug delivery. *Journal of Controlled Release*. 2014;192:262-270. doi:10.1016/j.jconrel.2014.07.042

148. Agrawal AK, Aqil F, Jeyabalan J, et al. Milk-derived exosomes for oral delivery of paclitaxel. *Nanomedicine: Nanotechnology, Biology and Medicine*. 2017;13(5):1627-1636. doi:10.1016/j.nano.2017.03.001

149. Wang C, Li N, Li Y, et al. Engineering a HEK-293T exosome-based delivery platform for efficient tumor-targeting chemotherapy/internal irradiation combination therapy. *J Nanobiotechnology*. 2022;20(1):247. doi:10.1186/s12951-022-01462-1

150. Yang X, Shi G, Guo J, Wang C, He Y. Exosome-encapsulated antibiotic against intracellular infections of methicillin-resistant Staphylococcus aureus. *International Journal of Nanomedicine*. 2018;13:8095-8104. doi:10.2147/IJN.S179380

151. Saari H, Lázaro-Ibáñez E, Viitala T, Vuorimaa-Laukkanen E, Siljander P, Yliperttula M. Microvesicle- and exosome-mediated drug delivery enhances the cytotoxicity of Paclitaxel in autologous prostate cancer cells. *Journal of Controlled Release*. 2015;220:727-737. doi:10.1016/j.jconrel.2015.09.031

152. Fuhrmann G, Serio A, Mazo M, Nair R, Stevens MM. Active loading into extracellular vesicles significantly improves the cellular uptake and photodynamic effect of porphyrins. *Journal of Controlled Release*. 2015;205:35-44. doi:10.1016/j.jconrel.2014.11.029

153. Johnsen KB, Gudbergsson JM, Skov MN, Pilgaard L, Moos T, Duroux M. A comprehensive overview of exosomes as drug delivery vehicles — Endogenous nanocarriers for targeted cancer therapy. *Biochimica et Biophysica Acta (BBA) - Reviews on Cancer*. 2014;1846(1):75-87. doi:10.1016/j.bbcan.2014.04.005

154. Haney MJ, Zhao Y, Jin YS, et al. Macrophage-Derived Extracellular Vesicles as Drug Delivery Systems for Triple Negative Breast Cancer (TNBC) Therapy. *J Neuroimmune Pharmacol*. Published online November 13, 2019. doi:10.1007/s11481-019-09884-9

155. Mane R, Dhumal A, Shinde S, Vardikar A, Ali M Osmani R, Rajput A. Exosomes as a roadmap from research to clinical development in the management of skin diseases. *Journal of Drug Delivery Science and Technology*. 2024;97:105832. doi:10.1016/j.jddst.2024.105832

156. Tsong TY. Electroporation of Cell Membranes. In: Neumann E, Sowers AE, Jordan CA, eds. *Electroporation and Electrofusion in Cell Biology*. Springer US; 1989:149-163. doi:10.1007/978-1-4899-2528-2_9

157. Liang G, Zhu Y, Ali DJ, et al. Engineered exosomes for targeted co-delivery of miR-21 inhibitor and chemotherapeutics to reverse drug resistance in colon cancer. *J Nanobiotechnology*. 2020;18(1):10. doi:10.1186/s12951-019-0563-2

158. Kooijmans SAA, Stremersch S, Braeckmans K, et al. Electroporation-induced siRNA precipitation obscures the efficiency of siRNA loading into extracellular vesicles. *Journal of Controlled Release*. 2013;172(1):229-238. doi:10.1016/j.jconrel.2013.08.014

159. Wu G, Zhang J, Zhao Q, et al. Molecularly Engineered Macrophage-Derived Exosomes with Inflammation Tropism and Intrinsic Heme Biosynthesis for Atherosclerosis Treatment. *Angewandte Chemie International Edition*. 2020;59(10):4068-4074. doi:10.1002/anie.201913700

160. Kim MS, Haney MJ, Zhao Y, et al. Development of exosome-encapsulated paclitaxel to overcome MDR in cancer cells. *Nanomedicine: Nanotechnology, Biology and Medicine*. 2016;12(3):655-664. doi:10.1016/j.nano.2015.10.012

161. Hajipour H, Farzadi L, Roshangar L, et al. A human chorionic gonadotropin (hCG) delivery platform using engineered uterine exosomes to improve endometrial receptivity. *Life Sciences*. 2021;275:119351. doi:10.1016/j.lfs.2021.119351

162. Shany S, Bernheimer AW, Grushoff PS, Kim KS. Evidence for membrane cholesterol as the common binding site for cereolysin, streptolysin O and saponin. *Mol Cell Biochem*. 1974;3(3):179-186. doi:10.1007/BF01686643

163. Luan X, Sansanaphongpricha K, Myers I, Chen H, Yuan H, Sun D. Engineering exosomes as refined biological nanoplatforms for drug delivery. *Acta Pharmacologica Sinica*. 2017;38(6):754-763. doi:10.1038/aps.2017.12

164. Oskouie MN, Moghaddam NSA, Butler AE, Zamani P, Sahebkar A. Therapeutic use of curcumin-encapsulated and curcumin-primed exosomes. *Journal of Cellular Physiology*. 2019;234(6):8182-8191. doi:10.1002/jcp.27615

165. Zhang Y, Liu Y, Teng Z, et al. Human umbilical cord mesenchymal stem cells (hUC-MSCs) alleviate paclitaxel-induced spermatogenesis defects and maintain male fertility. *Biol Res*. 2023;56:47. doi:10.1186/s40659-023-00459-w

166. Kim MS, Haney MJ, Zhao Y, et al. Engineering macrophage-derived exosomes for targeted paclitaxel delivery to pulmonary metastases: in vitro and in vivo evaluations. *Nanomedicine: Nanotechnology, Biology and Medicine*. 2018;14(1):195-204. doi:10.1016/j.nano.2017.09.011

167. Wang P, Wang H, Huang Q, et al. Exosomes from M1-Polarized Macrophages Enhance Paclitaxel Antitumor Activity by Activating Macrophages-Mediated Inflammation. *Theranostics*. 2019;9(6):1714-1727. doi:10.7150/thno.30716

168. Li YJ, Wu JY, Wang JM, Hu XB, Cai JX, Xiang DX. Gemcitabine loaded autologous exosomes for effective and safe chemotherapy of pancreatic cancer. *Acta Biomaterialia*. 2020;101:519-530. doi:10.1016/j.actbio.2019.10.022

169. Kumar DN, Chaudhuri A, Kumar D, Singh S, Agrawal AK. Impact of the Drug Loading Method on the Drug Distribution and Biological Efficacy of Exosomes. *AAPS PharmSciTech*. 2023;24(6):166. doi:10.1208/s12249-023-02624-6

170. Al Faruque H, Choi ES, Kim JH, Kim E. Enhanced effect of autologous EVs delivering paclitaxel in pancreatic cancer. *Journal of Controlled Release*. 2022;347:330-346. doi:10.1016/j.jconrel.2022.05.012

171. Gao ZS, Zhang CJ, Xia N, et al. Berberine-loaded M2 macrophage-derived exosomes for spinal cord injury therapy. *Acta Biomaterialia*. 2021;126:211-223. doi:10.1016/j.actbio.2021.03.018

172. Yerneni SS, Yalcintas EP, Smith JD, Averick S, Campbell PG, Ozdoganlar OB. Skin-targeted delivery of extracellular vesicle-encapsulated curcumin using dissolvable microneedle arrays. *Acta Biomaterialia*. 2022;149:198-212. doi:10.1016/j.actbio.2022.06.046

173. González-Sarrías A, Iglesias-Aguirre CE, Cortés-Martín A, et al. Milk-Derived Exosomes as Nanocarriers to Deliver Curcumin and Resveratrol in Breast Tissue and Enhance Their Anticancer Activity. *Int J Mol Sci*. 2022;23(5):2860. doi:10.3390/ijms23052860

174. Du J, Wan Z, Wang C, et al. Designer exosomes for targeted and efficient ferroptosis induction in cancer via chemo-photodynamic therapy. *Theranostics*. 2021;11(17):8185-8196. doi:10.7150/thno.59121

175. Yang X, Xie B, Peng H, et al. Eradicating intracellular MRSA *via* targeted delivery of lysostaphin and vancomycin with mannose-modified exosomes. *Journal of Controlled Release*. 2021;329:454-467. doi:10.1016/j.jconrel.2020.11.045

176. Tran PHL, Wang T, Yin W, et al. Development of a nanoamorphous exosomal delivery system as an effective biological platform for improved encapsulation of hydrophobic drugs. *International Journal of Pharmaceutics*. 2019;566:697-707. doi:10.1016/j.ijpharm.2019.06.028

177. Gul R, Bashir H, Sarfraz M, et al. Human plasma derived exosomes: Impact of active and passive drug loading approaches on drug delivery. *Saudi Pharmaceutical Journal*. 2024;32(6):102096. doi:10.1016/j.jsps.2024.102096

178. Zeng H, Guo S, Ren X, Wu Z, Liu S, Yao X. Current Strategies for Exosome Cargo Loading and Targeting Delivery. *Cells*. 2023;12(10):1416. doi:10.3390/cells12101416

179. Nizamudeen ZA, Xerri R, Parmenter C, et al. Low-Power Sonication Can Alter Extracellular Vesicle Size and Properties. *Cells*. 2021;10(9):2413. doi:10.3390/cells10092413

180. Mukhopadhya A, Tsiapalis D, McNamee N, Talbot B, O'Driscoll L. Doxorubicin Loading into Milk and Mesenchymal Stem Cells' Extracellular Vesicles as Drug Delivery Vehicles. *Pharmaceutics*. 2023;15(3):718. doi:10.3390/pharmaceutics15030718

181. Verhaegen PDHM, Van Zuijlen PPM, Pennings NM, et al. Differences in collagen architecture between keloid, hypertrophic scar, normotrophic scar, and normal skin: An objective histopathological analysis. *Wound Repair and Regeneration*. 2009;17(5):649-656. doi:10.1111/j.1524-475X.2009.00533.x

182. Peter Craig RD, David Schofield J, Jackson DS. Collagen biosynthesis in normal and hypertrophic scars and keloid as a function of the duration of the scar. *British Journal of Surgery*. 1975;62(9):741-744. doi:10.1002/bjs.1800620917

183. Sabino F, Keller U auf dem. Matrix metalloproteinases in impaired wound healing. *MNM*. 2015;2:1-8. doi:10.2147/MNM.S68420

184. Page-McCaw A, Ewald AJ, Werb Z. Matrix metalloproteinases and the regulation of tissue remodelling. *Nat Rev Mol Cell Biol*. 2007;8(3):221-233. doi:10.1038/nrm2125

185. Fujiwara M, Muragaki Y, Ooshima A. Keloid-derived fibroblasts show increased secretion of factors involved in collagen turnover and depend on matrix metalloproteinase for migration. *Br J Dermatol*. 2005;153(2):295-300. doi:10.1111/j.1365-2133.2005.06698.x

186. Cristodor PL, Nechifor A, Fotea S, et al. New Antifibroblastic Medication in Dermatology: Could Nintedanib Treat Scarring? *International Journal of General Medicine*. 2022;15:7169. doi:10.2147/IJGM.S377073

187. Hall CL, Wells AR, Leung KP. Pirfenidone reduces profibrotic responses in human dermal myofibroblasts, in vitro. *Lab Invest*. 2018;98(5):640-655. doi:10.1038/s41374-017-0014-3

188. Armendariz-Borunda J, Lyra-Gonzalez I, Medina-Preciado D, et al. A controlled clinical trial with pirfenidone in the treatment of pathological skin scarring caused by burns in pediatric patients. *Ann Plast Surg*. 2012;68(1):22-28. doi:10.1097/SAP.0b013e31821b6d08

189. Chen J, Wang H, Mei L, et al. A pirfenidone loaded spray dressing based on lyotropic liquid crystals for deep partial thickness burn treatment: healing promotion and scar prophylaxis. *J Mater Chem B*. 2020;8(13):2573-2588. doi:10.1039/C9TB02929J

190. Satish L, Evdokiou A, Geletu E, Hahn JM, Supp DM. Pirfenidone inhibits epithelial–mesenchymal transition in keloid keratinocytes. *Burns Trauma*. 2020;8:tkz007. doi:10.1093/burnst/tkz007

191. He J, Meng X, Meng C, et al. Layer-by-Layer Pirfenidone/Cerium Oxide Nanocapsule Dressing Promotes Wound Repair and Prevents Scar Formation. *Molecules*. 2022;27(6):1830. doi:10.3390/molecules27061830

192. Nanoparticles Encapsulated with LL37 and Serpin A1 Promotes Wound Healing and Synergistically Enhances Antibacterial Activity | Molecular Pharmaceutics. Accessed April 16, 2024. https://pubs.acs.org/doi/full/10.1021/acs.molpharmaceut.6b00099

193. Han X, Wu P, Li L, et al. Exosomes derived from autologous dermal fibroblasts promote diabetic cutaneous wound healing through the Akt/β-catenin pathway. *Cell Cycle*. 2021;20(5-6):616-629. doi:10.1080/15384101.2021.1894813

194. Xia W, Li M, Jiang X, et al. Young fibroblast-derived exosomal microRNA-125b transfers beneficial effects on aged cutaneous wound healing. *Journal of Nanobiotechnology*. 2022;20(1):144. doi:10.1186/s12951-022-01348-2

195. In vitro scratch assay: a convenient and inexpensive method for analysis of cell migration in vitro - PubMed. Accessed December 23, 2021. https://pubmed-ncbi-nlm-nih-gov.proxy.lib.uwaterloo.ca/17406593/

196. Horibe S, Tanahashi T, Kawauchi S, Murakami Y, Rikitake Y. Mechanism of recipient cell-dependent differences in exosome uptake. *BMC Cancer*. 2018;18(1):47. doi:10.1186/s12885-017-3958-1

197. Liu H, Shen M, Zhao D, et al. The Effect of Triptolide-Loaded Exosomes on the Proliferation and Apoptosis of Human Ovarian Cancer SKOV3 Cells. BioMed Research International. doi:https://doi.org/10.1155/2019/2595801

198. Clément V, Roy V, Paré B, et al. Tridimensional cell culture of dermal fibroblasts promotes exosome-mediated secretion of extracellular matrix proteins. *Sci Rep*. 2022;12(1):19786. doi:10.1038/s41598-022-23433-0

199. Nojima H, Freeman CM, Schuster RM, et al. Hepatocyte exosomes mediate liver repair and regeneration via sphingosine-1-phosphate. *Journal of Hepatology*. 2016;64(1):60-68. doi:10.1016/j.jhep.2015.07.030

200. Huang J, Ding Z, Luo Q, Xu W. Cancer cell-derived exosomes promote cell proliferation and inhibit cell apoptosis of both normal lung fibroblasts and non-small cell lung cancer cell through delivering alpha-smooth muscle actin. *Am J Transl Res*. 2019;11(3):1711-1723.

201. Cheng S, Xi Z, Chen G, Liu K, Ma R, Zhou C. Extracellular vesicle-carried microRNA-27b derived from mesenchymal stem cells accelerates cutaneous wound healing via E3 ubiquitin ligase ITCH. *Journal of Cellular and Molecular Medicine*. 2020;24(19):11254-11271. doi:10.1111/jcmm.15692

202. Pelley JW. 20 - Tissue Biochemistry. In: Pelley JW, ed. *Elsevier's Integrated Biochemistry*. Mosby; 2007:179-190. doi:10.1016/B978-0-323-03410-4.50026-2

203. Shi K, Wang F, Xia J, Zuo B, Wang Z, Cao X. Pirfenidone inhibits epidural scar fibroblast proliferation and differentiation by regulating TGF-β1-induced Smad-dependent and -independent pathways. *Am J Transl Res*. 2019;11(3):1593-1604.

204. Honda N, Jinnin M, Kajihara I, et al. TGF-β-mediated downregulation of microRNA-196a contributes to the constitutive upregulated type I collagen expression in scleroderma dermal fibroblasts. *J Immunol*. 2012;188(7):3323-3331. doi:10.4049/jimmunol.1100876

205. Zhang Y, Kang J, Chen X, et al. Ag nanocomposite hydrogels with immune and regenerative microenvironment regulation promote scarless healing of infected wounds. *Journal of Nanobiotechnology*. 2023;21(1):435. doi:10.1186/s12951-023-02209-2

206. Ludwig N, Razzo BM, Yerneni SS, Whiteside TL. Optimization of cell culture conditions for exosome isolation using mini-size exclusion chromatography (mini-SEC). *Exp Cell Res*. 2019;378(2):149-157. doi:10.1016/j.yexcr.2019.03.014

207. Patel DB, Gray KM, Santharam Y, Lamichhane TN, Stroka KM, Jay SM. Impact of cell culture parameters on production and vascularization bioactivity of mesenchymal stem cell-derived extracellular vesicles. *Bioeng Transl Med*. 2017;2(2):170-179. doi:10.1002/btm2.10065

208. Zhang B, Gong J, He L, et al. Exosomes based advancements for application in medical aesthetics. *Front Bioeng Biotechnol*. 2022;10:1083640. doi:10.3389/fbioe.2022.1083640

209. Ban JJ, Lee M, Im W, Kim M. Low pH increases the yield of exosome isolation. *Biochemical and Biophysical Research Communications*. 2015;461(1):76-79. doi:10.1016/j.bbrc.2015.03.172

210. Shirejini SZ, Inci F. The Yin and Yang of exosome isolation methods: conventional practice, microfluidics, and commercial kits. *Biotechnology Advances*. 2022;54:107814. doi:10.1016/j.biotechadv.2021.107814

211. Aqil F, Munagala R, Jeyabalan J, et al. Milk exosomes - Natural nanoparticles for siRNA delivery. *Cancer Letters*. 2019;449:186-195. doi:10.1016/j.canlet.2019.02.011

212. Yim N, Ryu SW, Choi K, et al. Exosome engineering for efficient intracellular delivery of soluble proteins using optically reversible protein–protein interaction module. *Nature Communications*. 2016;7(1):1-9. doi:10.1038/ncomms12277

213. Thakur A, Sidu RK, Zou H, Alam MK, Yang M, Lee Y. Inhibition of Glioma Cells' Proliferation by Doxorubicin-Loaded Exosomes via Microfluidics. *International Journal of Nanomedicine*. 2020;15:8331-8343. doi:10.2147/IJN.S263956

214. Gandek TB, van der Koog L, Nagelkerke A. A Comparison of Cellular Uptake Mechanisms, Delivery Efficacy, and Intracellular Fate between Liposomes and Extracellular Vesicles. *Advanced Healthcare Materials*. 2023;12(25):2300319. doi:10.1002/adhm.202300319

215. M. Bjørge I, Y. Kim S, F. Mano J, Kalionis B, Chrzanowski W. Extracellular vesicles, exosomes and shedding vesicles in regenerative medicine – a new paradigm for tissue repair. *Biomaterials Science*. 2018;6(1):60-78. doi:10.1039/C7BM00479F